

CERN-TH/2001-107
CLNS 01/1728
PITHA 01/01
SHEP 01/11
hep-ph/0104110
April 11, 2001

QCD Factorization in $B \rightarrow \pi K, \pi\pi$ Decays and Extraction of Wolfenstein Parameters

M. BENEKE^a, G. BUCHALLA^b, M. NEUBERT^c AND C.T. SACHRAJDA^d

^a*Institut für Theoretische Physik E, RWTH Aachen
D-52056 Aachen, Germany*

^b*Theory Division, CERN, CH-1211 Geneva 23, Switzerland*

^c*Newman Laboratory of Nuclear Studies, Cornell University
Ithaca, NY 14853, USA*

^d*Department of Physics and Astronomy, University of Southampton
Southampton SO17 1BJ, UK*

Abstract

In the heavy-quark limit, the hadronic matrix elements entering nonleptonic B -meson decays into two light mesons can be calculated from first principles including “nonfactorizable” strong-interaction corrections. The $B \rightarrow \pi K, \pi\pi$ decay amplitudes are computed including electroweak penguin contributions, SU(3) violation in the light-cone distribution amplitudes, and an estimate of power corrections from chirally-enhanced terms and annihilation graphs. The results are then used to reduce the theoretical uncertainties in determinations of the weak phases γ and α . In that way, new constraints in the $(\bar{\rho}, \bar{\eta})$ plane are derived. Predictions for the $B \rightarrow \pi K, \pi\pi$ branching ratios and CP asymmetries are also presented. A good global fit to the (in part preliminary) experimental data on the branching fractions is obtained without taking recourse to phenomenological models.

1 Introduction

The study of nonleptonic two-body decays of B mesons is of primary importance for the exploration of CP violation and the determination of the flavour parameters of the Standard Model. Because of the interference of several competing amplitudes, these processes allow for the presence of different weak and strong-interaction phases, which play a crucial role for CP violation. In the Standard Model, all CP-violating observables are related to the complex phase of the quark mixing matrix, which in turn implies nontrivial angles in the “unitarity triangle” $V_{ud}V_{ub}^* + V_{cd}V_{cb}^* + V_{td}V_{tb}^* = 0$. With the standard choice of phase conventions, one defines the weak phases $\beta = -\arg(V_{td})$ and $\gamma = \arg(V_{ub}^*)$, as well as $\alpha = 180^\circ - \beta - \gamma$. In the Standard Model, $\sin 2\beta$ can be extracted in a theoretically clean way by measuring the time-dependent rates for the decays $B^0, \bar{B}^0 \rightarrow J/\psi K_S$. The measurement of γ (or α) is more difficult, since it requires controlling the hadronic dynamics in nonleptonic B decays.

A promising strategy for the determination of γ is based on rate measurements for the charged modes $B^\pm \rightarrow (\pi K)^\pm$ and $B^\pm \rightarrow \pi^\pm \pi^0$ [1]. Hadronic uncertainties in this method can be reduced to a minimum by exploiting the structure of the effective weak Hamiltonian and using isospin and SU(3) flavour symmetries [2, 3, 4, 5]. If only measurements of CP-averaged branching ratios are available, it is still possible to derive bounds on γ [3, 6], or to determine γ under the assumption of only a moderate strong-interaction phase ϕ between penguin and tree amplitudes. A different strategy for extracting γ uses SU(3)-symmetry relations between the various contributions to the time-dependent $B_d, \bar{B}_d \rightarrow \pi^+ \pi^-$ and $B_s, \bar{B}_s \rightarrow K^+ K^-$ decay amplitudes [7]. The main theoretical limitation of these methods is in the accuracy with which the effects of SU(3) breaking can be estimated.

The angle α can be determined from the time-dependent CP asymmetry in the decays $B^0, \bar{B}^0 \rightarrow \pi^+ \pi^-$, if the subdominant penguin contribution to the decay amplitudes can be subtracted in some way. This can be achieved by an isospin analysis [8]; however, in practice that route is extremely challenging due to the difficulty in measuring the very small $B^0, \bar{B}^0 \rightarrow \pi^0 \pi^0$ branching ratios. One must therefore rely on dynamical input for the penguin-to-tree ratio [9, 10, 11]. Alternatively, α can be measured in related decays such as $B \rightarrow \rho \pi$, for which the penguin contribution can be eliminated using a time-dependent analysis of the $B \rightarrow \pi^+ \pi^- \pi^0$ Dalitz plot [12].

Most of the above-mentioned determinations of γ or α have theoretical limitations, which would be reduced if some degree of theoretical control over two-body nonleptonic B decays could be attained. However, in the past this has proven to be a very difficult problem. Even advanced methods such as lattice gauge theory, QCD sum rules, or the large- N_c expansion have little to say about the QCD dynamics relevant to hadronic B decays. In recent work, we have developed a systematic approach to this problem. It is based on the observation that, in the heavy-quark limit $m_b \gg \Lambda_{\text{QCD}}$, a rigorous QCD factorization formula holds for the two-body decays $B \rightarrow M_1 M_2$, if the “emission particle” M_2 (the meson not obtaining the spectator quark from the B meson) is a light meson. (It has been argued that perhaps the large- N_c limit may be more relevant

to factorization than the heavy-quark limit [13]. However, the dramatic decrease of “nonfactorizable” effects seen when comparing $K \rightarrow \pi\pi$, $D \rightarrow \pi K$ and $B \rightarrow \pi K$ decays shows that the heavy-quark limit is of crucial importance.) We have previously applied the factorization formula to $B \rightarrow \pi\pi$ decays and obtained results for the decay amplitudes at next-to-leading order in α_s and to leading power in Λ_{QCD}/m_b [14]. The conceptual foundations of our approach have been discussed in detail in [15], which focused on the simpler case of decays into heavy–light final states (where M_1 is a charm meson). In the present work, the QCD factorization formula is applied to the general case of B decays into a pair of light, flavour-nonsinglet pseudoscalar mesons. (Preliminary results of this analysis have been presented in [16].) The present analysis contains three new theoretical ingredients in addition to a much more detailed phenomenological analysis:

1. Matrix elements of electroweak penguin operators are included, which play an important role in charmless decays based on $b \rightarrow s\bar{q}q$ transitions. This is a straightforward extension of our previous analysis. However, a sensible implementation of QCD corrections to electroweak penguin matrix elements implies that one departs from the usual renormalization-group counting, in which the initial conditions for the electroweak penguin operators at the scale $\mu = M_W$ are treated as a next-to-leading order effect.
2. Hard-scattering kernels are derived for general, asymmetric meson light-cone distribution amplitudes. This is important for addressing the question of nonfactorizable SU(3)-breaking corrections, since the distribution amplitudes of strange mesons are, in general, not symmetric with respect to the quark and antiquark momenta.
3. The leading power corrections to the heavy-quark limit are estimated by analyzing “chirally-enhanced” power corrections related to certain twist-3 distribution amplitudes for pseudoscalar mesons. We also discuss potentially large power corrections arising from annihilation topologies, noted first in [17]. This is essential for controlling the theoretical uncertainties of our approach.

The second and third items have not been considered in previous generalizations of the results of [14] to the case of $B \rightarrow \pi K$ decays [18, 19, 20, 21]. Chirally-enhanced power corrections were discussed in [22, 23], but we disagree with some of the results obtained by these authors.

The QCD factorization approach provides us with model-independent predictions for the decays amplitudes including, in particular, their strong-interaction phases. The same method can also be applied to other charmless decays, such as vector–pseudoscalar [19] or vector–vector modes. Our main focus here is on the development of the new conceptual aspects of the approach that are important for a comprehensive phenomenological analysis. This includes a detailed discussion of various sources of potentially large power corrections to the heavy-quark limit. We then perform a comprehensive study of CP-averaged branching fractions and direct CP asymmetries in decays to πK and $\pi\pi$ final states, including a detailed discussion of the theoretical uncertainties from all inputs to the QCD factorization approach. In many of the phenomenological applications discussed in this work the dynamical information obtained using the QCD factorization

formalism is used in a “minimal way”, to reduce the hadronic uncertainties in methods that are theoretically clean up to “nonfactorizable” SU(3)-breaking effects. Most importantly, these strategies do not suffer from uncertainties related to weak annihilation contributions. In this way, it is possible to reduce the hadronic uncertainties in the strategies for determining γ from $B^\pm \rightarrow \pi K, \pi\pi$ decays proposed in [1, 4] to the level of “nonfactorizable” corrections that simultaneously violate SU(3) symmetry and are power suppressed in the heavy-quark limit. These corrections are parametrically suppressed by the product of three small quantities: $1/N_c$, $(m_s - m_d)/\Lambda_{\text{QCD}}$, and Λ_{QCD}/m_b . As a consequence, we argue it will eventually be possible to determine γ with a theoretical accuracy of about 10° (unless γ is much different from its expected value in the Standard Model). More accurately, the strategies discussed here can constrain the Wolfenstein parameters $\bar{\rho}$ and $\bar{\eta}$ with accuracies similar those obtained from the standard global fit to $|V_{ub}|$, ϵ_K , and $B-\bar{B}$ mixing. Given the theoretical input discussed in this paper even the present, preliminary data on the rare hadronic decays exclude at 95% confidence level half of the parameter space obtained from the standard fit.

The QCD factorization approach provides a complete theoretical description of all $B \rightarrow PP$ decay amplitudes. This allows for a large variety of predictions, which go far beyond those explored in the present work. In the future, this will offer the possibility of several nontrivial experimental tests of the factorization formula. A more detailed discussion of these predictions will be presented elsewhere.

The remainder of this paper is organized as follows: In Section 2, we collect some basic formulae and express the $B \rightarrow \pi K, \pi\pi$ decay amplitudes in terms of parameters a_i and b_i appearing in the effective, factorized transition operators for these decays (including weak annihilation contributions). Section 3 contains the technical details of the calculations based on the factorization formula, a discussion of annihilation effects, and a compilation of the relevant formulae for the numerical evaluation of our results. Readers not interested in the technical aspects of our work can proceed directly to Sections 4 and 5, where we present numerical values for the amplitude parameters a_i and b_i (Section 4) and discuss phenomenological applications of our results (Section 5). Specifically, we consider strategies to bound and determine the weak phase γ and to extract $\sin 2\alpha$ from mixing-induced CP violation in $B \rightarrow \pi^+\pi^-$ decay. We also present predictions for CP-averaged branching fractions and CP asymmetries, and perform a global fit in the $(\bar{\rho}, \bar{\eta})$ plane to all measured $B \rightarrow \pi K, \pi\pi$ branching fractions. A critical comparison of our formalism with other theoretical approaches to hadronic B decays is performed in Section 6.

2 Parameterizations of the decay amplitudes

The effective weak Hamiltonian for charmless hadronic B decays consists of a sum of local operators Q_i multiplied by short-distance coefficients C_i and products of elements of the quark mixing matrix, $\lambda_p = V_{pb}V_{ps}^*$ or $\lambda'_p = V_{pb}V_{pd}^*$. Below we will focus on $B \rightarrow \pi K$ decays to be specific; however, with obvious substitutions a similar discussion holds for

all other B decays into two light, flavour-nonsinglet pseudoscalar mesons. Using the unitarity relation $-\lambda_t = \lambda_u + \lambda_c$, we write

$$\mathcal{H}_{\text{eff}} = \frac{G_F}{\sqrt{2}} \sum_{p=u,c} \lambda_p \left(C_1 Q_1^p + C_2 Q_2^p + \sum_{i=3,\dots,10} C_i Q_i + C_{7\gamma} Q_{7\gamma} + C_{8g} Q_{8g} \right) + \text{h.c.}, \quad (1)$$

where $Q_{1,2}^p$ are the left-handed current-current operators arising from W -boson exchange, $Q_{3,\dots,6}$ and $Q_{7,\dots,10}$ are QCD and electroweak penguin operators, and $Q_{7\gamma}$ and Q_{8g} are the electromagnetic and chromomagnetic dipole operators. They are given by

$$\begin{aligned} Q_1^p &= (\bar{p}b)_{V-A} (\bar{s}p)_{V-A}, & Q_2^p &= (\bar{p}_i b_j)_{V-A} (\bar{s}_j p_i)_{V-A}, \\ Q_3 &= (\bar{s}b)_{V-A} \sum_q (\bar{q}q)_{V-A}, & Q_4 &= (\bar{s}_i b_j)_{V-A} \sum_q (\bar{q}_j q_i)_{V-A}, \\ Q_5 &= (\bar{s}b)_{V-A} \sum_q (\bar{q}q)_{V+A}, & Q_6 &= (\bar{s}_i b_j)_{V-A} \sum_q (\bar{q}_j q_i)_{V+A}, \\ Q_7 &= (\bar{s}b)_{V-A} \sum_q \frac{3}{2} e_q (\bar{q}q)_{V+A}, & Q_8 &= (\bar{s}_i b_j)_{V-A} \sum_q \frac{3}{2} e_q (\bar{q}_j q_i)_{V+A}, \\ Q_9 &= (\bar{s}b)_{V-A} \sum_q \frac{3}{2} e_q (\bar{q}q)_{V-A}, & Q_{10} &= (\bar{s}_i b_j)_{V-A} \sum_q \frac{3}{2} e_q (\bar{q}_j q_i)_{V-A}, \\ Q_{7\gamma} &= \frac{-e}{8\pi^2} m_b \bar{s} \sigma_{\mu\nu} (1 + \gamma_5) F^{\mu\nu} b, & Q_{8g} &= \frac{-g_s}{8\pi^2} m_b \bar{s} \sigma_{\mu\nu} (1 + \gamma_5) G^{\mu\nu} b, \end{aligned} \quad (2)$$

where $(\bar{q}_1 q_2)_{V\pm A} = \bar{q}_1 \gamma_\mu (1 \pm \gamma_5) q_2$, i, j are colour indices, e_q are the electric charges of the quarks in units of $|e|$, and a summation over $q = u, d, s, c, b$ is implied. (The definition of the dipole operators $Q_{7\gamma}$ and Q_{8g} corresponds to the sign convention $iD^\mu = i\partial^\mu + g_s A_a^\mu t_a$ for the gauge-covariant derivative.) The Wilson coefficients are calculated at a high scale $\mu \sim M_W$ and evolved down to a characteristic scale $\mu \sim m_b$ using next-to-leading order renormalization-group equations. The essential problem obstructing the calculation of nonleptonic decay amplitudes resides in the evaluation of the hadronic matrix elements of the local operators contained in the effective Hamiltonian.

Applying the QCD factorization formula and neglecting power-suppressed effects, the matrix elements of the effective weak Hamiltonian can be written in the form [14, 15]

$$\langle \pi K | \mathcal{H}_{\text{eff}} | \bar{B} \rangle = \frac{G_F}{\sqrt{2}} \sum_{p=u,c} \lambda_p \langle \pi K | \mathcal{T}_p + \mathcal{T}_p^{\text{ann}} | \bar{B} \rangle, \quad (3)$$

where

$$\begin{aligned} \mathcal{T}_p &= a_1(\pi K) \delta_{pu} (\bar{u}b)_{V-A} \otimes (\bar{s}u)_{V-A} \\ &+ a_2(\pi K) \delta_{pu} (\bar{s}b)_{V-A} \otimes (\bar{u}u)_{V-A} \\ &+ a_3(\pi K) \sum_q (\bar{s}b)_{V-A} \otimes (\bar{q}q)_{V-A} \\ &+ a_4^p(\pi K) \sum_q (\bar{q}b)_{V-A} \otimes (\bar{s}q)_{V-A} \\ &+ a_5(\pi K) \sum_q (\bar{s}b)_{V-A} \otimes (\bar{q}q)_{V+A} \end{aligned}$$

$$\begin{aligned}
& + a_6^p(\pi K) \sum_q (-2)(\bar{q}b)_{S-P} \otimes (\bar{s}q)_{S+P} \\
& + a_7(\pi K) \sum_q (\bar{s}b)_{V-A} \otimes \frac{3}{2}e_q(\bar{q}q)_{V+A} \\
& + a_8^p(\pi K) \sum_q (-2)(\bar{q}b)_{S-P} \otimes \frac{3}{2}e_q(\bar{s}q)_{S+P} \\
& + a_9(\pi K) \sum_q (\bar{s}b)_{V-A} \otimes \frac{3}{2}e_q(\bar{q}q)_{V-A} \\
& + a_{10}^p(\pi K) \sum_q (\bar{q}b)_{V-A} \otimes \frac{3}{2}e_q(\bar{s}q)_{V-A}.
\end{aligned} \tag{4}$$

Here $(\bar{q}_1 q_2)_{S\pm P} = \bar{q}_1(1 \pm \gamma_5)q_2$, and a summation over $q = u, d$ is implied. The symbol \otimes indicates that the matrix elements of the operators in \mathcal{T}_p are to be evaluated in the factorized form $\langle \pi K | j_1 \otimes j_2 | \bar{B} \rangle \equiv \langle \pi | j_1 | \bar{B} \rangle \langle K | j_2 | 0 \rangle$ or $\langle K | j_1 | \bar{B} \rangle \langle \pi | j_2 | 0 \rangle$, as appropriate. “Nonfactorizable” corrections are, by definition, included in the coefficients a_i . The matrix elements for B mesons (i.e., mesons containing a \bar{b} -antiquark) are obtained from (3) by CP conjugation. A corresponding result, with obvious substitutions, holds for other decays such as $B \rightarrow \pi\pi$.

The term $\mathcal{T}_p^{\text{ann}}$ in (3) arises from weak annihilation contributions and introduces a set of coefficients $b_i(\pi K)$, which we shall define and discuss in detail in Section 3.5. Annihilation contributions are suppressed by a power of Λ_{QCD}/m_b and not calculable within the QCD factorization approach. Nevertheless, we will include the coefficients b_i in the amplitude parameterizations in this section.

The coefficients a_i multiplying products of vector or axial-vector currents are renormalization-scheme invariant, as are the hadronic matrix elements of these currents. For the coefficients a_6 and a_8 a scheme dependence remains, which exactly compensates the scheme dependence of the hadronic matrix elements of the scalar or pseudoscalar densities associated with these coefficients. These matrix elements are power suppressed by the ratio

$$r_\chi^K(\mu) = \frac{2m_K^2}{\bar{m}_b(\mu) (\bar{m}_q(\mu) + \bar{m}_s(\mu))}, \tag{5}$$

which is formally of order Λ_{QCD}/m_b but numerically close to unity. In the following we shall use the same notation for charged ($q = u$) and neutral kaons ($q = d$), since the difference is tiny. A corresponding ratio

$$r_\chi^\pi(\mu) = \frac{2m_\pi^2}{\bar{m}_b(\mu) (\bar{m}_u(\mu) + \bar{m}_d(\mu))} \tag{6}$$

appears in the discussion of the $B \rightarrow \pi\pi$ decay amplitudes. For a phenomenological analysis of nonleptonic B decays it is necessary to estimate these “chirally-enhanced” corrections despite the fact that they are formally power suppressed. A detailed discussion of these corrections will be presented in Section 3.2, and their numerical importance will be investigated in Section 4.

In terms of the parameters a_i , the $B \rightarrow \pi K$ decay amplitudes (without annihilation contributions) are expressed as

$$\mathcal{A}(B^- \rightarrow \pi^- \bar{K}^0) = \lambda_p \left[\left(a_4^p - \frac{1}{2} a_{10}^p \right) + r_\chi^K \left(a_6^p - \frac{1}{2} a_8^p \right) \right] A_{\pi K},$$

$$\begin{aligned}
-\sqrt{2}\mathcal{A}(B^- \rightarrow \pi^0 K^-) &= \left[\lambda_u a_1 + \lambda_p (a_4^p + a_{10}^p) + \lambda_p r_\chi^K (a_6^p + a_8^p) \right] A_{\pi K} \\
&\quad + \left[\lambda_u a_2 + \lambda_p \frac{3}{2} (-a_7 + a_9) \right] A_{K\pi}, \\
-\mathcal{A}(\bar{B}^0 \rightarrow \pi^+ K^-) &= \left[\lambda_u a_1 + \lambda_p (a_4^p + a_{10}^p) + \lambda_p r_\chi^K (a_6^p + a_8^p) \right] A_{\pi K}, \\
\sqrt{2}\mathcal{A}(\bar{B}^0 \rightarrow \pi^0 \bar{K}^0) &= \mathcal{A}(B^- \rightarrow \pi^- \bar{K}^0) + \sqrt{2}\mathcal{A}(B^- \rightarrow \pi^0 K^-) \\
&\quad - \mathcal{A}(\bar{B}^0 \rightarrow \pi^+ K^-). \tag{7}
\end{aligned}$$

Here $\lambda_p = V_{pb}V_{ps}^*$, $a_i \equiv a_i(\pi K)$, and a summation over $p = u, c$ is implicitly understood in expressions like $\lambda_p a_i^p$. The last relation follows from isospin symmetry. The CP-conjugate decay amplitudes are obtained from the above by replacing $\lambda_p \rightarrow \lambda_p^*$. We have defined the factorized matrix elements

$$\begin{aligned}
A_{\pi K} &= i \frac{G_F}{\sqrt{2}} (m_B^2 - m_\pi^2) F_0^{B \rightarrow \pi}(m_K^2) f_K, \\
A_{K\pi} &= i \frac{G_F}{\sqrt{2}} (m_B^2 - m_K^2) F_0^{B \rightarrow K}(m_\pi^2) f_\pi, \tag{8}
\end{aligned}$$

where $F_0^{B \rightarrow M}(q^2)$ are semileptonic form factors. Weak annihilation effects contribute further terms to the decay amplitudes, which can be parameterized as

$$\begin{aligned}
\mathcal{A}_{\text{ann}}(B^- \rightarrow \pi^- \bar{K}^0) &= \left[\lambda_u b_2 + (\lambda_u + \lambda_c)(b_3 + b_3^{\text{EW}}) \right] B_{\pi K}, \\
-\sqrt{2}\mathcal{A}_{\text{ann}}(B^- \rightarrow \pi^0 K^-) &= \mathcal{A}_{\text{ann}}(B^- \rightarrow \pi^- \bar{K}^0), \\
-\mathcal{A}_{\text{ann}}(\bar{B}^0 \rightarrow \pi^+ K^-) &= (\lambda_u + \lambda_c) \left(b_3 - \frac{1}{2} b_3^{\text{EW}} \right) B_{\pi K}, \\
\sqrt{2}\mathcal{A}_{\text{ann}}(\bar{B}^0 \rightarrow \pi^0 \bar{K}^0) &= -\mathcal{A}_{\text{ann}}(\bar{B}^0 \rightarrow \pi^+ K^-), \tag{9}
\end{aligned}$$

where

$$B_{\pi K} = i \frac{G_F}{\sqrt{2}} f_B f_\pi f_K. \tag{10}$$

The coefficients $b_i \equiv b_i(\pi K)$ will be defined in Section 3.5, but we may note here that $b_{1,2}$ are related to the current-current operators Q_1^p and Q_2^p in the effective Hamiltonian (1), and $b_{3,4}$ ($b_{3,4}^{\text{EW}}$) are related to QCD (electroweak) penguin operators.

The $B \rightarrow \pi\pi$ decay amplitudes are given by

$$\begin{aligned}
-\mathcal{A}(\bar{B}^0 \rightarrow \pi^+ \pi^-) &= \left[\lambda'_u a_1 + \lambda'_p (a_4^p + a_{10}^p) + \lambda'_p r_\chi^\pi (a_6^p + a_8^p) \right] A_{\pi\pi}, \\
-\sqrt{2}\mathcal{A}(B^- \rightarrow \pi^- \pi^0) &= \left[\lambda'_u (a_1 + a_2) + \frac{3}{2} \lambda'_p (-a_7 + r_\chi^\pi a_8^p + a_9 + a_{10}^p) \right] A_{\pi\pi}, \\
\mathcal{A}(\bar{B}^0 \rightarrow \pi^0 \pi^0) &= \sqrt{2}\mathcal{A}(B^- \rightarrow \pi^- \pi^0) - \mathcal{A}(\bar{B}^0 \rightarrow \pi^+ \pi^-), \tag{11}
\end{aligned}$$

where now $\lambda'_p = V_{pb}V_{pd}^*$, $a_i \equiv a_i(\pi\pi)$, and

$$A_{\pi\pi} = i\frac{G_F}{\sqrt{2}}(m_B^2 - m_\pi^2)F_0^{B\rightarrow\pi}(m_\pi^2)f_\pi. \quad (12)$$

The additional annihilation contributions are

$$\begin{aligned} -\mathcal{A}_{\text{ann}}(\bar{B}^0 \rightarrow \pi^+\pi^-) &= \left[\lambda'_u b_1 + (\lambda'_u + \lambda'_c) \left(b_3 + 2b_4 - \frac{1}{2}b_3^{\text{EW}} + \frac{1}{2}b_4^{\text{EW}} \right) \right] B_{\pi\pi}, \\ -\sqrt{2}\mathcal{A}_{\text{ann}}(B^- \rightarrow \pi^-\pi^0) &= 0, \\ \mathcal{A}_{\text{ann}}(\bar{B}^0 \rightarrow \pi^0\pi^0) &= -\mathcal{A}_{\text{ann}}(\bar{B}^0 \rightarrow \pi^+\pi^-), \end{aligned} \quad (13)$$

where $b_i \equiv b_i(\pi\pi)$, and

$$B_{\pi\pi} = i\frac{G_F}{\sqrt{2}}f_B f_\pi^2. \quad (14)$$

Neglecting tiny mass corrections of order $(m_{\pi,K}/m_B)^2$,

$$R_{\pi K} \equiv \frac{A_{K\pi}}{A_{\pi K}} \simeq \frac{F_0^{B\rightarrow K}(0)f_\pi}{F_0^{B\rightarrow\pi}(0)f_K}, \quad \frac{A_{\pi K}}{A_{\pi\pi}} \simeq \frac{f_K}{f_\pi}. \quad (15)$$

These ratios will play an important role in the discussion of SU(3) violations in Section 5.

The expressions collected above provide a complete description of the decay amplitudes in terms of the parameters a_i and b_i for the various processes. They are the basis for most of the phenomenological applications discussed in this work. However, in the literature several alternative parameterizations of the $B \rightarrow \pi K$ decay amplitudes have been introduced, which are sometimes useful when considering CP asymmetries or ratios of branching fractions. We briefly elaborate on one such parameterization here, adopting the notations of [4]. The dominant contributions to the $B \rightarrow \pi K$ decay amplitudes come from QCD penguin operators. Because the corresponding operators in the effective weak Hamiltonian preserve isospin, this contribution is the same (up to trivial Clebsch–Gordon coefficients) for all decay modes. Isospin-violating contributions to the decay amplitudes are subdominant and arise from the current–current operators Q_1^u and Q_2^u (so-called “tree” contributions), and from electroweak penguins. The latter are suppressed by a power of α/α_s , whereas the former are suppressed by the ratio

$$\epsilon_{\text{KM}} e^{-i\gamma} \equiv \frac{\lambda_u}{\lambda_c} = \tan^2\theta_C R_b e^{-i\gamma}, \quad (16)$$

where θ_C is the Cabibbo angle,

$$R_b = \cot\theta_C \frac{|V_{ub}|}{|V_{cb}|} = \sqrt{\bar{\rho}^2 + \bar{\eta}^2} \quad (17)$$

is one of the sides of the unitarity triangle, and $\bar{\rho}$ and $\bar{\eta}$ are the Wolfenstein parameters. A general parameterization of the decay amplitudes is

$$\begin{aligned} \mathcal{A}(B^- \rightarrow \pi^- \bar{K}^0) &= P \left(1 + \varepsilon_a e^{i\phi_a} e^{-i\gamma} \right), \\ -\sqrt{2} \mathcal{A}(B^- \rightarrow \pi^0 K^-) &= P \left[1 + \varepsilon_a e^{i\phi_a} e^{-i\gamma} - \varepsilon_{3/2} e^{i\phi} (e^{-i\gamma} - q e^{i\omega}) \right], \\ -\mathcal{A}(\bar{B}^0 \rightarrow \pi^+ K^-) &= P \left[1 + \varepsilon_a e^{i\phi_a} e^{-i\gamma} - \varepsilon_T e^{i\phi_T} (e^{-i\gamma} - q_C e^{i\omega_C}) \right]. \end{aligned} \quad (18)$$

(The phase $e^{i\phi_a}$ was denoted $-e^{i\eta}$ in [4].) The amplitude $\mathcal{A}(\bar{B}^0 \rightarrow \pi^0 \bar{K}^0)$ is then determined by the isospin relation shown in the last line of (7). The dominant penguin amplitude P is defined as the sum of all contributions to the $B^- \rightarrow \pi^- \bar{K}^0$ amplitude that are not proportional to $e^{-i\gamma}$. This quantity cancels whenever one takes ratios of decay amplitudes, such as CP asymmetries or ratios of branching fractions. The parameters $\varepsilon_{3/2}$ and ε_T measure the relative strength of tree and QCD penguin contributions, q and q_C measure the relative strength of electroweak penguin and tree contributions, and ε_a parameterizes a rescattering contribution to the $B^- \rightarrow \pi^- \bar{K}^0$ amplitude arising from up-quark penguin topologies. Moreover, ϕ , ϕ_T , ω , ω_C , and ϕ_a are strong rescattering phases. (The strong-interaction phase of P is not observable and can be set to zero.) All parameters except $q e^{i\omega}$ receive weak annihilation contributions.

It is straightforward to express the various amplitude parameters in terms of the parameters $a_i \equiv a_i(\pi K)$ and $b_i \equiv b_i(\pi K)$ defined earlier. We obtain

$$P = \lambda_c \left\{ \left[\left(a_4^c - \frac{1}{2} a_{10}^c \right) + r_\chi^K \left(a_6^c - \frac{1}{2} a_8^c \right) \right] A_{\pi K} + (b_3 + b_3^{\text{EW}}) B_{\pi K} \right\} \quad (19)$$

for the leading penguin amplitude, and for the remaining parameters

$$\begin{aligned} \varepsilon_{3/2} e^{i\phi} &= -\epsilon_{\text{KM}} \frac{(a_1 + R_{\pi K} a_2) + \frac{3}{2} [a_{10}^u + r_\chi^K a_8^u + R_{\pi K} (a_9 - a_7)]}{(a_4^c + r_\chi^K a_6^c) - \frac{1}{2} (a_{10}^c + r_\chi^K a_8^c) + r_A (b_3 + b_3^{\text{EW}})}, \\ \varepsilon_T e^{i\phi_T} &= -\epsilon_{\text{KM}} \frac{a_1 + \frac{3}{2} (a_{10}^u + r_\chi^K a_8^u) - r_A (b_2 + \frac{3}{2} b_3^{\text{EW}})}{(a_4^c + r_\chi^K a_6^c) - \frac{1}{2} (a_{10}^c + r_\chi^K a_8^c) + r_A (b_3 + b_3^{\text{EW}})}, \\ \varepsilon_a e^{i\phi_a} &= \epsilon_{\text{KM}} \frac{(a_4^u + r_\chi^K a_6^u) - \frac{1}{2} (a_{10}^u + r_\chi^K a_8^u) + r_A (b_2 + b_3 + b_3^{\text{EW}})}{(a_4^c + r_\chi^K a_6^c) - \frac{1}{2} (a_{10}^c + r_\chi^K a_8^c) + r_A (b_3 + b_3^{\text{EW}})}, \\ q e^{i\omega} &= -\frac{3}{2\epsilon_{\text{KM}}} \frac{a_{10}^c + r_\chi^K a_8^c + R_{\pi K} (a_9 - a_7)}{(a_1 + R_{\pi K} a_2) + \frac{3}{2} [a_{10}^u + r_\chi^K a_8^u + R_{\pi K} (a_9 - a_7)]}, \\ q_C e^{i\omega_C} &= -\frac{3}{2\epsilon_{\text{KM}}} \frac{a_{10}^c + r_\chi^K a_8^c - r_A b_3^{\text{EW}}}{a_1 + \frac{3}{2} (a_{10}^u + r_\chi^K a_8^u) - r_A (b_2 + \frac{3}{2} b_3^{\text{EW}})}, \end{aligned} \quad (20)$$

where $R_{\pi K} = A_{K\pi}/A_{\pi K}$ is the ratio of the two factorized amplitudes given in (15), and

$$r_A = \frac{B_{\pi K}}{A_{\pi K}} \simeq \frac{f_B f_\pi}{m_B^2 F_0^{B \rightarrow \pi}(0)}. \quad (21)$$

Our notation for amplitude ratios is such that the ratio $R_{\pi K}$ (denoted by a capital R) deviates from 1 only by SU(3)-breaking corrections, whereas the ratios r_A and r_χ^K (denoted by a lower-case r) are formally of order Λ_{QCD}/m_b in the heavy-quark limit. However, whereas $r_A \approx 0.003$ is indeed very small, $r_\chi^K \approx 0.7$ (at a scale $\mu \approx 1.45$ GeV) is numerically large for real B mesons. Finally, note that the electroweak penguin coefficients $a_{7,\dots,10}$ could be safely neglected in all quantities other than $q e^{i\omega}$ and $q_C e^{i\omega_C}$, because they are tiny compared with the other coefficients $a_{1,\dots,6}$. In (20), they are included only for completeness. (The systematics of including electroweak penguin contributions will be discussed in more detail later.)

An important quantity affecting the determination of $\sin 2\alpha$ from the time-dependent CP asymmetry in the decays $B^0, \bar{B}^0 \rightarrow \pi^+\pi^-$ is the ratio of penguin to tree amplitudes. In this case the tree contribution is no longer CKM suppressed, since

$$\frac{\lambda'_u}{\lambda'_c} = -R_b e^{-i\gamma} \quad (22)$$

is of order unity. The $\bar{B}^0 \rightarrow \pi^+\pi^-$ decay amplitude in (11) can be written as

$$- \mathcal{A}(\bar{B}^0 \rightarrow \pi^+\pi^-) \propto e^{-i\gamma} + \frac{P_{\pi\pi}}{T_{\pi\pi}}, \quad (23)$$

where

$$\frac{P_{\pi\pi}}{T_{\pi\pi}} = -\frac{1}{R_b} \frac{(a_4^c + r_\chi^\pi a_6^c) + (a_{10}^c + r_\chi^\pi a_8^c) + r_A[b_3 + 2b_4 - \frac{1}{2}(b_3^{\text{EW}} - b_4^{\text{EW}})]}{(a_1 + a_4^u + r_\chi^\pi a_6^u) + (a_{10}^u + r_\chi^\pi a_8^u) + r_A[b_1 + b_3 + 2b_4 - \frac{1}{2}(b_3^{\text{EW}} - b_4^{\text{EW}})]}, \quad (24)$$

and $r_A = B_{\pi\pi}/A_{\pi\pi}$. In this case the electroweak penguin terms are very small, because they are not CKM enhanced with respect to the tree contribution.

This concludes the discussion of parameterizations of the decay amplitudes. The following section is devoted to a detailed description of the QCD factorization formalism, the calculation of the parameters a_i for the various nonleptonic decay amplitudes, and an estimation of the annihilation parameters b_i . The reader mainly interested in the phenomenological applications of our results can proceed directly to Section 4, where we present numerical results for these parameters, which will be used in the subsequent analysis in Section 5.

3 QCD factorization in $B \rightarrow \pi K$ decays

Based on the underlying physical principle of colour transparency (see [24, 25, 26] for early discussions in the context of decays to heavy–light final states), supported by a detailed diagrammatic analysis of infrared cancellations at leading power in the heavy-quark expansion, we have shown in previous work that the complexity of the hadronic matrix elements governing energetic, two-body hadronic decays of B mesons simplifies greatly in the heavy-quark limit $m_b \gg \Lambda_{\text{QCD}}$ [14, 15]. Consider $B \rightarrow \pi K$ decays as an

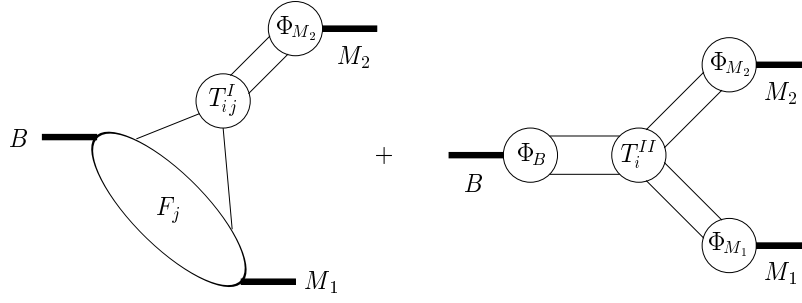


Figure 1: Graphical representation of the factorization formula. Only one of the two form-factor terms in (25) is shown for simplicity.

example. To leading power in Λ_{QCD}/m_b , but to all orders in perturbation theory, the matrix elements of the local operators Q_i in the effective weak Hamiltonian in (1) obey the factorization formula

$$\begin{aligned} \langle \pi K | Q_i | B \rangle = & F_0^{B \rightarrow \pi} T_{K,i}^I * f_K \Phi_K + F_0^{B \rightarrow K} T_{\pi,i}^I * f_\pi \Phi_\pi \\ & + T_i^{II} * f_B \Phi_B * f_K \Phi_K * f_\pi \Phi_\pi, \end{aligned} \quad (25)$$

where Φ_M are leading-twist light-cone distribution amplitudes, and the $*$ -products imply an integration over the light-cone momentum fractions of the constituent quarks inside the mesons. A graphical representation of this result is shown in Figure 1. Because the energetic, collinear light-quark pair that ultimately evolves into the emission particle at the “upper vertex” is created by a point-like source, soft gluon exchange between this pair and the other quarks in the decay is power suppressed in the heavy-quark limit (colour transparency). In other words, whereas the hadronic physics governing the semileptonic $B \rightarrow M_1$ transition and the formation of the emission particle M_2 is genuinely nonperturbative, “nonfactorizable” interactions connecting the two systems are dominated by hard gluon exchange.

The hard-scattering kernels $T_i^{I,II}$ in (25) are calculable in perturbation theory. $T_{M,i}^I$ starts at tree level and, at higher order in α_s , contains “nonfactorizable” corrections from hard gluon exchange or light-quark loops (penguin topologies). Hard, “nonfactorizable” interactions involving the spectator quark are part of T_i^{II} . The relevant Feynman diagrams contributing to these kernels at next-to-leading are shown in Figure 2. Although individually these graphs contain infrared-sensitive regions at leading power, all soft and collinear divergences cancel in their sum, thus yielding a calculable short-distance contribution. Annihilation topologies are not included in (25) and Figure 2, because they do not contribute at leading order in Λ_{QCD}/m_b . These power-suppressed contributions will be discussed separately in Section 3.5.

We stress that the factorization formula does not imply that hadronic B decays are perturbative in nature. Dominant soft contributions to the decay amplitudes exist, which cannot be controlled in a hard-scattering approach. However, at leading power all these nonperturbative effects are contained in the semileptonic form factors and light-cone

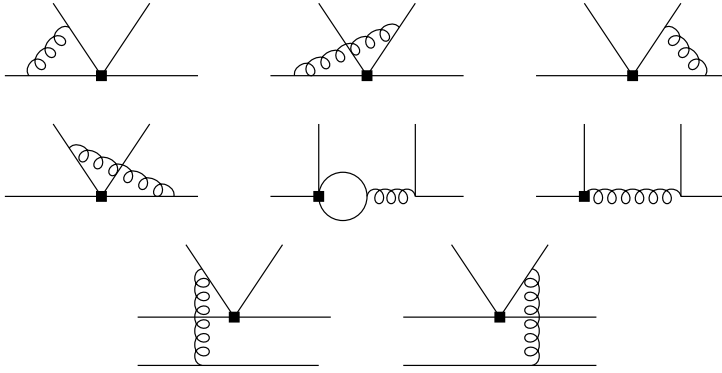


Figure 2: Order α_s corrections to the hard-scattering kernels $T_{M,i}^{\text{I}}$ (first two rows) and T_i^{II} (last row). In the case of $T_{M,i}^{\text{I}}$, the spectator quark does not participate in the hard interaction and is not drawn. The two lines directed upwards represent the quarks that make up one of the light mesons (the emission particle) in the final state.

distribution amplitudes. Once these quantities are given, the nonleptonic decay amplitudes can be derived using perturbative approximations to the hard-scattering kernels. This allows us to compute perturbative corrections to “naive factorization” estimates of nonleptonic amplitudes, which is crucial for obtaining results that are independent of the renormalization scheme adopted in the calculation of the effective weak Hamiltonian. The hard-scattering kernels also contain imaginary parts, which determine the strong rescattering phases of the decay amplitudes. At leading power in Λ_{QCD}/m_b these imaginary parts are of perturbative origin.

In the remainder of this section, we discuss in detail the various issues to be addressed in the evaluation of the factorization formula. In Section 3.1, a modified renormalization-group treatment of electroweak penguin effects is introduced, which is more appropriate than the standard scheme as far as applications to rare hadronic B decays are concerned. Each of the diagrams in Figure 2 contains a leading-power contribution relevant to (25) and power-suppressed terms, which do not factorize in general. An important class of such power-suppressed effects is related to certain higher-twist meson distribution amplitudes. These amplitudes are defined in Section 3.2, and their leading, chirally-enhanced contributions to the nonleptonic decay amplitudes are evaluated. Section 3.4 contains a compendium of the relevant formulae for the calculation of the parameters a_i . Section 3.5 is devoted to annihilation topologies and the definition of the parameters b_i .

3.1 Wilson coefficients of electroweak penguin operators

In the conventional treatment of the effective weak Hamiltonian (1), the initial conditions for the electroweak penguin coefficients at the scale $\mu = M_W$ are considered a next-to-leading order effect, because they are proportional to the electroweak gauge coupling α (see [27, 28] for a detailed discussion). For our purposes, however, it is preferable

to deviate from this standard power counting and introduce a modified approximation scheme. The reason is that the electroweak penguin contributions in $B \rightarrow \pi K$ decays and other rare processes based on $b \rightarrow s\bar{q}q$ transitions are important only because they compete with strongly CKM-suppressed tree topologies. Electroweak penguins and tree topologies together are responsible for the isospin-violating contributions to the decay amplitudes [29]. Therefore, their effects are important even though they are suppressed with respect to the leading QCD penguin amplitude, which conserves isospin. The ratio of electroweak penguin to tree amplitudes scales like $\alpha/\lambda^2 \sim 1$, where $\lambda = 0.22$ is the Wolfenstein parameter. Moreover, the dominant electroweak penguin effects are enhanced by a factor of $(m_t/M_W)^2$ and $1/\sin^2\theta_W$. Hence it is not appropriate to count α as a small parameter in the renormalization-group evolution, if the effect of interest is related to isospin breaking.

We now describe a systematic modification of the usual leading and next-to-leading approximations, in which the dominant part of the electroweak penguin coefficients at the scale $\mu = M_W$ is treated as a leading-order effect. It is then consistent to include the QCD radiative corrections to the enhanced terms in the initial conditions for the electroweak penguin coefficients and, at the same time, the corrections of order α_s to the matrix elements of the electroweak penguin operators, which represent the next-to-leading order corrections to the hard-scattering kernels in the factorization formula.

Using a compact matrix notation, the solution to the renormalization-group equation for the Wilson coefficients C_1, \dots, C_{10} in (1) can be written as

$$\vec{C}(\mu) = \left[\mathbf{U}_0 + \frac{\alpha_s(\mu)}{4\pi} \mathbf{J} \mathbf{U}_0 - \frac{\alpha_s(M_W)}{4\pi} \mathbf{U}_0 \mathbf{J} + \frac{\alpha}{4\pi} \left(\frac{4\pi}{\alpha_s(\mu)} \mathbf{R}_0 + \mathbf{R}_1 \right) \right] \vec{C}(M_W). \quad (26)$$

The matrices \mathbf{U}_0 , \mathbf{J} , \mathbf{R}_0 , and \mathbf{R}_1 depend on the ratio $\alpha_s(\mu)/\alpha_s(M_W)$ and on the anomalous dimensions and β -function. At leading order, the evolution matrix reduces to $\mathbf{U}_0 + (\alpha/\alpha_s)\mathbf{R}_0$. The remaining terms shown above are the next-to-leading corrections.

We now expand the coefficients $\vec{C}(M_W)$ at the weak scale as

$$\vec{C}(M_W) = \vec{C}_s^{(0)} + \frac{\alpha_s(M_W)}{4\pi} \vec{C}_s^{(1)} + \frac{\alpha}{4\pi} \left(\vec{C}_e^{(0)} + \frac{\alpha_s(M_W)}{4\pi} \vec{C}_e^{(1)} + \vec{R}_e^{(0)} \right), \quad (27)$$

where superscripts indicate the order in the strong coupling constant $\alpha_s(M_W)$. The term proportional to α represents the electroweak contribution originating from photon-penguin, Z -penguin and box diagrams. We split this term into a contribution \vec{C}_e containing all terms enhanced by the large top-quark mass and/or a factor of $1/\sin^2\theta_W$, and a remainder \vec{R}_e . As explained above, we treat \vec{C}_e as a leading effect and hence include the first two terms in its expansion in powers of $\alpha_s(M_W)$. The remainder \vec{R}_e is considered a next-to-leading effect, and so we only keep the first term in its perturbative expansion. Explicitly, the nonvanishing contributions to the initial conditions in the electroweak sector ($i = 7, 8, 9, 10$) are

$$C_{e,7}^{(0)} = \frac{x_t}{3}, \quad C_{e,9}^{(0)} = \frac{x_t}{3} + \frac{2}{3\sin^2\theta_W} [10B_0(x_t) - 4C_0(x_t)], \quad (28)$$

and

$$R_{e,7}^{(0)} = R_{e,9}^{(0)} = \frac{8}{3} C_0(x_t) + \frac{2}{3} \tilde{D}_0(x_t) - \frac{x_t}{3}, \quad (29)$$

where $x_t = m_t^2/M_W^2$ with $m_t = \bar{m}_t(m_t)$. The Inami–Lim functions $B_0(x)$, $C_0(x)$ and $\tilde{D}_0(x)$ can be found, e.g., in [30]. Numerically, the remainder $\vec{R}_e^{(0)}$ is indeed much smaller than $\vec{C}_e^{(0)}$, justifying our approximation scheme. Note that $\vec{C}_e^{(0)}$ is gauge and renormalization-scheme independent. The remainder $\vec{R}_e^{(0)}$ is gauge-independent, but it carries the usual next-to-leading order scheme dependence of the electroweak coefficients. Explicit expressions for the QCD corrections contributing to $\vec{C}_e^{(1)}$ have been obtained in [31]. Using these results, we obtain the approximate expressions (valid for a high-energy matching scale $\mu_W = M_W$)

$$\begin{aligned} C_{e,7}^{(1)} &\simeq -29.60 x_t^{1.142} + 28.52 x_t^{1.148}, \\ C_{e,8}^{(1)} &\simeq 0.94 x_t^{0.661}, \\ C_{e,9}^{(1)} &\simeq -571.62 x_t^{0.580} + 566.40 x_t^{0.590}, \\ C_{e,10}^{(1)} &\simeq -5.51 x_t^{1.107}. \end{aligned} \quad (30)$$

In the conventional treatment $\vec{C}_e^{(1)}$ would be absent, while the sum $(\vec{C}_e^{(0)} + \vec{R}_e^{(0)})$ would be the usual initial condition for the electroweak coefficients at the scale $\mu = M_W$, counted as a next-to-leading order effect.

In addition to the modified counting scheme for powers of coupling constants, we make a further, numerically excellent approximation, which greatly simplifies the systematic evaluation of the Wilson coefficients. In essence, it amounts to neglecting QED effects in the calculation of the Wilson coefficients C_1, \dots, C_6 . The values of these coefficients are obtained using the standard next-to-leading order approximation including only strong-interaction effects. At the same time, we neglect QED corrections to the matrix elements of the operators Q_1, \dots, Q_6 . (In fact, the virtual corrections of order α are infrared divergent and require the inclusion of photon bremsstrahlung contributions in order to obtain physical results. Our approximation scheme avoids this complication.) This treatment can be justified by noting that QED and electroweak contributions to the decay amplitudes in (18) are only important if they contribute to the parameters $q e^{i\omega}$ and $q_C e^{i\omega_C}$. From (20), it follows that the terms of order α contained in the coefficients $a_{7,\dots,10}$ are enhanced by the prefactor $1/\epsilon_{\text{KM}}$. It is thus sufficient for all practical purposes to only include the order α corrections from the coefficients $a_{7,\dots,10}$. On the contrary, QED corrections to the other amplitude parameters can be safely neglected (i.e., the coefficients $a_{1,\dots,6}$ do not contain terms proportional to α). Precisely this is achieved by our approximation scheme.

At the technical level, the approximation described above can be explained in terms of the 10×10 anomalous-dimension matrix for the operators Q_1, \dots, Q_{10} , written in block form as

$$\gamma = \left(\begin{array}{c|c} \mathbf{A}_{6 \times 6} & \mathbf{B}_{6 \times 4} \\ \hline \mathbf{C}_{4 \times 6} & \mathbf{D}_{4 \times 4} \end{array} \right). \quad (31)$$

Table 1: Wilson coefficients C_i in the NDR scheme and based on our modified approximation scheme (see text). Input parameters are $\Lambda_{\overline{\text{MS}}}^{(5)} = 0.225 \text{ GeV}$, $m_t(m_t) = 167 \text{ GeV}$, $m_b(m_b) = 4.2 \text{ GeV}$, $M_W = 80.4 \text{ GeV}$, $\alpha = 1/129$, and $\sin^2\theta_W = 0.23$.

| | | | | | | |
|---------------|--------------|--------------|--------------|-----------------|----------------------------|-----------------------|
| NLO | C_1 | C_2 | C_3 | C_4 | C_5 | C_6 |
| $\mu = m_b/2$ | 1.137 | -0.295 | 0.021 | -0.051 | 0.010 | -0.065 |
| $\mu = m_b$ | 1.081 | -0.190 | 0.014 | -0.036 | 0.009 | -0.042 |
| $\mu = 2m_b$ | 1.045 | -0.113 | 0.009 | -0.025 | 0.007 | -0.027 |
| | C_7/α | C_8/α | C_9/α | C_{10}/α | $C_{7\gamma}^{\text{eff}}$ | C_{8g}^{eff} |
| $\mu = m_b/2$ | -0.024 | 0.096 | -1.325 | 0.331 | — | — |
| $\mu = m_b$ | -0.011 | 0.060 | -1.254 | 0.223 | — | — |
| $\mu = 2m_b$ | 0.011 | 0.039 | -1.195 | 0.144 | — | — |
| LO | C_1 | C_2 | C_3 | C_4 | C_5 | C_6 |
| $\mu = m_b/2$ | 1.185 | -0.387 | 0.018 | -0.038 | 0.010 | -0.053 |
| $\mu = m_b$ | 1.117 | -0.268 | 0.012 | -0.027 | 0.008 | -0.034 |
| $\mu = 2m_b$ | 1.074 | -0.181 | 0.008 | -0.019 | 0.006 | -0.022 |
| | C_7/α | C_8/α | C_9/α | C_{10}/α | $C_{7\gamma}^{\text{eff}}$ | C_{8g}^{eff} |
| $\mu = m_b/2$ | -0.012 | 0.045 | -1.358 | 0.418 | -0.364 | -0.169 |
| $\mu = m_b$ | -0.001 | 0.029 | -1.276 | 0.288 | -0.318 | -0.151 |
| $\mu = 2m_b$ | 0.018 | 0.019 | -1.212 | 0.193 | -0.281 | -0.136 |

We set $\mathbf{C} = \mathbf{0}$, thereby neglecting the mixing of the electroweak penguin operators into the operators Q_1, \dots, Q_6 , and ignore contributions of order α to \mathbf{A} . At the same time, we drop the terms of order α in the matching conditions (27) for C_1, \dots, C_6 . We also omit terms of order α in \mathbf{D} , which would yield second-order corrections in α . For the matrix \mathbf{B} , we use the complete next-to-leading order result including terms of order α .

Numerical results for the Wilson coefficients obtained at leading and next-to-leading order in our modified approximation scheme are given in Table 1. Throughout this work, we use the “naive dimensional regularization” (NDR) scheme with anticommuting γ_5 , as defined in [27]. The matrix elements of the dipole operators $Q_{7\gamma}$ and Q_{8g} enter the decay amplitudes only at next-to-leading order. Consequently, the standard leading-logarithmic approximation is sufficient for the coefficients $C_{7\gamma}$ and C_{8g} . In practice, it is advantageous to work with so-called “effective” coefficients, which in the NDR scheme are defined as $C_{7\gamma}^{\text{eff}} = C_{7\gamma} - \frac{1}{3}C_5 - C_6$ and $C_{8g}^{\text{eff}} = C_{8g} + C_5$. In the numerical analysis of (26) we consistently drop all terms of higher than next-to-leading order according to our modified counting scheme. Throughout we use the two-loop expression for the running coupling $\alpha_s(\mu)$ evaluated with $n_f = 5$ light quark flavours.

3.2 Meson distribution amplitudes and twist-3 projections

Referring to the factorization formula shown graphically in Figure 1, we denote by x the longitudinal momentum fraction of the constituent quark in the emission meson M_2 (the meson at the “upper vertex”), and by y the momentum fraction of the quark in the meson M_1 . For a \bar{B} meson decaying into two light mesons, we define light-cone distribution amplitudes by choosing the $+$ direction along the decay path of the light emission particle and denote by ξ the light-cone momentum fraction of the light spectator antiquark. A massive pseudoscalar meson has two leading-twist light-cone distribution amplitudes [15, 32], but only one of them enters our results. This amplitude is called $\Phi_B(\xi)$ and coincides with the function $\Phi_{B1}(\xi)$ defined in Section 2.3.3 of [15]. The meson distribution amplitudes are normalized to 1 once the decay constants are factored out as in (25). For a light meson, we define the leading-twist amplitude $\Phi(x)$ in the usual way and assume that $\Phi(x) = O(1)$ if both x and $(1 - x)$ are of order unity, and $\Phi(x) = O(x)$ for $x \rightarrow 0$ (and similarly for $x \rightarrow 1$). For the B meson, almost all momentum is carried by the heavy quark, and hence $\Phi_B(\xi) = O(m_b/\Lambda_{\text{QCD}})$ and $\xi = O(\Lambda_{\text{QCD}}/m_b)$.

Higher-twist light-cone distribution amplitudes for the light mesons give power-suppressed contributions in the heavy-quark limit. However, as has been explained in Section 2, these can sometimes be large if they appear in conjunction with the chiral enhancement factors $r_\chi^M(\mu)$ defined in (5) and (6). The corresponding terms are associated with twist-3 quark–antiquark distribution amplitudes and can be identified completely. Since the calculation of these contributions in momentum space is less straightforward than for the leading-twist contributions, we summarize the relevant projection operators below, following the discussion in [33].

The relevant definitions of the light-cone distribution amplitudes of a light pseudoscalar meson P in terms of bilocal operator matrix elements are [34]

$$\begin{aligned} \langle P(p) | \bar{q}(z_2) \gamma_\mu \gamma_5 q(z_1) | 0 \rangle &= -i f_P p_\mu \int_0^1 dx e^{i(x p \cdot z_2 + \bar{x} p \cdot z_1)} \Phi(x), \\ \langle P(p) | \bar{q}(z_2) i \gamma_5 q(z_1) | 0 \rangle &= f_P \mu_P \int_0^1 dx e^{i(x p \cdot z_2 + \bar{x} p \cdot z_1)} \Phi_p(x), \\ \langle P(p) | \bar{q}(z_2) \sigma_{\mu\nu} \gamma_5 q(z_1) | 0 \rangle &= i f_P \mu_P (p_\mu z_\nu - p_\nu z_\mu) \int_0^1 dx e^{i(x p \cdot z_2 + \bar{x} p \cdot z_1)} \frac{\Phi_\sigma(x)}{6}, \end{aligned} \quad (32)$$

where f_P is the decay constant, and we have defined $z = z_2 - z_1$ and $\bar{x} = 1 - x$. The parameter $\mu_P = m_P^2/(m_1 + m_2)$, where $m_{1,2}$ are the current quark masses of the meson constituents, is proportional to the chiral quark condensate. (This definition does not hold for the π^0 meson, in which case $\mu_{\pi^0} = m_{\pi^0}^2/(m_u + m_d)$ as for the charged pions [15].) $\Phi(x)$ is the leading-twist (twist-2) distribution amplitude, whereas $\Phi_p(x)$ and $\Phi_\sigma(x)$ have subleading twist (twist-3). All three distribution amplitudes are normalized to 1, as follows by taking the limit $z_1 \rightarrow z_2$. The above definitions can be combined into the matrix

$$\langle P(p) | \bar{q}_\beta(z_2) q_\alpha(z_1) | 0 \rangle$$

$$= \frac{if_P}{4} \int_0^1 dx e^{i(xp \cdot z_2 + \bar{x}p \cdot z_1)} \left\{ \not{p} \gamma_5 \Phi(x) - \mu_P \gamma_5 \left(\Phi_p(x) - \sigma_{\mu\nu} p^\mu z^\nu \frac{\Phi_\sigma(x)}{6} \right) \right\}_{\alpha\beta}. \quad (33)$$

We implicitly assume that the bilocal matrix elements are supplied with the appropriate path-ordered exponentials of gluon fields so as to make the definitions of the light-cone distribution amplitudes gauge invariant. (These exponentials are absent in light-cone gauge.) The distribution amplitudes depend on the renormalization scale μ . This scale dependence is compensated by higher-order corrections to the hard-scattering kernels, which however are beyond the accuracy of the present calculation. We thus suppress the argument μ in the distribution amplitudes, because it is irrelevant to our discussion.

To obtain the corresponding projector of the quark–antiquark amplitude in momentum space, the transverse components of the coordinate z must be taken into account. The collinear approximation can be taken only after the projection has been applied. We therefore assign momenta

$$k_1^\mu = xp^\mu + k_\perp^\mu + \frac{\vec{k}_\perp^2}{2x p \cdot \bar{p}} \bar{p}^\mu, \quad k_2^\mu = \bar{x}p^\mu - k_\perp^\mu + \frac{\vec{k}_\perp^2}{2\bar{x} p \cdot \bar{p}} \bar{p}^\mu \quad (34)$$

to the quark and antiquark in the light meson, where \bar{p} is a light-like vector whose 3-components point into the opposite direction of \vec{p} . Then the exponential in (33) becomes $e^{i(k_1 \cdot z_2 + k_2 \cdot z_1)}$. (Meson mass effects are neglected, so that p and \bar{p} can be considered as light-like.) The transverse components k_\perp^μ are defined with respect to the vectors p and \bar{p} . Note that $k_1^2 = k_2^2 = 0$. In general, the projector (33) is part of a diagram expressed in configuration space. Transformation to momentum space is achieved by performing the integrations over z_i , which reduce to momentum-space δ -functions after substituting

$$z^\nu \rightarrow (-i) \frac{\partial}{\partial k_{1\nu}} = (-i) \left(\frac{\bar{p}^\nu}{p \cdot \bar{p}} \frac{\partial}{\partial x} + \frac{\partial}{\partial k_{\perp\nu}} + \dots \right). \quad (35)$$

The ellipses denote a term proportional to p^ν , which does not contribute to the result. We also omit terms of order k_\perp^2 , which cannot contribute in the limit $k_\perp \rightarrow 0$. As written above, the derivative acts on the hard-scattering amplitude in the momentum-space representation. Using an integration by parts, the derivative with respect to x can be made to act on the light-cone distribution amplitude. The second term, which involves the derivative with respect to the transverse momentum, must be evaluated before the collinear limit $k_1 \rightarrow xp$, $k_2 \rightarrow \bar{x}p$ is taken. The light-cone projection operator of a light pseudoscalar meson in momentum space, including twist-3 two-particle contributions, then reads

$$M_{\alpha\beta}^P = \frac{if_P}{4} \left\{ \not{p} \gamma_5 \Phi(x) - \mu_P \gamma_5 \left(\Phi_p(x) - i\sigma_{\mu\nu} \frac{p^\mu \bar{p}^\nu}{p \cdot \bar{p}} \frac{\Phi'_\sigma(x)}{6} + i\sigma_{\mu\nu} p^\mu \frac{\Phi_\sigma(x)}{6} \frac{\partial}{\partial k_{\perp\nu}} \right) \right\}_{\alpha\beta}. \quad (36)$$

It is understood that, after the derivative is taken, the momenta k_1 and k_2 are set equal to xp and $\bar{x}p$, respectively. A complete description of the pseudoscalar meson at the twist-3 level would also include three-particle quark–antiquark–gluon contributions (see

[34] for a detailed discussion), which do not involve the large normalization factor μ_P and thus are omitted here. (Note that the overall sign of (36) as well as of (41) below depends on the convention of ordering the quark fields in (33).)

The asymptotic limit of the leading-twist distribution amplitude, valid for $\mu \rightarrow \infty$, is $\Phi(x) = 6x(1-x)$. For finite value of the renormalization scale, it is convenient and conventional to employ an expansion in Gegenbauer polynomials of the form

$$\Phi_M(x, \mu) = 6x(1-x) \left[1 + \sum_{n=1}^{\infty} \alpha_n^M(\mu) C_n^{(3/2)}(2x-1) \right]. \quad (37)$$

In numerical evaluations it will be sufficient to truncate this expansion at $n=2$, using $C_1^{(3/2)}(u) = 3u$ and $C_2^{(3/2)}(u) = \frac{3}{2}(5u^2 - 1)$. The Gegenbauer moments $\alpha_n^M(\mu)$ are multiplicatively renormalized. The scale dependence of these coefficients enters our results only at order α_s^2 , which is beyond the accuracy of a next-to-leading order calculation.

The twist-3 two-particle distribution amplitudes are determined by the three-particle distributions via the equations of motion, except for a single term [34]. In the approximation adopted here, where only terms proportional to μ_P are kept and all three-particle distributions are neglected, the twist-3 amplitudes must obey the equations of motion

$$\frac{x}{2} \left(\Phi_p(x) + \frac{\Phi'_\sigma(x)}{6} \right) = \frac{\Phi_\sigma(x)}{6}, \quad \frac{1-x}{2} \left(\Phi_p(x) - \frac{\Phi'_\sigma(x)}{6} \right) = \frac{\Phi_\sigma(x)}{6}. \quad (38)$$

These equations enforce that we must use the asymptotic forms $\Phi_p(x) = 1$ and $\Phi_\sigma(x) = 6x(1-x)$. It will be important below that $\Phi_p(x)$ and $\Phi'_\sigma(x)$ do not vanish at the endpoints $x=0$ or 1 . We finally observe that the k_\perp -derivative in (36) can be substituted by

$$\frac{\partial}{\partial k_{\perp\nu}} \rightarrow \frac{2k_\perp^\nu}{k_\perp^2}. \quad (39)$$

This is because we may expand the amplitude to first order in k_\perp (higher powers do not contribute in the $k_\perp \rightarrow 0$ limit), and use

$$\frac{\partial}{\partial k_{\perp\nu}} k_\perp^\lambda = \frac{\langle 2k_\perp^\nu k_\perp^\lambda \rangle}{k_\perp^2} = g_\perp^{\nu\lambda}, \quad (40)$$

which holds after averaging k_\perp over the azimuthal angle (denoted by $\langle \dots \rangle$). We use the definition $g_\perp^{\nu\lambda} = \text{diag}(0, -1, -1, 0)$. The twist-3 terms in (36) can now be combined into the projector [35]

$$- \frac{i f_P \mu_P}{4} \gamma_5 \frac{\not{k}_2 \not{k}_1}{k_2 \cdot k_1} \Phi_p(x), \quad (41)$$

where $k_{1,2}$ are the quark and antiquark momenta defined in (34), and the factor of $\Phi_p(x) = 1$ is simply there to remind us that this is a twist-3 projection. In our analysis below, we will quote the results of the twist-3 projections in this form, i.e., after eliminating $\Phi_\sigma^{(\prime)}(x)$ using the equations of motion. Expressions in terms of two functions $\Phi_p(x)$ and $\Phi_\sigma(x)$ are ambiguous, but reduce to the same expression upon substituting the asymptotic forms of the distribution amplitudes.

3.3 Comments on the calculation

We now describe some technical aspects of the calculation of the various diagrams in more detail. The complete results for the parameters a_i will be given in Section 3.4.

Vertex corrections

The calculation of the four one-loop vertex diagrams (first four diagrams in Figure 2) involves the trace

$$\text{tr} \left(M^{M_2} \left[\frac{(2k_1^\rho + \gamma^\rho \not{\ell})\Gamma}{(xq + \ell)^2} - \frac{\Gamma(2k_2^\rho + \not{\ell}\gamma^\rho)}{(\bar{x}q + \ell)^2} \right] \right), \quad (42)$$

where M^{M_2} is the projector from (36), q the momentum of the meson M_2 , k_1 (k_2) the momentum of the quark (antiquark) in this meson, and ℓ the momentum of the gluon. We have used that $M^{M_2} \not{k}_1 = \not{k}_2 M^{M_2} = 0$ by the equations of motion, and that we can put $k_1 = xq$ and $k_2 = \bar{x}q$ in the denominator. A Fierz transformation may be necessary in order to arrive at the trace (42). The possible Γ structures are therefore $V - A$ (contributing to $a_{1,\dots,4,9,10}$), $V + A$ (contributing to $a_{5,7}$), and $S + P$ (contributing to $a_{6,8}$).

If $\Gamma = V \pm A$, only the leading-twist light-cone distribution amplitude $\Phi(x)$ in (36) contributes under the trace. We then recover the results of [14, 15] and find that there exist no chirally-enhanced power corrections to $a_{1,\dots,5,7,9,10}$ from the vertex diagrams. If $\Gamma = S + P$, the leading-twist contribution to the trace vanishes, while the twist-3 result is proportional to $r_\chi^{M_2} = 2\mu_{M_2}/m_b$. This gives an order α_s correction to the coefficients $a_{6,8}$, which are multiplied by $r_\chi^{M_2}$ already in naive factorization. We can now exploit the fact that $\text{tr} \sigma_{\mu\nu} = 0$ to show that the term involving the transverse-momentum derivative in (36) does not contribute to the trace. At this stage, the collinear limit can be taken to compute the kernel in the usual way. The projection on $\Phi_p(x)$ yields a result containing symmetric and antisymmetric parts under the exchange of x and $(1-x)$. As explained above, in the approximation of keeping only chirally-enhanced terms we are forced to assume the asymptotic form for $\Phi_p(x)$, so that the antisymmetric part of the kernel integrates to zero. The symmetric part turns out to be a scheme-dependent constant and is responsible for the “-6” in the expressions for $a_{6,8}$ in (46) below. The kernel resulting from the $\Phi'_\sigma(x)$ projection is symmetric under $x \leftrightarrow (1-x)$ and thus vanishes after integration with $\Phi'_\sigma(x)$.

Penguin diagrams

We now consider the penguin contractions (fifth diagram in Figure 2), restricting our attention first to the twist-2 part of the projector (36). The corresponding contributions to the hard-scattering kernels have been given in our previous work [14]. Because there have been conflicting results for the penguin terms in the recent literature (see Section 6), we wish to clarify the origin of the discrepancies here.

The point to note is that, depending on the structure of the $(V - A) \otimes (V \pm A)$ four fermion operators in the effective weak Hamiltonian (without Fierz transformation!),



Figure 3: The two different penguin contractions.

there exist two distinct penguin contractions with different contractions of spinor indices, as indicated in Figure 3. Although the two diagrams are related by Fierz transformations in four dimensions, in dimensional regularization they give different results in the NDR scheme with anticommuting γ_5 , because this scheme does not preserve the Fierz identities in d dimensions [27]. The results for the two contractions shown in the figure involve

$$\text{left: } \frac{2}{3} \ln \frac{m_b^2}{\mu^2} - G(s), \quad \text{right: } \frac{2}{3} \left(\ln \frac{m_b^2}{\mu^2} + 1 \right) - G(s), \quad (43)$$

where the function $G(s)$ is given in (50) below. The first contraction appears in matrix elements of the operators $Q_{4,6}$, while the second one enters in matrix elements of $Q_{1,3}$. This assumes the standard Fierz-form of the effective Hamiltonian, which is employed in the calculation of the Wilson coefficients in the NDR scheme. The operator Q_5 is special, because its contribution is a pure ultraviolet effect which, by definition, is absorbed into the definition of the “effective” Wilson coefficient $C_{8g}^{\text{eff}} = C_{8g} + C_5$ of the chromomagnetic dipole operator [30]. The discrepancies between our results and some of the papers discussed in Section 6 seem to arise from the fact that Q_4 and Q_6 are treated like $Q_{1,3}$.

Including now the twist-3 part of the projector (36), we still find that the penguin contractions can be straightforwardly evaluated in terms of four-quark operators, before the actual projection is made. The on-shell conditions for the external quarks connected to the gluon need to be used in this step. The projection is then very simple and only the γ_5 projector multiplied by $\Phi_p(x)$ contributes. The resulting kernel is identical to that obtained with the twist-2 projection.

The calculation of the matrix element of the chromomagnetic dipole operator (sixth diagram in Figure 2) is more interesting in this respect. In this case it is no longer possible to reduce the amplitude to the usual structures involving four-quark operators. This is related to the fact that at the twist-3 level the k_\perp momenta cannot immediately be put to zero. The complete twist-3 projection (36) has to be performed to evaluate the diagram, which leads to the expression

$$\frac{1}{(1-x)m_b^2} \bar{u}_q(p_q) \gamma^\mu M^{M_2} (\not{P} \gamma_\mu - \gamma_\mu \not{P}) (1 + \gamma_5) u_b(p_b), \quad (44)$$

where $P = p_q + k_2 = p_b - k_1$ denotes the momentum of the gluon, and the prefactor comes from the gluon propagator. M^{M_2} projects on the emission particle M_2 with momentum q , and p_b, p_q denote the momenta of the b quark and the quark in M_1 , respectively. We

find that all four terms of the projector contribute when evaluated on this expression, giving the result

$$\begin{aligned}
if_P \bar{u}_q(p_q) & \left[(1 + \gamma_5) \frac{\Phi(x)}{\bar{x}} + \frac{\mu_P}{m_b} (1 - \gamma_5) \left(\frac{3}{2} \Phi_p(x) + \frac{1}{2} \frac{\Phi'_\sigma(x)}{6} + \frac{1}{\bar{x}} \frac{\Phi_\sigma(x)}{6} \right) \right] u_b(p_b) \\
& = if_P \bar{u}_q(p_q) \left[(1 + \gamma_5) \frac{\Phi(x)}{\bar{x}} + \frac{2\mu_P}{m_b} (1 - \gamma_5) \Phi_p(x) \right] u_b(p_b). \tag{45}
\end{aligned}$$

The second line is obtained after using the equations of motion (38) for the twist-3 distribution amplitudes, so that the asymptotic form $\Phi_p(x) = 1$ is understood. We observe that the factor $1/\bar{x}$ from the gluon propagator is cancelled in the twist-3 term, and so the convolution integral has no endpoint divergence.

One can see from (45) that the matrix element of the chromomagnetic operator is obtained incorrectly at the twist-3 level if the incomplete projector containing only $\Phi_p(x)$ is used. Note that, in general, this leads to gauge-dependent results, since the equations of motion are not respected.

Hard spectator interaction

The calculation of the two diagrams in the third row of Figure 2 leads to the same trace as in (42). It therefore follows that, for $\Gamma = S + P$, the projection on M_2 can result at most in a constant multiplying the distribution amplitude $\Phi_p(x)$. However, the constant obtained for the vertex diagrams resulted entirely from a term of order $\epsilon = (2 - d/2)$ in the trace multiplying the ultraviolet-divergent loop diagram. Since the hard spectator contributions result from tree diagrams, the trace can be evaluated in four dimensions, and this constant is absent. We thus conclude that there is no hard spectator correction to the parameters $a_{6,8}$ at order α_s .

If $\Gamma = V \pm A$, only the twist-2 distribution amplitude contributes for the emission particle M_2 , but all four terms in the projector for M_1 contribute to the result. We also find that both terms in the B -meson projection (as given in [15]) contribute, but one of the two B -meson light-cone distribution amplitudes drops out after implementing the equations of motion (38). Contrary to the other corrections, the kernels T_i^{II} resulting from hard spectator interactions have logarithmic endpoint singularities at twist-3 level. They arise from integrals of the form $\int_0^1 dy/\bar{y}$, where \bar{y} is the momentum of the antiquark in the meson that picks up the spectator antiquark from the B meson. These endpoint singularities prevent a reliable perturbative calculation of the chirally-enhanced power corrections to the hard spectator interactions. (The endpoint singularities are missed if the incomplete light-meson projector with only the γ_5 projection at twist-3 is employed.)

3.4 Results for the parameters a_i

After these preliminaries, we now present the results for the coefficients a_i obtained at next-to-leading order in α_s , and including the complete set of chirally-enhanced power

corrections to the heavy-quark limit. We focus on the case of $B \rightarrow \pi K$ decays, but similar results (with obvious substitutions) hold for all other B decays into two flavour-nonsinglet pseudoscalar mesons. For later convenience, every coefficient $a_i(\pi K)$ is split into two terms: $a_i(\pi K) = a_{i,\text{I}}(\pi K) + a_{i,\text{II}}(\pi K)$. The first term contains the naive factorization contribution and the sum of vertex and penguin corrections (the form-factor terms in the factorization formula (25)), while the second one arises from the hard spectator interactions (the hard-scattering term in the factorization formula). Weak annihilation effects are not included here; they will be discussed separately in Section 3.5. The calculation of the kernels described above results in

$$\begin{aligned}
a_{1,\text{I}} &= C_1 + \frac{C_2}{N_c} \left[1 + \frac{C_F \alpha_s}{4\pi} V_K \right], & a_{1,\text{II}} &= \frac{C_2}{N_c} \frac{C_F \pi \alpha_s}{N_c} H_{K\pi}, \\
a_{2,\text{I}} &= C_2 + \frac{C_1}{N_c} \left[1 + \frac{C_F \alpha_s}{4\pi} V_\pi \right], & a_{2,\text{II}} &= \frac{C_1}{N_c} \frac{C_F \pi \alpha_s}{N_c} H_{\pi K}, \\
a_{3,\text{I}} &= C_3 + \frac{C_4}{N_c} \left[1 + \frac{C_F \alpha_s}{4\pi} V_\pi \right], & a_{3,\text{II}} &= \frac{C_4}{N_c} \frac{C_F \pi \alpha_s}{N_c} H_{\pi K}, \\
a_{4,\text{I}}^p &= C_4 + \frac{C_3}{N_c} \left[1 + \frac{C_F \alpha_s}{4\pi} V_K \right] + \frac{C_F \alpha_s}{4\pi} \frac{P_{K,2}^p}{N_c}, & a_{4,\text{II}} &= \frac{C_3}{N_c} \frac{C_F \pi \alpha_s}{N_c} H_{K\pi}, \\
a_{5,\text{I}} &= C_5 + \frac{C_6}{N_c} \left[1 + \frac{C_F \alpha_s}{4\pi} (-V'_\pi) \right], & a_{5,\text{II}} &= \frac{C_6}{N_c} \frac{C_F \pi \alpha_s}{N_c} (-H'_{\pi K}), \\
a_{6,\text{I}}^p &= C_6 + \frac{C_5}{N_c} \left(1 - 6 \cdot \frac{C_F \alpha_s}{4\pi} \right) + \frac{C_F \alpha_s}{4\pi} \frac{P_{K,3}^p}{N_c}, & a_{6,\text{II}} &= 0, \\
a_{7,\text{I}} &= C_7 + \frac{C_8}{N_c} \left[1 + \frac{C_F \alpha_s}{4\pi} (-V'_\pi) \right], & a_{7,\text{II}} &= \frac{C_8}{N_c} \frac{C_F \pi \alpha_s}{N_c} (-H'_{\pi K}), \\
a_{8,\text{I}}^p &= C_8 + \frac{C_7}{N_c} \left(1 - 6 \cdot \frac{C_F \alpha_s}{4\pi} \right) + \frac{\alpha}{9\pi} \frac{P_{K,3}^{p,\text{EW}}}{N_c}, & a_{8,\text{II}} &= 0, \\
a_{9,\text{I}} &= C_9 + \frac{C_{10}}{N_c} \left[1 + \frac{C_F \alpha_s}{4\pi} V_\pi \right], & a_{9,\text{II}} &= \frac{C_{10}}{N_c} \frac{C_F \pi \alpha_s}{N_c} H_{\pi K}, \\
a_{10,\text{I}}^p &= C_{10} + \frac{C_9}{N_c} \left[1 + \frac{C_F \alpha_s}{4\pi} V_K \right] + \frac{\alpha}{9\pi} \frac{P_{K,2}^{p,\text{EW}}}{N_c}, & a_{10,\text{II}} &= \frac{C_9}{N_c} \frac{C_F \pi \alpha_s}{N_c} H_{K\pi}, \quad (46)
\end{aligned}$$

where $C_i \equiv C_i(\mu)$, $\alpha_s \equiv \alpha_s(\mu)$, $C_F = (N_c^2 - 1)/(2N_c)$, and $N_c = 3$. The quantities $V_M^{(l)}$, $H_{M_2 M_1}^{(l)}$, $P_{K,2}^p$, $P_{K,3}^p$, $P_{K,2}^{p,\text{EW}}$, and $P_{K,3}^{p,\text{EW}}$ are hadronic parameters that contain all nonperturbative dynamics. These quantities consist of convolutions of hard-scattering kernels with meson distribution amplitudes. Specifically, the terms $V_M^{(l)}$ result from the vertex corrections (first four diagrams in Figure 2), $P_{K,2}^p$ and $P_{K,3}^p$ ($P_{K,2}^{p,\text{EW}}$ and $P_{K,3}^{p,\text{EW}}$) arise from QCD (electroweak) penguin contractions and the contributions from the dipole operators (fifth and sixth diagrams in Figure 2), and $H_{M_2 M_1}^{(l)}$ are due hard gluon exchange involving the spectator quark in the B meson (last two diagrams in Figure 2). For the penguin terms, the subscript 2 or 3 indicates the twist of the corresponding projection.

In the numerical evaluation of these expressions we consistently drop higher-order terms in the products of the Wilson coefficients with the next-to-leading order corrections. Also, in the computation of the $O(\alpha)$ corrections we confine ourselves to the penguin contractions of the current–current operators Q_1 and Q_2 and to the contribution of the electromagnetic dipole operator, which have the largest Wilson coefficients. These contributions, which are contained in the quantities $P_{K,2}^{p,\text{EW}}$ and $P_{K,3}^{p,\text{EW}}$, suffice to cancel the renormalization-scheme dependence of the electroweak penguin coefficients $C_{7,\dots,10}$ at next-to-leading order. Additional $O(\alpha)$ corrections proportional to the Wilson coefficients $C_{3,\dots,6}$ of the QCD penguin operators exist, but because these coefficients are very small their effects can be safely neglected.

Vertex and penguin contributions

We now collect the relevant formulae needed for the calculation of the coefficients $a_{i,1}$. The vertex corrections are given by ($M = \pi, K$)

$$\begin{aligned}
V_M &= 12 \ln \frac{m_b}{\mu} - 18 + \int_0^1 dx g(x) \Phi_M(x), \\
V'_M &= 12 \ln \frac{m_b}{\mu} - 6 + \int_0^1 dx g(1-x) \Phi_M(x), \\
g(x) &= 3 \left(\frac{1-2x}{1-x} \ln x - i\pi \right) \\
&\quad + \left[2 \text{Li}_2(x) - \ln^2 x + \frac{2 \ln x}{1-x} - (3 + 2i\pi) \ln x - (x \leftrightarrow 1-x) \right], \quad (47)
\end{aligned}$$

where $\text{Li}_2(x)$ is the dilogarithm. The constants 18 and 6 are specific to the NDR scheme. The function $g(x)$ can be obtained from the corresponding function relevant to, e.g., $\bar{B}^0 \rightarrow D^+ K^-$ decays [15] by taking the limit $m_c \rightarrow 0$. (Recently, a partial two-loop result for the vertex corrections has been obtained in [36], where the terms of order $\beta_0 \alpha_s^2$ were calculated analytically. To be consistent with the next-to-leading order analysis of this paper, we will not make use of this result.)

If the leading-twist light-cone distribution amplitudes are expanded in Gegenbauer polynomials as shown in (37), the relevant convolution integral can be evaluated analytically, giving

$$\int_0^1 dx g(x) \Phi_M(x) = -\frac{1}{2} - 3i\pi + \left(\frac{11}{2} - 3i\pi \right) \alpha_1^M - \frac{21}{20} \alpha_2^M + \dots \quad (48)$$

The integral with $g(x) \rightarrow g(1-x)$ is obtained by changing the sign of the odd Gegenbauer coefficients. Since the pion distribution amplitude $\Phi_\pi(x)$ is symmetric under the exchange $x \leftrightarrow (1-x)$, it follows that $V'_\pi = V_\pi + 12$.

Next, the penguin contributions are

$$P_{K,2}^p = C_1 \left[\frac{4}{3} \ln \frac{m_b}{\mu} + \frac{2}{3} - G_K(s_p) \right] + C_3 \left[\frac{8}{3} \ln \frac{m_b}{\mu} + \frac{4}{3} - G_K(0) - G_K(1) \right]$$

$$\begin{aligned}
& + (C_4 + C_6) \left[\frac{4n_f}{3} \ln \frac{m_b}{\mu} - (n_f - 2)G_K(0) - G_K(s_c) - G_K(1) \right] \\
& - 2C_{8g}^{\text{eff}} \int_0^1 \frac{dx}{1-x} \Phi_K(x), \\
P_{K,2}^{p,\text{EW}} & = (C_1 + N_c C_2) \left[\frac{4}{3} \ln \frac{m_b}{\mu} + \frac{2}{3} - G_K(s_p) \right] - 3C_{7\gamma}^{\text{eff}} \int_0^1 \frac{dx}{1-x} \Phi_K(x), \quad (49)
\end{aligned}$$

where $n_f = 5$ is the number of light quark flavours, and $s_u = 0$, $s_c = (m_c/m_b)^2$ are mass ratios involved in the evaluation of the penguin diagrams. Small electroweak corrections from C_7, \dots, C_{10} are consistently neglected in $P_{K,2}^p$ within our approximations. In principle, in $P_{K,2}^{p,\text{EW}}$ also contributions from C_3, \dots, C_6 appear. Their impact is extremely small numerically and we drop them for simplicity. Similar comments apply to (54) below. The function $G_K(s)$ is given by

$$G_K(s) = \int_0^1 dx G(s - i\epsilon, 1 - x) \Phi_K(x), \quad (50)$$

$$\begin{aligned}
G(s, x) & = -4 \int_0^1 du u(1-u) \ln[s - u(1-u)x] \\
& = \frac{2(12s + 5x - 3x \ln s)}{9x} - \frac{4\sqrt{4s-x}(2s+x)}{3x^{3/2}} \arctan \sqrt{\frac{x}{4s-x}}. \quad (51)
\end{aligned}$$

Its expansion in terms of Gegenbauer moments reads

$$\begin{aligned}
G_K(s_c) & = \frac{5}{3} - \frac{2}{3} \ln s_c + \frac{\alpha_1^K}{2} + \frac{\alpha_2^K}{5} + \frac{4}{3} (8 + 9\alpha_1^K + 9\alpha_2^K) s_c \\
& + 2(8 + 63\alpha_1^K + 214\alpha_2^K) s_c^2 - 24(9\alpha_1^K + 80\alpha_2^K) s_c^3 + 2880\alpha_2^K s_c^4 \\
& - \frac{2}{3} \sqrt{1-4s_c} \left[1 + 2s_c + 6(4 + 27\alpha_1^K + 78\alpha_2^K) s_c^2 \right. \\
& \left. - 36(9\alpha_1^K + 70\alpha_2^K) s_c^3 + 4320\alpha_2^K s_c^4 \right] (2 \operatorname{arctanh} \sqrt{1-4s_c} - i\pi) \\
& + 12s_c^2 \left[1 + 3\alpha_1^K + 6\alpha_2^K - \frac{4}{3} (1 + 9\alpha_1^K + 36\alpha_2^K) s_c \right. \\
& \left. + 18(\alpha_1^K + 10\alpha_2^K) s_c^2 - 240\alpha_2^K s_c^3 \right] (2 \operatorname{arctanh} \sqrt{1-4s_c} - i\pi)^2 + \dots, \\
G_K(0) & = \frac{5}{3} + \frac{2i\pi}{3} + \frac{\alpha_1^K}{2} + \frac{\alpha_2^K}{5} + \dots, \\
G_K(1) & = \frac{85}{3} - 6\sqrt{3}\pi + \frac{4\pi^2}{9} - \left(\frac{155}{2} - 36\sqrt{3}\pi + 12\pi^2 \right) \alpha_1^K \\
& + \left(\frac{7001}{5} - 504\sqrt{3}\pi + 136\pi^2 \right) \alpha_2^K + \dots \quad (52)
\end{aligned}$$

The contribution of the dipole operators in (49) involve the integral

$$\int_0^1 \frac{dx}{1-x} \Phi_M(x) = 3(1 + \alpha_1^M + \alpha_2^M + \dots). \quad (53)$$

The twist-3 terms from the penguin diagrams are related to the twist-2 terms by the simple replacement $\Phi_K(x) \rightarrow \Phi_p^K(x) = 1$. For the terms proportional to $C_{7\gamma}^{\text{eff}}$ and C_{8g}^{eff} , however, the twist-3 projection yields an additional factor of $(1-x)$, which cancels the denominator in (53). We therefore find

$$\begin{aligned} P_{K,3}^p &= C_1 \left[\frac{4}{3} \ln \frac{m_b}{\mu} + \frac{2}{3} - \hat{G}_K(s_p) \right] + C_3 \left[\frac{8}{3} \ln \frac{m_b}{\mu} + \frac{4}{3} - \hat{G}_K(0) - \hat{G}_K(1) \right] \\ &\quad + (C_4 + C_6) \left[\frac{4n_f}{3} \ln \frac{m_b}{\mu} - (n_f - 2)\hat{G}_K(0) - \hat{G}_K(s_c) - \hat{G}_K(1) \right] - 2C_{8g}^{\text{eff}}, \\ P_{K,3}^{p,\text{EW}} &= (C_1 + N_c C_2) \left[\frac{4}{3} \ln \frac{m_b}{\mu} + \frac{2}{3} - \hat{G}_K(s_p) \right] - 3C_{7\gamma}^{\text{eff}}, \end{aligned} \quad (54)$$

with

$$\hat{G}_K(s) = \int_0^1 dx G(s - i\epsilon, 1-x) \Phi_p^K(x). \quad (55)$$

Inserting $\Phi_p^K(x) = 1$, this integral is evaluated to

$$\begin{aligned} \hat{G}_K(s_c) &= \frac{16}{9} (1 - 3s_c) - \frac{2}{3} \left[\ln s_c + (1 - 4s_c)^{3/2} \left(2 \operatorname{arctanh} \sqrt{1 - 4s_c} - i\pi \right) \right], \\ \hat{G}_K(0) &= \frac{16}{9} + \frac{2\pi}{3} i, \quad \hat{G}_K(1) = \frac{2\pi}{\sqrt{3}} - \frac{32}{9}. \end{aligned} \quad (56)$$

The typical parton off-shellness in the loop diagrams contributing to the vertex and penguin contributions to the hard-scattering kernels is of order m_b , and hence it is appropriate to choose a value $\mu \sim m_b$ for the renormalization scale in the Wilson coefficients C_i and in the kernels T_i^{I} when evaluating the quantities $a_{i,\text{I}}$. The μ -dependent terms in expressions (47), (49) and (54) cancel the renormalization-scale dependence of the Wilson coefficients $C_i(\mu)$ at next-to-leading order. Similarly, the constants accompanying the various logarithms in these expressions are renormalization-scheme dependent and combine with scheme-dependent constants in the expressions for the Wilson coefficients to give renormalization-group invariant results.

The coefficients $a_{i,\text{I}}$ contain strong-interaction phases via the imaginary parts of the functions $g(x)$ and $G(s, x)$. At next-to-leading order and to leading power in Λ_{QCD}/m_b , these phases yield the asymptotic contributions to the final-state rescattering phases of the $B \rightarrow \pi K$ decay amplitudes. The presence of a strong-interaction phase in the penguin function $G(s, x)$ is well known and commonly referred to as the Bander–Silverman–Soni mechanism [37]. It was included in many phenomenological investigations of non-leptonic B decays; however, there was always an argument as to how to choose the gluon

momentum, k_g^2 , in the fourth diagram in Figure 2. In our approach there is no ambiguity to this choice, because the distribution of $k_g^2 = (1-x)m_b^2$ is determined by the kaon distribution amplitudes. The imaginary part of the function $g(x)$ is another source of rescattering phases, which arises from hard gluon exchanges between the two outgoing mesons [14, 15]. The appearance of this phase is a new element of the QCD factorization approach.

Hard-scattering contributions

The hard spectator interactions shown in the last two diagrams in Figure 2 give leading-twist and chirally-enhanced twist-3 contributions to the kernels T_i^{II} . We include these hard-scattering contributions as parts of the coefficients a_i , although they are not related to factorized matrix elements in the usual sense. Only the twist-2 terms are dominated by hard gluon exchange and thus calculable. Nevertheless, for consistency with our treatment of the penguin coefficients we should also include the chirally-enhanced terms of subleading twist, which however have logarithmic endpoint singularities.

At tree level, the integrals over meson distribution amplitudes for the hard spectator contributions factorize. We find (the momentum fractions x and y are defined in Section 3.2)

$$\begin{aligned}
H_{K\pi} &= \frac{f_B f_\pi}{m_B^2 F_0^{B \rightarrow \pi}(0)} \int_0^1 \frac{d\xi}{\xi} \Phi_B(\xi) \int_0^1 \frac{dx}{\bar{x}} \Phi_K(x) \int_0^1 \frac{dy}{\bar{y}} \left[\Phi_\pi(y) + \frac{2\mu_\pi \bar{x}}{m_b x} \Phi_p^\pi(y) \right] \\
&= \frac{f_B f_\pi}{m_B \lambda_B F_0^{B \rightarrow \pi}(0)} \left[\langle \bar{x}^{-1} \rangle_K \langle \bar{y}^{-1} \rangle_\pi + r_\chi^\pi \langle x^{-1} \rangle_K X_H^\pi \right], \\
H_{\pi K} &= \frac{f_B f_K}{m_B^2 F_0^{B \rightarrow K}(0)} \int_0^1 \frac{d\xi}{\xi} \Phi_B(\xi) \int_0^1 \frac{dx}{\bar{x}} \Phi_\pi(x) \int_0^1 \frac{dy}{\bar{y}} \left[\Phi_K(y) + \frac{2\mu_K \bar{x}}{m_b x} \Phi_p^K(y) \right] \\
&= \frac{f_B f_K}{m_B \lambda_B F_0^{B \rightarrow K}(0)} \left[\langle \bar{x}^{-1} \rangle_\pi \langle \bar{y}^{-1} \rangle_K + r_\chi^K \langle x^{-1} \rangle_\pi X_H^K \right], \\
H'_{\pi K} &= \frac{f_B f_K}{m_B^2 F_0^{B \rightarrow K}(0)} \int_0^1 \frac{d\xi}{\xi} \Phi_B(\xi) \int_0^1 \frac{dx}{x} \Phi_\pi(x) \int_0^1 \frac{dy}{\bar{y}} \left[\Phi_K(y) + \frac{2\mu_K x}{m_b \bar{x}} \Phi_p^K(y) \right] \\
&= \frac{f_B f_K}{m_B \lambda_B F_0^{B \rightarrow K}(0)} \left[\langle x^{-1} \rangle_\pi \langle \bar{y}^{-1} \rangle_K + r_\chi^K \langle \bar{x}^{-1} \rangle_\pi X_H^K \right], \tag{57}
\end{aligned}$$

where we have defined the moments

$$\int_0^1 \frac{d\xi}{\xi} \Phi_B(\xi) \equiv \frac{m_B}{\lambda_B}, \quad \int_0^1 dx x^n \Phi_M(x) \equiv \langle x^n \rangle_M. \tag{58}$$

The quantity λ_B parameterizes our ignorance about the B -meson distribution amplitude [14]. Not much is known about this parameter except for the upper bound $3\lambda_B \leq 4\bar{\Lambda}$ [38], where $\bar{\Lambda} = m_B - m_b$ is a scheme-dependent parameter. In practice, this just means that λ_B is expected to be less than 600 MeV or so. The ratios $2\mu_K/m_b$ and $2\mu_\pi/m_b$

multiplying the twist-3 terms coincide with the parameters r_χ^K and r_χ^π introduced in (5) and (6), respectively. The twist-3 contribution involves the logarithmically divergent integral ($M = \pi$ or K)

$$X_H^M \equiv \int_0^1 \frac{dy}{1-y} \Phi_p^M(y) = \int_0^1 \frac{dy}{1-y}. \quad (59)$$

As previously we have to use the asymptotic form for $\Phi_p^M(y)$, so no distinction between pion and kaon is necessary. (Consequently, the superscript “ M ” will often be dropped from now on.) The divergence results from the region where the spectator quark in the B meson enters the light final-state meson at the “lower vertex” in Figure 1 as a soft quark. The twist-3 hard-scattering kernels do not provide sufficient endpoint suppression to render this contribution subleading. In practice, the singularity will be smoothed out by soft physics related to the intrinsic transverse momentum and off-shellness of the partons, which unfortunately does not admit a perturbative treatment (see also the discussion in Section 6). In particular, the resulting contribution may be complex due to soft rescattering in higher orders. For the purpose of power counting, we note that the effect of transverse momentum and off-shellness would be to modify $(1-y) \rightarrow (1-y) + \epsilon$ with $\epsilon = O(\Lambda_{\text{QCD}}/m_b)$ in the denominator in (59). We thus expect that $X_H^M \sim \ln(m_b/\Lambda_{\text{QCD}})$, however, with a potentially complex coefficient.

Considering the off-shellness of the gluon in the last two diagrams in Figure 2, it is natural to associate a scale $\mu_h \sim (\Lambda_{\text{QCD}} m_b)^{1/2}$, rather than $\mu \sim m_b$, with the hard-scattering contributions of leading power. Hence, we set $\alpha_s = \alpha_s(\mu_h)$ (and also evaluate the Wilson coefficients at the scale μ_h) for the twist-2 contributions to the quantities $a_{i,\text{II}}$ in (46). Specifically, we use $\mu_h = \sqrt{\Lambda_h \mu}$ with $\Lambda_h = 0.5 \text{ GeV}$ for the scale in the hard-scattering diagrams. However, because of the endpoint divergence the contributions proportional to X_H^M must be considered as nonperturbative effects dominated by small-momentum interactions. For this reason, we should more properly write

$$H_{K\pi} = \frac{f_B f_\pi}{m_B \lambda_B F_0^{B \rightarrow \pi}(0)} \left[\langle \bar{x}^{-1} \rangle_K \langle \bar{y}^{-1} \rangle_\pi + \frac{\alpha_s(\mu_s) r_\chi^\pi(\mu_s)}{\alpha_s(\mu_h)} \langle x^{-1} \rangle_K X_H^\pi \right], \quad (60)$$

and similarly for the other two quantities in (57). Here μ_s may be a soft scale. In other words, in principle there is no reason to expect that the twist-3 contributions should be governed by a perturbative coupling constant. However, it turns out that the product $\alpha_s(\mu_s) r_\chi^\pi(\mu_s)$ is almost renormalization-group invariant (it scales only as $[\alpha_s(\mu)]^{1/25}$ with $N_c = 3$ and four flavours), and therefore we may evaluate it at the scale μ_h , so that the ratio of running couplings in (60) equals 1.

The expressions for the hard-scattering contributions in (57) contain many poorly known parameters. Besides the divergent quantity X_H and the wave-function parameter λ_B , they depend on the B -meson decay constant and heavy-to-light form factors. Fortunately, it turns out that ratios of the different hard-scattering contribution have very small uncertainties. Using the symmetry of the pion distribution amplitude, we find that

$$H'_{\pi K} = H_{\pi K}, \quad H_{K\pi} \simeq R_{\pi K} H_{\pi K}, \quad (61)$$

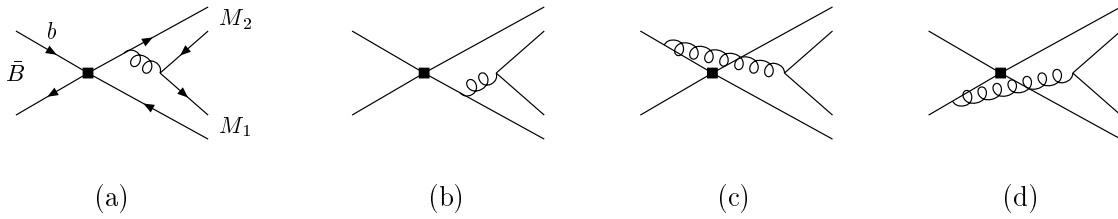


Figure 4: Annihilation diagrams.

where $R_{\pi K} = A_{K\pi}/A_{\pi K}$ is the ratio of factorized matrix elements defined in (15). As argued in Section 3.2, in the approximation where only chirally-enhanced power corrections are included one is forced to employ the asymptotic forms of the twist-3 distribution amplitudes $\Phi_p(x)$ and $\Phi_\sigma(x)$. It is then not necessary to keep other nonasymptotic effects in the twist-3 terms. That is, we are free to replace the moments of twist-2 amplitudes multiplying X_H by their asymptotic values. In this approximation, the twist-3 contributions in (57) reduce to a universal, multiplicative correction of the twist-2 term, and we obtain the approximate form of the second relation in (61). In other words, up to small SU(3) violations the main uncertainties in the description of the hard-scattering terms combine into a single poorly-known quantity $H_{\pi K}$.

Finally, note that in (57) we have not assumed any symmetry properties of the twist-2 light-meson distribution amplitudes. Therefore, with obvious substitutions our results can be applied directly to other decays, such as $B \rightarrow \pi\pi$ and $B_s \rightarrow K^+K^-$.

3.5 Weak annihilation contributions b_i

Weak annihilation contributions to charmless hadronic B decays are power suppressed in the heavy-quark limit and hence do not appear in the factorization formula (25). Nevertheless, as emphasized in [17], these contributions may be numerically important for realistic B -meson decays. Besides their power suppression, weak annihilation effects differ from the hard spectator interactions discussed earlier in that they exhibit endpoint singularities even at twist-2 order in the light-cone expansion for the final-state mesons, and therefore cannot be computed self-consistently in the context of a hard-scattering approach. In the following discussion, we will ignore the soft endpoint divergences and derive results for the annihilation contributions in terms of convolutions of “hard-scattering” kernels with light-cone distribution amplitudes, including again the chirally-enhanced twist-3 projections. Despite the fact that such a treatment is not entirely self-consistent, it is nevertheless useful to estimate the importance of annihilation for particular final states.

At leading order in α_s , the annihilation kernels follow from the diagrams shown in Figure 4. They result in a further contribution to the hard-scattering term in the factorization formula, in addition to the hard spectator scattering discussed in Section 3.2. It will be convenient for future applications to keep the discussion of annihilation contributions general. We thus consider a generic b -quark decay and use the convention that

M_2 contains a quark from the weak decay vertex with longitudinal momentum fraction x , and M_1 contains an antiquark from the weak vertex with momentum fraction \bar{y} . The four-quark operators in the effective weak Hamiltonian are Fierz-transformed into the form $(\bar{q}_1 b)_{\Gamma_1} (\bar{q}_2 q_3)_{\Gamma_2}$, such that the quarks in the first bracket refer to the constituents of the \bar{B} meson. If the colour indices of this bracket are of the form $\bar{q}_{1i} b_i$, diagrams (c) and (d) do not contribute, while diagrams (a) and (b) give rise to a colour factor C_F/N_c . If the colour indices are of the form $\bar{q}_{1i} b_j$, then the colour factor of all four diagrams is C_F/N_c^2 . The projections onto the light-cone distribution amplitudes are done in the same manner as for the hard spectator scattering described in Section 3.2. At leading power (and assuming that $x, y \gg \xi$) the integration over the B -meson distribution amplitude is trivial and yields the B -meson decay constant, since the kernels are ξ independent. The remainders of the diagrams can be expressed in terms of the following building blocks:

$$\begin{aligned}
A_1^i &= \pi\alpha_s \int_0^1 dx dy \left\{ \Phi_{M_2}(x) \Phi_{M_1}(y) \left[\frac{1}{y(1-x\bar{y})} + \frac{1}{\bar{x}^2 y} \right] + \frac{4\mu_{M_1}\mu_{M_2}}{m_b^2} \frac{2}{\bar{x}y} \right\}, \\
A_1^f &= 0, \\
A_2^i &= \pi\alpha_s \int_0^1 dx dy \left\{ \Phi_{M_2}(x) \Phi_{M_1}(y) \left[\frac{1}{\bar{x}(1-x\bar{y})} + \frac{1}{\bar{x}y^2} \right] + \frac{4\mu_{M_1}\mu_{M_2}}{m_b^2} \frac{2}{\bar{x}y} \right\}, \\
A_2^f &= 0, \\
A_3^i &= \pi\alpha_s \int_0^1 dx dy \left\{ \frac{2\mu_{M_1}}{m_b} \Phi_{M_2}(x) \frac{2\bar{y}}{\bar{x}y(1-x\bar{y})} - \frac{2\mu_{M_2}}{m_b} \Phi_{M_1}(y) \frac{2x}{\bar{x}y(1-x\bar{y})} \right\}, \\
A_3^f &= \pi\alpha_s \int_0^1 dx dy \left\{ \frac{2\mu_{M_1}}{m_b} \Phi_{M_2}(x) \frac{2(1+\bar{x})}{\bar{x}^2 y} + \frac{2\mu_{M_2}}{m_b} \Phi_{M_1}(y) \frac{2(1+y)}{\bar{x}y^2} \right\}. \tag{62}
\end{aligned}$$

Here the superscripts i and f refer to gluon emission from the initial- and final-state quarks, respectively. The subscript k on $A_k^{i,f}$ refers to one of the three possible Dirac structures $\Gamma_1 \otimes \Gamma_2$, namely $k = 1$ for $(V - A) \otimes (V - A)$, $k = 2$ for $(V - A) \otimes (V + A)$, and $k = 3$ for $(-2)(S - P) \otimes (S + P)$. As always, $\Phi_M(x)$ denotes the leading-twist light-cone distribution amplitude of a pseudoscalar meson M , and the asymptotic forms of the twist-3 amplitudes have been used. Note that in the limit of symmetric (under $x \leftrightarrow \bar{x}$) distribution amplitudes, and assuming SU(3) flavour symmetry, we have $A_1^i = A_2^i$ and $A_3^i = 0$. In this approximation the annihilation contributions can be parameterized by only two quantities (A_1^i and A_3^f). For an estimate of these annihilation contributions we use the asymptotic form of the leading-twist distribution amplitudes to obtain

$$\begin{aligned}
A_1^i &\approx \pi\alpha_s \left[18 \left(X_A - 4 + \frac{\pi^2}{3} \right) + 2r_\chi^2 X_A^2 \right], \\
A_3^f &\approx 12\pi\alpha_s r_\chi (2X_A^2 - X_A), \tag{63}
\end{aligned}$$

where $X_A = \int_0^1 dy/y$ parameterizes the divergent endpoint integrals. Similar to the case of the twist-3 hard-scattering contributions parameterized by X_H , we will treat the

quantity X_A as a phenomenological parameter. Clearly, taking the same value of X_A for all annihilation terms is a crude model. We shall see below, however, that the parameter A_3^f (contributing to penguin annihilation topologies) gives the dominant contribution. Therefore, our treatment effectively amounts to defining a model for this particular parameter.

To complete the calculation we need to account for the flavour structure of the various operators. It is convenient to introduce the compact notation

$$\langle M_1 M_2 | j_1 \times j_2 | \bar{B}_q \rangle \equiv i c f_{B_q} f_{M_1} f_{M_2}, \quad (64)$$

where the constant c takes into account factors of (-1) or $1/\sqrt{2}$ appearing in the quark wave-functions of some of the mesons, and $c \neq 0$ only if the flavours of the ‘‘currents’’ j_1 and j_2 match those of the mesons M_1 and M_2 , respectively. It is apparent from Figure 4 that the products $j_1 \times j_2$ have the flavour structure

$$\sigma_{q_1}^{q_2} = \sum_{q'} (\bar{q}' q_2) \times (\bar{q}_1 q'), \quad (65)$$

where the sum over $q' = u, d, s$ arises from the $g \rightarrow q' \bar{q}'$ vertex in the annihilation diagrams. Effectively, the flavour structure $\sigma_{q_1}^{q_2}$ ‘‘creates’’ a quark q_1 (lower index) and an antiquark \bar{q}_2 (upper index), together with a flavour-singlet $q' \bar{q}'$ pair. It is then straightforward to find the set of meson final states to which a given flavour structure contributes. All σ operators contributing to charged B^- decays have the structure σ_d^u or σ_s^u . The corresponding two-particle final states with light (flavour-nonsinglet) pseudoscalar mesons are

$$\sigma_d^u : \pi^0 \pi^-, \pi^- \pi^0, K^- K^0; \quad \sigma_s^u : \pi^0 K^-, \pi^- \bar{K}^0. \quad (66)$$

Operators contributing to neutral \bar{B}_r decays (with $r = d, s$) have the structure $\sigma_d^r, \sigma_s^r, \sigma_u^r$, or one of the ‘‘penguin structures’’ $\text{tr}(\sigma) \equiv \sum_q \sigma_q^q$ and $\text{tr}(Q \sigma) \equiv \sum_q e_q \sigma_q^q$. Here Q is the charge operator for the quarks, and the sum (trace) over q is inherited from the QCD and electroweak penguin operators in the effective weak Hamiltonian. The final states to which these operators contribute are

$$\begin{aligned} \sigma_d^d : & \pi^+ \pi^-, \pi^0 \pi^0, \bar{K}^0 K^0; & \sigma_s^d : & \pi^+ K^-, \pi^0 \bar{K}^0; \\ \sigma_d^s : & K^+ \pi^-, K^0 \pi^0; & \sigma_s^s : & K^+ K^-, K^0 \bar{K}^0; \\ \sigma_u^u : & \pi^0 \pi^0, \pi^- \pi^+, K^- K^+; \\ \text{tr}(\sigma), \text{tr}(Q \sigma) : & \pi^0 \pi^0, \pi^- \pi^+, \pi^+ \pi^-, K^- K^+, K^+ K^-, K^0 \bar{K}^0, \bar{K}^0 K^0. \end{aligned} \quad (67)$$

It follows from the above discussion that the weak annihilation contributions to the decay amplitudes can be parameterized in terms of the coefficients

$$\begin{aligned} b_1 &= \frac{C_F}{N_c^2} C_1 A_1^i, & b_3 &= \frac{C_F}{N_c^2} [C_3 A_1^i + C_5 (A_3^i + A_3^f) + N_c C_6 A_3^f], \\ b_2 &= \frac{C_F}{N_c^2} C_2 A_1^i, & b_4 &= \frac{C_F}{N_c^2} [C_4 A_1^i + C_6 A_2^i], \end{aligned}$$

$$\begin{aligned}
b_3^{\text{EW}} &= \frac{C_F}{N_c^2} [C_9 A_1^i + C_7 (A_3^i + A_3^f) + N_c C_8 A_3^f], \\
b_4^{\text{EW}} &= \frac{C_F}{N_c^2} [C_{10} A_1^i + C_8 A_2^i].
\end{aligned} \tag{68}$$

They correspond to current–current annihilation (b_1, b_2), penguin annihilation (b_3, b_4), and electroweak penguin annihilation ($b_3^{\text{EW}}, b_4^{\text{EW}}$), where within each pair the two coefficients correspond to different flavour structures. The quantities b_i depend on the final-state mesons through the light-cone distribution amplitudes entering the expressions for $A_k^{i,f}$ and thus should be written as $b_i(M_1 M_2)$. We suppress this notation when confusion cannot arise. As for the hard spectator terms, we will evaluate the various quantities in (68) at the scale $\mu_h = \sqrt{\Lambda_h} \mu$.

The effective weak Hamiltonian for \bar{B} -meson decays contains a strangeness-conserving part ($\mathcal{H}_{\Delta S=0}$) and a strangeness-changing part ($\mathcal{H}_{\Delta S=1}$). Using the above definitions, the annihilation contributions to the matrix elements of $\mathcal{H}_{\Delta S=1}$ can be written as

$$\langle M_1 M_2 | \mathcal{H}_{\Delta S=1} | \bar{B} \rangle = \frac{G_F}{\sqrt{2}} \sum_{p=u,c} \lambda_p \langle M_1 M_2 | \mathcal{T}_p^{\text{ann}} | \bar{B} \rangle, \tag{69}$$

where $\lambda_p = V_{pb} V_{ps}^*$, and

$$\begin{aligned}
\mathcal{T}_p^{\text{ann}} &= \delta_{up} (\delta_{rn} b_1 \sigma_u^u + \delta_{ru} b_2 \sigma_s^u) + b_3 \sigma_s^r + \delta_{rn} b_4 \text{tr}(\sigma) \\
&\quad + \frac{3}{2} b_3^{\text{EW}} e_r \sigma_s^r + \frac{3}{2} \delta_{rn} b_4^{\text{EW}} \text{tr}(Q \sigma).
\end{aligned} \tag{70}$$

The index r refers to the flavour of the spectator quark inside the B meson in (69), and $\delta_{rn} = \delta_{rd} + \delta_{rs}$ equals 1 for neutral \bar{B} mesons and 0 for B^- . The matrix elements of $\mathcal{H}_{\Delta S=0}$ take an identical form, except that λ_p is replaced with $\lambda'_p = V_{pb} V_{pd}^*$ in this case, and σ_s^q must be replaced with σ_d^q .

It is now straightforward to derive the annihilation contribution to a particular final state in terms of the coefficients $b_i(M_1 M_2)$. The expressions for the decay modes discussed in this paper have been given earlier in (9) and (13). We will later use the approximation (63) for the quantities $A_k^{i,f}$ to estimate the annihilation coefficients b_i numerically. We should recall, however, that the annihilation kernels have been derived under the assumption of hard scattering. Specifically, we have neglected the momentum fraction ξ of the spectator quark in the B meson compared to x, \bar{x}, y, \bar{y} in deriving the kernels. This is the reason why the results for $A_k^{i,f}$ turned out to be independent of the form of the B -meson distribution amplitude. In the endpoint regions, one or two of the variables x, \bar{x}, y, \bar{y} can be of order ξ , invalidating this approximation. Therefore, our numerical results for the weak annihilation contributions presented in the next section must be considered as model-dependent estimates.

Table 2: Summary of theoretical input parameters.

| QCD Scale and Running Quark Masses | | | | |
|--|---------------|-----------------------------|------------------------------|------------------------------|
| $\Lambda_{\overline{\text{MS}}}^{(5)}$ | $m_b(m_b)$ | $m_c(m_b)$ | $m_s(2 \text{ GeV})$ | $(m_u + m_d)(2 \text{ GeV})$ |
| 225 MeV | 4.2 GeV | $(1.3 \pm 0.2) \text{ GeV}$ | $(110 \pm 25) \text{ MeV}$ | $(9.1 \pm 2.1) \text{ MeV}$ |
| Parameters Related to Hadronic Matrix Elements | | | | |
| f_π | f_K | f_B | $F_0^{B \rightarrow \pi}(0)$ | $R_{\pi K}$ |
| 131 MeV | 160 MeV | $(180 \pm 40) \text{ MeV}$ | 0.28 ± 0.05 | 0.9 ± 0.1 |
| Parameters of Distribution Amplitudes | | | | |
| α_1^K | α_2^K | α_1^π | α_2^π | λ_B |
| 0.3 ± 0.3 | 0.1 ± 0.3 | 0 | 0.1 ± 0.3 | $(350 \pm 150) \text{ MeV}$ |

4 Numerical analysis of amplitude parameters

In this section we summarize the numerical values of the parameters a_i and b_i entering the $B \rightarrow \pi K$ decay amplitudes and perform detailed estimates of various sources of theoretical uncertainties. Other decays such as $B \rightarrow \pi\pi$ will be discussed later.

The theoretical input parameters used in our analysis, together with their respective ranges of uncertainty, are summarized in Table 2. The quark masses are running masses in the $\overline{\text{MS}}$ scheme. Note that the value of the charm-quark mass is given at $\mu = m_b$. The ratio $s_c = (m_c/m_b)^2$ needed for the calculation of the penguin contributions is scale independent. The values of the light quark masses are such that $r_\chi^K = r_\chi^\pi$. We hold $(m_u + m_d)/m_s$ fixed and use m_s as an input parameter. (This implies that in our error estimation procedure $|P_{\pi\pi}/T_{\pi\pi}|$ indirectly depends on m_s .) The value of the QCD scale parameter corresponds to $\alpha_s(M_Z) = 0.118$ in the $\overline{\text{MS}}$ scheme. The values for the B -meson decay constant f_B , the semileptonic form factor $F_0^{B \rightarrow \pi}(0)$, and the hadronic parameter $R_{\pi K}$ in (15) are consistent with recent determinations of these quantities using light-cone QCD sum rules [39, 40], form-factor models (see, e.g., [41]), and lattice gauge theory (see, e.g., [42]). The last row in the table contains our values for the Gegenbauer moments of the pion and kaon light-cone distribution amplitudes, and for the B -meson wavefunction parameter λ_B . The Gegenbauer moments for the light mesons are adopted with a conservative error estimate that encompasses most of the parameter ranges obtained from phenomenological or QCD sum rule determinations of these quantities. The value of λ_B is an educated guess guided by the model determinations $\lambda_B \approx \frac{2}{3}\bar{\Lambda} \approx 300 \text{ MeV}$ [32] and $\lambda_B = (380 \pm 120) \text{ MeV}$ [38]. For comparison, using the models of [17] we obtain $\lambda_B = (410 \pm 170) \text{ MeV}$.

Table 3: Next-to-leading order results for the coefficients $a_{i,I}(\pi K)$ for three different choices of the renormalization scale. Numbers in parentheses show the maximal change in the last digit(s) under variation of the Gegenbauer moments of the light-cone distribution amplitudes; if present, numbers in square brackets show the change under variation of the charm-quark mass.

| μ | Real Part | | | Imaginary Part | | |
|-----------------------------|-------------|--------------|---------------|----------------|--------------|--------------|
| | $m_b/2$ | m_b | $2m_b$ | $m_b/2$ | m_b | $2m_b$ |
| $a_{1,I}$ | 1.073(8) | 1.054(4) | 1.037(2) | 0.048(11) | 0.026(6) | 0.015(3) |
| $a_{2,I}$ | -0.039(4) | 0.005(3) | 0.045(2) | -0.113 | -0.084 | -0.066 |
| $a_{3,I}$ | 0.008 | 0.006 | 0.004 | 0.004 | 0.002 | 0.001 |
| $-a_{4,I}^u$ | 0.031(4) | 0.029(3) | 0.027(2) | 0.023(0) | 0.017 | 0.014 |
| $-a_{4,I}^c$ | 0.036(9)[2] | 0.033(6)[1] | 0.030(4)[1] | 0.005(3)[4] | 0.004(3)[3] | 0.004(2)[2] |
| $-a_{5,I}$ | 0.011 | 0.007 | 0.004 | 0.005 | 0.003 | 0.001 |
| $-r_\chi^K a_{6,I}^u$ | 0.052 | 0.052 | 0.052 | 0.017 | 0.018 | 0.019 |
| $-r_\chi^K a_{6,I}^c$ | 0.056 | 0.056 | 0.056 | 0.005[3] | 0.007[3] | 0.008[3] |
| $a_{7,I}/\alpha$ | 0.007 | 0.011 | 0.025 | 0.004 | 0.002 | 0.001 |
| $r_\chi^K a_{8,I}^u/\alpha$ | 0.090 | 0.077 | 0.059 | -0.001 | -0.009 | -0.020 |
| $r_\chi^K a_{8,I}^c/\alpha$ | 0.090 | 0.075 | 0.055 | -0.000 | -0.005[1] | -0.010[3] |
| $-a_{9,I}/\alpha$ | 1.258(1) | 1.222(1) | 1.181 | 0.040 | 0.022 | 0.012 |
| $a_{10,I}^u/\alpha$ | 0.062(27) | 0.020(20) | -0.025(16) | 0.168(39) | 0.116(29) | 0.084(22) |
| $a_{10,I}^c/\alpha$ | 0.062(27) | 0.018(21)[1] | -0.028(17)[1] | 0.168(39) | 0.121(30)[1] | 0.093(25)[2] |

4.1 Vertex and penguin contributions

We begin the discussion with the vertex and penguin contributions, i.e., the terms $a_{i,I}(\pi K)$ in (46). In this case all convolution integrals are finite, even for the power-suppressed coefficients $r_\chi^K a_{6,I}(\pi K)$ and $r_\chi^K a_{8,I}(\pi K)$. Table 3 contains the values of the various coefficients for three different values of the renormalization scale, and with theoretical uncertainties due to the variation of the pion and kaon light-cone distribution amplitudes and the charm-quark mass, as specified in Table 2. We vary the Gegenbauer moments independently and quote the maximal variation in the table. The main characteristics of theoretical uncertainties are as follows:

Renormalization-scale dependence: The residual scale dependence at next-to-leading order depends on the size of the leading-order Wilson coefficients and the magnitude of the Wilson coefficient that multiplies the next-to-leading order correction. In general, we find a significant reduction of scale dependence compared to the a_i parameters obtained at leading order (corresponding to naive factorization). Only for the parameters a_2 and a_{10} a sizeable scale dependence remains at next-to-leading order, even though it

is reduced by about a factor of 2 relative to the leading order. In general, the imaginary parts of the coefficients $a_{i,I}$, which occur first at order α_s , have a larger scale dependence than the real parts.

Light-cone distribution amplitudes: The explicit expressions in Section 3.4 show that the second Gegenbauer moments α_2^K and α_2^π enter the results for the vertex and penguin contributions typically with small coefficients. Therefore, the main uncertainty comes from the first moment α_1^K of the kaon distribution amplitude, which affects only a_1 , a_4 and a_{10} . The real part of a_{10} is particularly uncertain. There is also some uncertainty in a_2 , because the dependence on the second moment of the pion light-cone distribution amplitude is amplified by the large Wilson coefficient C_1 . From Table 3, we conclude that the dependence on the distribution amplitudes is almost always smaller than the scale dependence. Since, for consistency, we must use the asymptotic twist-3 distribution amplitudes, the coefficients a_6 and a_8 show no dependence on the Gegenbauer moments. This is clearly an approximation, which is valid only if the chirally-enhanced power corrections dominate over the remaining power corrections. (This is a questionable approximation, because the quark–antiquark–gluon distribution amplitude impacts on $\Phi_p(x)$ with a large numerical coefficient [34].) As a consequence, we cannot control SU(3)-breaking effects at twist-3 order. In practice, we expect such SU(3) violations to have a similar (hence, small) effect as those at leading twist.

Charm and strange-quark masses: The value of the charm-quark mass affects the penguin contributions with a charm-quark loop. This leads to a significant uncertainty in the imaginary parts of a_4^c and a_6^c . The real parts of the coefficients are much less affected. Note that the chiral enhancement factor r_χ^K multiplying the coefficients a_6 and a_8 in Table 3 is inversely proportional to the strange-quark mass. The ± 25 MeV uncertainty in the value of m_s leads to a sizeable uncertainty in the values of the products $r_\chi^K a_{6,8}$ which, except for the imaginary parts of $r_\chi^K a_{6,8}^c$, is a much larger effect than the dependence on the charm-quark mass.

Unknown power corrections: A source of theoretical uncertainty that is difficult to estimate arises from power corrections which cannot be computed using the QCD factorization approach. Naive dimensional analysis suggests that such corrections are of order $\Lambda_{\text{QCD}}/m_b \sim (10\text{--}20)\%$, but they could be enhanced, e.g., by large Wilson coefficients. This situation may potentially be realized for the parameters a_2 and a_{10} . Recently, some power corrections to QCD factorization for the $\pi\pi$ final state have been investigated in the framework of QCD sum rules [43] and using the renormalon calculus [36]. (Power corrections for final states with one heavy meson were also considered in [15, 44].) In none of these cases particularly large corrections have been identified.

4.2 Hard spectator interactions

We have argued in Section 3.4 that the description of the hard-scattering contributions to the coefficients a_i suffers from large theoretical uncertainties, which however can be parameterized in terms of a single (complex) quantity $H_{\pi K}$ defined in (57). If this quantity is fixed, then the hard-scattering contributions $a_{i,II}$ can be calculated with

Table 4: Coefficients $a_{i,\text{II}}(\pi K)$ for three different choices of the renormalization scale and fixed default values of the quantity $H_{\pi K}$. All scale-dependent quantities are evaluated at the scale $\mu_h = \sqrt{\Lambda_h} \mu$ with $\Lambda_h = 0.5 \text{ GeV}$. Numbers in parentheses show the maximal change in the last digit(s) under variation of the Gegenbauer moments; numbers in square brackets show the dependence under variation of $R_{\pi K}$.

| μ | $m_b/2$ | m_b | $2m_b$ |
|------------------------------|----------------|----------------|----------------|
| μ_h | 1.02 GeV | 1.45 GeV | 2.05 GeV |
| $H_{\pi K}^{\text{default}}$ | 0.92 | 0.99 | 1.05 |
| $a_{1,\text{II}}$ | -0.087(16)[10] | -0.061(14)[7] | -0.045(12)[5] |
| $a_{2,\text{II}}$ | 0.231 | 0.192 | 0.167 |
| $a_{3,\text{II}}$ | -0.010 | -0.007 | -0.005 |
| $a_{4,\text{II}}$ | 0.004(1) | 0.003(1) | 0.002(1) |
| $a_{5,\text{II}}$ | 0.016 | 0.010 | 0.008 |
| $a_{7,\text{II}}/\alpha$ | -0.014 | -0.009 | -0.006 |
| $a_{9,\text{II}}/\alpha$ | 0.112 | 0.080 | 0.060 |
| $a_{10,\text{II}}/\alpha$ | -0.221(42)[25] | -0.182(42)[20] | -0.157(42)[17] |

relatively small uncertainties. In Table 4, we show the results for these coefficients obtained by keeping $H_{\pi K}$ fixed at its central value (using central values for all input parameters and setting $X_H = \ln(m_B/\Lambda_h) \approx 2.4$). Because the hard-scattering terms arise first at order α_s , they exhibit a relatively strong scale dependence. In addition, the coefficients a_1 , a_4 and a_{10} have some dependence on the Gegenbauer moments and on the value of the ratio $R_{\pi K}$. Although the twist-3 correction is sizeable, it does not dominate the result for the hard spectator term. With our default value for X_H we obtain an enhancement of the leading twist-2 term by about 40%.

Comparison of the results for $a_{i,\text{I}}$ and $a_{i,\text{II}}$ in Tables 3 and 4 shows that in most cases the hard spectator terms are of a similar magnitude as the vertex corrections. Notable exceptions are the coefficients a_2 and a_{10} , for which the hard-scattering contributions are the dominant effects. The predictions for these coefficients are correspondingly uncertain. On the other hand, the hard spectator contributions are very small (or absent) in the case of the coefficients a_4 , a_6 and a_8 .

So far we have ignored the large overall uncertainty in the hard-scattering terms resulting from the uncertainty in the value of $H_{\pi K}$. For an estimate of this quantity, we parameterize the divergent integral X_H in (59) in the form

$$X_H = \left(1 + \varrho_H e^{i\varphi_H}\right) \ln \frac{m_B}{\Lambda_h}; \quad \varrho_H \leq 1 \quad (71)$$

with an arbitrary phase φ_H , which may be caused by soft rescattering. In other words,

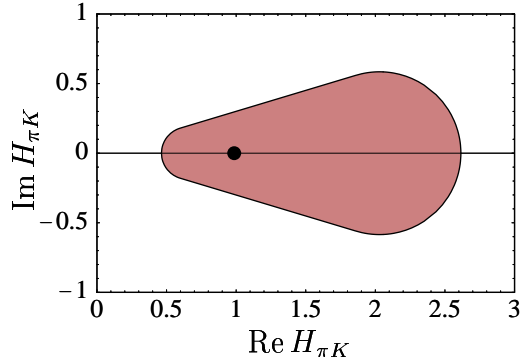


Figure 5: Ranges for the complex parameter $H_{\pi K}$. The dot shows the default value used in obtaining the results in Table 4.

we assign a 100% uncertainty to the “default value” $X_H = \ln(m_M/\Lambda_h) \approx 2.4$. If, in addition, the parameters λ_B , f_B and $F_0^{B \rightarrow \pi}(0)$ are varied within the ranges shown in Table 2, the result for $H_{\pi K}$ is confined to the interior of a region in the complex plane shown in Figure 5. (Variations of the Gegenbauer moments or the parameter $R_{\pi K}$ have a minor effect and can be safely neglected in this plot.) The obtained values for $H_{\pi K}$ are of order unity, but with an uncertainty of at least a factor 2 and a potentially significant strong-interaction phase (of up to about $\pm 17^\circ$ with our choice of parameters).

4.3 Annihilation contributions

As emphasized earlier, the results for the weak annihilation contributions derived in Section 3.5 are based on the assumption of hard scattering, which is invalidated by the presence of endpoint singularities. Nevertheless, eqs. (63) and (68) can be employed as a model for the annihilation terms, which we expect to give the correct order of magnitude of the effects. In analogy with the previous section, we parameterize the divergent integral X_A in the form

$$X_A = \left(1 + \varrho_A e^{i\varphi_A}\right) \ln \frac{m_B}{\Lambda_h}; \quad \varrho_A \leq 1 \quad (72)$$

with an arbitrary phase φ_A . Table 5 shows the results for the annihilation contributions obtained with the default value $X_A = \ln(m_B/\Lambda_h)$. They have an overall uncertainty of about 30% due to the error in the value of the ratio $r_A = (3.0 \pm 0.9) \cdot 10^{-3}$ defined in (21).

We observe that the default values for the annihilation contributions are rather small, compatible with being first-order power corrections of a canonical size. Specifically, from the relations for the amplitude parameters in (20) it follows that for an estimate of the most important annihilation effects in $B \rightarrow \pi K$ decays we should compare $r_A b_3$ with $(a_4^c + r_\chi^K a_6^c)$ (denominator of $\varepsilon_{3/2}$, ε_T , ε_a), $r_A(b_2 + b_3)$ with $(a_4^u + r_\chi^K a_6^u)$ (numerator of ε_a), and $r_A b_3^{\text{EW}}$ with $(a_{10}^c + r_\chi^K a_8^c)$ (numerator of q_C). Similarly, from (24) it follows that in $B \rightarrow \pi\pi$ decays we should compare $r_A(b_3 + 2b_4)$ with $(a_4^c + r_\chi^\pi a_6^c)$ (numerator of $P_{\pi\pi}/T_{\pi\pi}$).

Table 5: Annihilation coefficients $r_A b_i^{(\text{EW})}$ for three different choices of the renormalization scale and fixed default values of all input parameters.

| μ | $m_b/2$ | m_b | $2m_b$ |
|------------------------------|----------|----------|----------|
| μ_h | 1.02 GeV | 1.45 GeV | 2.05 GeV |
| $r_A b_1$ | 0.025 | 0.021 | 0.018 |
| $r_A b_2$ | -0.011 | -0.008 | -0.006 |
| $r_A b_3$ | -0.008 | -0.006 | -0.005 |
| $r_A b_4$ | -0.003 | -0.002 | -0.001 |
| $r_A b_3^{\text{EW}}/\alpha$ | -0.021 | -0.018 | -0.016 |
| $r_A b_4^{\text{EW}}/\alpha$ | 0.014 | 0.010 | 0.007 |

In all cases, annihilation effects can be neglected in comparison with $a_1 \approx 1$. With the default values from Table 5 the annihilation contributions are always a moderate correction of less than 25% to the leading terms obtained from the QCD factorization formula. However, these estimates have a large uncertainty.

Phenomenologically most relevant are the penguin annihilation effects parameterized by b_3 and b_4 . They tend to increase the penguin amplitudes P in $B \rightarrow \pi K$ decays and $P_{\pi\pi}$ in $B \rightarrow \pi\pi$ decays, thereby reducing the values of the tree-to-penguin ratios $\varepsilon_{3/2}$ and ε_T , and increasing the value of the penguin-to-tree ratio $P_{\pi\pi}/T_{\pi\pi}$. The fact that penguin annihilation graphs can significantly enhance the penguin amplitude has been noted first in [17]. We confirm this effect; however, with our default parameter variations we find a more moderate enhancement than these authors. In order to illustrate the effect and its dependence on the value of the quantity X_A , we show in Figure 6 the combinations $r_A b_3$ and $r_A(b_3 + 2b_4)$ parameterizing the penguin annihilation contributions in $B \rightarrow \pi K$ and $B \rightarrow \pi\pi$ decays. The default values for the leading penguin coefficients ($a_4^c + r_\chi a_6^c$) are shown for comparison. The regions bounded by the solid lines refer to our standard choice $\varrho_A \leq 1$ in (72). In this case, the annihilation contribution can increase the penguin amplitudes by up to 30–40%. The dashed curves show the accessible parameter space in the more extreme case where we let $\varrho_A \leq 2$ (corresponding to a 200% uncertainty in the value of the divergent integral X_A). Then the annihilation contributions can be almost as large as the leading penguin terms. We will see later that there are no experimental indications of such large annihilation effects.

4.4 Amplitude parameters for $B \rightarrow \pi K, \pi\pi$ decays

We are now in a position to combine the results for the parameters $a_{i,\text{I}}$, $a_{i,\text{II}}$ and b_i discussed in the previous subsections into complete predictions for the decay amplitudes. We focus first on the amplitude parameters defined in (20). They are sufficient to calculate any ratio of $B \rightarrow \pi K$ decay amplitudes, such as CP asymmetries and ratios

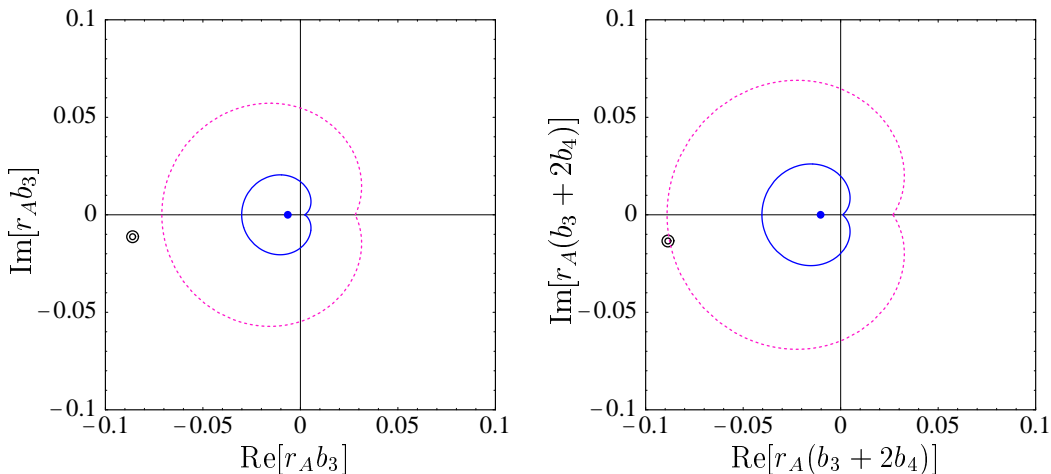


Figure 6: Ranges for $r_A b_3$ (left) and $r_A(b_3 + 2b_4)$ (right) parameterizing, respectively, penguin annihilation effects in $B \rightarrow \pi K$ and $B \rightarrow \pi\pi$ decays. Solid lines refer to $\varrho_A = 1$, dashed ones to $\varrho_A = 2$. The dots show the default values. For comparison, the central values for the leading penguin coefficients ($a_4^c + r_\chi a_6^c$) are shown by the double circles.

of CP-averaged branching fractions. We also study the ratio $P_{\pi\pi}/T_{\pi\pi}$ in $B \rightarrow \pi\pi$ decays defined in (24). A more extensive phenomenological analysis will be performed in Section 5.

It will be important to distinguish two types of theoretical uncertainties: those arising from the variation of input parameters to the factorization formula, and those associated with power corrections to factorization. Uncertainties of the first kind have a well-defined meaning and can, at least in principle, be reduced in a systematic way. They include the dependence on the renormalization scale, quark masses, moments of light-cone distribution amplitudes, and hadronic quantities such as f_B and $F_0^{B \rightarrow \pi}(0)$. The errors in the input parameters can be reduced, e.g., by using experimental data or lattice calculations. The residual dependence on the renormalization scale can be reduced by calculating higher-order corrections to the hard-scattering kernels. Our predictions also depend on the value of $|V_{ub}/V_{cb}|$; however, this should not be considered a theoretical uncertainty. Ultimately, the goal is to use hadronic B decays to learn about such CKM parameters.

Theoretical uncertainties related to power corrections to the factorization formula are of a different quality. Since factorization does, in general, not hold beyond leading power, there is no systematic formalism known that would allow us to analyze power corrections in a model-independent way. This is a general problem of QCD factorization theorems in cases where no operator product expansion can be applied. (Another familiar example are event-shape variables in e^+e^- annihilation to hadrons.) In the present work, we have identified sources of potentially large power corrections (chirally-enhanced contributions and weak annihilation terms) and estimated their effects. These estimates are uncertain

due to logarithmically divergent endpoint contributions, which indicate the dominance of soft gluon exchange. Without significant conceptual progress in the understanding of power corrections to observables that do not admit a local operator product expansion, it will be difficult to reduce these uncertainties in a systematic way.

Our results for the amplitude parameters including all theoretical uncertainties of the first kind are shown in Table 6. They are obtained by keeping the parameters X_H and X_A entering the power corrections fixed at the default value $X_H = X_A = \ln(m_B/\Lambda_h)$. All other input parameters are varied within the ranges shown in Table 2. Following common practice, we vary the renormalization scale μ between $m_b/2$ and $2m_b$. The individual contributions to the error are then added in quadrature to obtain the total theoretical uncertainty of the first kind. The two most important contributions to the total error are shown in the last column of the table. The sign convention is such that the upper (lower) sign corresponds to increasing (decreasing) the value of an input parameter. Finally, the second error on the central value (if present) indicates the sensitivity to the uncertainty in the ratio $|V_{ub}/V_{cb}| = 0.085 \pm 0.017$, which we assume to be 20%. This is not a hadronic uncertainty and therefore should not be combined with the first error. The amplitude parameters are either proportional (or inversely proportional) to $|V_{ub}/V_{cb}|$ or independent of this parameter, so that this error can easily be readjusted if needed.

In almost all cases the theoretical uncertainty is dominated by a single source. With the exception of the strong-interaction phase ω_C , our next-to-leading order results for the amplitude parameters are very stable under variation of the renormalization scale. The uncertainty in the values of the tree-to-penguin ratios $\varepsilon_{3/2}$, ε_T , and $|P_{\pi\pi}/T_{\pi\pi}|$ is dominated by the error on the strange-quark mass, whereas the corresponding strong-interaction phases ϕ , ϕ_T , and $\arg(P_{\pi\pi}/T_{\pi\pi})$, as well as the phase ϕ_a , are most sensitive to the error on the charm-quark mass. The largest uncertainty in the electroweak-penguin parameter q comes from the SU(3) violations parameterized by the amplitude ratio $R_{\pi K}$ in (15). The uncertainty in the value of the wave-function parameter λ_B is the dominant source of uncertainty for the electroweak-penguin parameter q_C . Note that the Gegenbauer moments of the pion and kaon light-cone distribution amplitudes are never the dominant contribution to the error. This shows that the precise shapes of these amplitudes are of minor importance for phenomenological applications of QCD factorization.

In order to study the theoretical uncertainties of the second kind, related to our estimate of potentially large power corrections to the factorization formula, we show in Figure 7 results for amplitude parameters obtained using central values for all input parameters, but varying the complex quantities X_H and X_A according to the parameterizations (71) and (72). The dots with error bars show the central results for the amplitude parameters as given in Table 6 (for fixed $|V_{ub}/V_{cb}| = 0.085$). The dashed curves (visible only for $\varepsilon_{3/2}$ and q_C) bound the parameter space obtained by variation of X_H , whereas the solid curves (present for all parameters except q) define the region obtained by variation of X_A . It is evident that the chirally-enhanced twist-3 corrections to the hard spectator interactions do not lead to a dominant uncertainty. Their effect is always smaller than the uncertainty due to parameter variations of the first kind. The

Table 6: Predictions for the amplitude parameters including all theoretical uncertainties of the first kind (see text), but using default values for the power corrections to QCD factorization. The first error on the central value is the sum of all theoretical uncertainties added in quadrature. The second error (if present) shows the dependence on $|V_{ub}/V_{cb}|$. The last column indicates the two most important contributions to the theoretical uncertainty. For each quantity, the second line shows the result without weak annihilation contributions (except for q and ω , which do not receive annihilation terms).

| Parameter | Central Value | Dominant Errors | |
|-------------------------------|-------------------------|-----------------------|------------------------|
| $\varepsilon_{3/2}$ (%) | $23.9 \pm 4.5 \pm 4.8$ | $\pm 3.5 (m_s)$ | $\pm 1.4 (\mu)$ |
| | $25.7 \pm 4.8 \pm 5.1$ | $\pm 3.6 (m_s)$ | $\pm 1.6 (\alpha_2^K)$ |
| ϕ (deg) | -9.6 ± 3.8 | $\pm 3.5 (m_c)$ | $\pm 1.4 (\alpha_1^K)$ |
| | -10.2 ± 4.1 | $\pm 3.7 (m_c)$ | $\pm 1.5 (\alpha_1^K)$ |
| ε_T (%) | $20.6 \pm 3.5 \pm 4.1$ | $\pm 3.2 (m_s)$ | $\pm 0.9 (\mu)$ |
| | $22.0 \pm 3.6 \pm 4.4$ | $\pm 3.3 (m_s)$ | $\pm 0.8 (\alpha_2^K)$ |
| ϕ_T (deg) | -5.7 ± 4.4 | $\pm 3.5 (m_c)$ | $\mp 2.3 (\mu)$ |
| | -6.2 ± 4.6 | $\pm 3.7 (m_c)$ | $\mp 2.2 (\mu)$ |
| ε_a (%) | $2.0 \pm 0.1 \pm 0.4$ | $\pm 0.1 (m_c)$ | $\mp 0.1 (\mu)$ |
| | $1.9 \pm 0.1 \pm 0.4$ | $\pm 0.1 (m_c)$ | — |
| ϕ_a (deg) | 13.6 ± 4.4 | $\pm 3.7 (m_c)$ | $\pm 1.7 (\alpha_1^K)$ |
| | 16.6 ± 5.2 | $\pm 3.9 (m_c)$ | $\mp 2.8 (\mu)$ |
| q (%) | $58.8 \pm 6.7 \mp 11.8$ | $\pm 6.4 (R_{\pi K})$ | $\pm 1.3 (\mu)$ |
| ω (deg) | -2.5 ± 2.8 | $\pm 1.9 (\mu)$ | $\mp 1.8 (\alpha_1^K)$ |
| q_C (%) | $8.3 \pm 4.5 \mp 1.7$ | $\mp 2.7 (\lambda_B)$ | $\pm 2.3 (\alpha_1^K)$ |
| | $8.9 \pm 4.9 \mp 1.8$ | $\mp 3.1 (\lambda_B)$ | $\pm 2.3 (\alpha_1^K)$ |
| ω_C (deg) | -60.2 ± 49.5 | $\pm 31.7 (\mu)$ | $\mp 27.9 (\lambda_B)$ |
| | -54.2 ± 44.2 | $\pm 29.5 (\mu)$ | $\mp 24.1 (\lambda_B)$ |
| $ P_{\pi\pi}/T_{\pi\pi} $ (%) | $28.5 \pm 5.1 \mp 5.7$ | $\mp 4.6 (m_s)$ | $\mp 1.8 (\mu)$ |
| | $25.9 \pm 4.3 \mp 5.2$ | $\mp 4.1 (m_s)$ | $\mp 0.8 (\mu)$ |
| $\arg(P_{\pi\pi}/T_{\pi\pi})$ | 8.2 ± 3.8 | $\mp 3.3 (m_c)$ | $\pm 2.0 (\mu)$ |
| (deg) | 9.0 ± 4.1 | $\mp 3.6 (m_c)$ | $\pm 1.8 (\mu)$ |

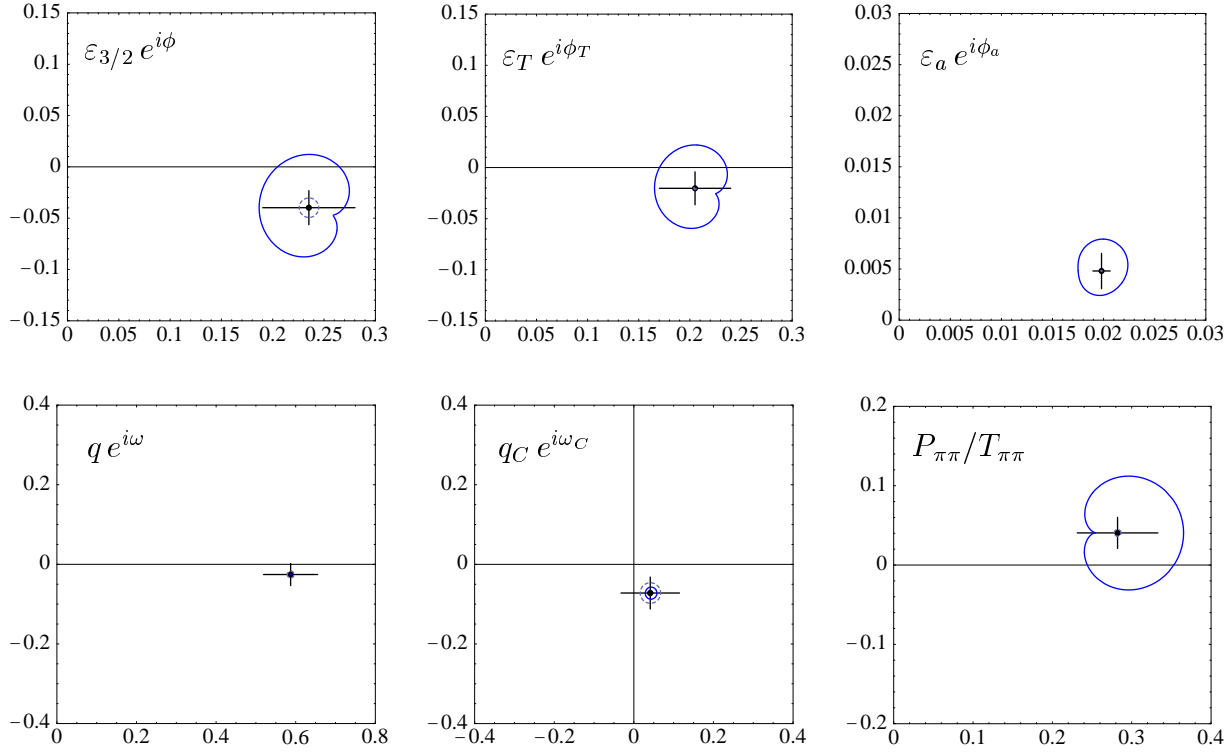


Figure 7: Results for the amplitude parameters. Dots with error bars show the default values and uncertainties of the first kind, while the regions bounded by the curves show the variation of the central values under variation of X_H with $\varrho_H = 1$ (dashed curves), and variation of X_A with $\varrho_A = 1$ (solid curves).

uncertainty in the description of weak annihilation is significant for the tree-to-penguin ratios $\varepsilon_{3/2}$, ε_T , $P_{\pi\pi}/T_{\pi\pi}$ and their phases. The resulting variation is typically as large as the total theoretical uncertainty of the first kind. Although the modelling of weak annihilation thus introduces sizeable uncertainties, we stress that their impact on the values of the amplitude parameters is still a moderate correction (see also Table 6). Moreover, it is important that the dominant effect is a universal contribution to the leading penguin amplitudes P and $P_{\pi\pi}$, which leads to correlations between the various amplitude parameters. Ultimately, this will help to constrain the annihilation contributions using experimental data (see Section 5.3 below).

5 Phenomenological applications

This section, which can be read without studying the technical details of our analysis, illustrates several applications of our result to the phenomenology of $B \rightarrow \pi K$ and $B \rightarrow \pi\pi$ decays. The main goal will be to obtain information about the Wolfenstein parameters $\bar{\rho}$ and $\bar{\eta}$ defining the unitarity triangle. After some general remarks in Section 5.1, we

start by considering methods for constraining $\bar{\rho}$ and $\bar{\eta}$ that depend on a minimal amount of theoretical input about QCD dynamics. The simplest such strategy is the Fleischer–Mannel bound [6] discussed in Section 5.2. In the following Section 5.3, we review analysis strategies developed by Rosner and one of us [1, 3, 4], which are based on CP-averaged rate measurements for the charged modes $B^\pm \rightarrow \pi K, \pi\pi$. These methods provide powerful constraints in the $(\bar{\rho}, \bar{\eta})$ plane with minimal theoretical uncertainties. The third method, the determination of $\sin 2\alpha$ from the time-dependent CP asymmetry in $B^0, \bar{B}^0 \rightarrow \pi^+\pi^-$ decays, is explored in Section 5.4. Towards the end of our discussion we will then rely more heavily on the new theoretical results obtained in the present work. In Section 5.5, we give predictions for the absolute values of branching fractions and results for various ratios of CP-averaged branching ratios as a function of γ . We then perform a global fit to the experimental data on the branching ratios and extract the corresponding allowed region in the $(\bar{\rho}, \bar{\eta})$ plane. In the final Section 5.6, we show predictions for the direct CP asymmetries in the various $B \rightarrow \pi K$ and $B \rightarrow \pi\pi$ decay modes. Because of their sensitivity to strong-interaction phases, these results have the largest theoretical uncertainties.

5.1 General observations

Several points following from the numerical analysis in Section 4.4 are worth repeating here, because they will have a direct impact on some of the analysis strategies mentioned below:

1. The rescattering effects parameterized by ε_a are very small and not much affected by theoretical uncertainties. Therefore, the decay amplitude for $B^- \rightarrow \pi^- \bar{K}^0$ in (18) is, to a very good approximation, given by the pure penguin amplitude P . This has two important consequences: first, it is a safe approximation to neglect terms of order ε_a^2 in the squared decay amplitudes; secondly, it follows that the direct CP asymmetry in the decays $B^\pm \rightarrow \pi^\pm K^0$,

$$A_{\text{CP}}(\pi^+ K^0) = -2\varepsilon_a \sin \phi_a \sin \gamma + O(\varepsilon_a^2) \approx -1\% \times \sin \gamma, \quad (73)$$

is tiny and unobservable in the foreseeable future. (We define the CP asymmetries as the difference of the B -meson minus \bar{B} -meson decay rates divided by their sum.) An experimental finding of a sizeable asymmetry in this decay mode would have to be interpreted as a sign of physics beyond the Standard Model, or as a gross failure of the QCD factorization formula, indicating the presence of large, uncontrollable power corrections. For completeness, we note that the prediction that ε_a is small can be tested experimentally by measuring the CP-averaged branching ratio for the decays $B^\pm \rightarrow K^\pm K^0$ [4, 45].

2. The strong-interaction phase $\omega = -(2.5 \pm 2.8)^\circ$ is accurately predicted and tiny, consistent with zero within errors. Also, the value of q is not affected by annihilation contributions. These observations confirm a theoretical argument presented in [2, 3], which uses Fierz identities and top-quark dominance in the electroweak penguin diagrams

to show that $\omega \approx 0$, and that q can be calculated in a model-independent way up to SU(3)-breaking corrections. The argument is based on the fact that in the limit of V-spin ($s \leftrightarrow u$) symmetry the leading electroweak penguin contributions parameterized by $q e^{i\omega}$ can be related to the current-current contributions from the operators Q_1^u and Q_2^u using Fierz identities. Neglecting the small contributions from the operators Q_7 , Q_8 , and $Q_{7\gamma}$, one then obtains

$$q e^{i\omega} \simeq -\frac{3}{2\epsilon_{\text{KM}}} \frac{C_9 + C_{10}}{C_1 + C_2} \simeq \frac{1}{\epsilon_{\text{KM}}} \frac{\alpha}{8\pi} \frac{x_t}{\sin^2\theta_W} \left(1 + \frac{3 \ln x_t}{x_t - 1} \right), \quad (74)$$

where the ratio of Wilson coefficients is renormalization-scheme invariant and can thus be evaluated at the electroweak scale. The strong-interaction phase ω vanishes in this approximation. When SU(3)-breaking corrections and small electromagnetic contributions are included, the above result is rescaled by a factor $R_q = (0.84 \pm 0.10) e^{-i(2.5 \pm 2.8)^\circ}$. About half of the deviation from 1 is due to (mostly “factorizable”) SU(3) violations. The important point to note is that the smallness of ω is a model-independent result that does not rely on the QCD factorization formula. It follows that terms of second order in ω can be safely neglected.

3. The electroweak penguin contributions to the $\bar{B}^0 \rightarrow \pi^+ K^-$ decay amplitude, parameterized by q_C in (18), are small and can also be treated to first order to good approximation. In the literature, these effects are sometimes referred to as “colour-suppressed” electroweak penguin contributions.

4. The strong-interaction phases ϕ , ϕ_T , and $\arg(P_{\pi\pi}/T_{\pi\pi})$ are small. We find central values of order 10° or less in magnitude, with an uncertainty of about a factor 2 due to potentially large annihilation contributions and higher-order perturbative corrections to the hard-scattering kernels. It follows that the cosines of these phases deviate from 1 by only a few percent, and the direct CP asymmetries are suppressed by a factor $|\sin \phi_i| \sim 0.1\text{--}0.3$. We note, in this context, that the smallness of the phase difference $\phi_T - \phi \approx 4^\circ$ (see Table 6) can be understood based on simple physical arguments and implies a strong correlation between the direct CP asymmetries in the decays $B^\pm \rightarrow \pi^0 K^\pm$ and $B^0 \rightarrow \pi^\mp K^\pm$ [46].

In the following sections, we explain how these general observations can be put to work in different analysis strategies. We start with those strategies that avoid theoretical input on tree-to-penguin ratios such as $\varepsilon_{3/2}$ and ε_T . This eliminates the sensitivity to weak annihilation effects and hence the main uncertainty of the QCD factorization approach. As a result, these strategies are particularly clean from a theoretical point of view.

Experimental data for the CP-averaged $B \rightarrow \pi K$ and $B \rightarrow \pi\pi$ branching fractions as reported by several experimental groups are collected in Table 7. The last column shows our naive averages of these results neglecting correlations. We use the average result for the $B^\pm \rightarrow \pi^\pm \pi^0$ branching ratio in despite of the fact that the individual measurements of this mode have less than 3σ significance.

Table 7: Experimental results for the CP-averaged $B \rightarrow \pi K$ and $B \rightarrow \pi\pi$ branching ratios in units of 10^{-6} . The BaBar and Belle results are preliminary. Our averages ignore correlations.

| Decay Mode | CLEO [47] | BaBar [48] | Belle [49] | Average |
|----------------------------------|------------------------------|------------------------------|------------------------------|----------------|
| $B^0 \rightarrow \pi^+\pi^-$ | $4.3^{+1.6}_{-1.4} \pm 0.5$ | $4.1 \pm 1.0 \pm 0.7$ | $5.9^{+2.4}_{-2.1} \pm 0.5$ | 4.4 ± 0.9 |
| $B^\pm \rightarrow \pi^\pm\pi^0$ | $5.6^{+2.6}_{-2.3} \pm 1.7$ | $5.1^{+2.0}_{-1.8} \pm 0.8$ | $7.1^{+3.6+0.9}_{-3.0-1.2}$ | 5.6 ± 1.5 |
| | < 12.7 (90% C.L.) | < 9.0 (90% C.L.) | < 12.6 (90% C.L.) | |
| $B^0 \rightarrow \pi^\mp K^\pm$ | $17.2^{+2.5}_{-2.4} \pm 1.2$ | $16.7 \pm 1.6^{+1.2}_{-1.7}$ | $18.7^{+3.3}_{-3.0} \pm 1.6$ | 17.2 ± 1.5 |
| $B^\pm \rightarrow \pi^0 K^\pm$ | $11.6^{+3.0+1.4}_{-2.7-1.3}$ | $10.8^{+2.1+1.0}_{-1.9-1.2}$ | $17.0^{+3.7+2.0}_{-3.3-2.2}$ | 12.1 ± 1.7 |
| $B^\pm \rightarrow \pi^\pm K^0$ | $18.2^{+4.6}_{-4.0} \pm 1.6$ | $18.2^{+3.3+1.6}_{-3.0-2.0}$ | $13.1^{+5.5}_{-4.6} \pm 2.6$ | 17.2 ± 2.5 |
| $B^0 \rightarrow \pi^0 K^0$ | $14.6^{+5.9+2.4}_{-5.1-3.3}$ | $8.2^{+3.1+1.1}_{-2.7-1.2}$ | $14.6^{+6.1}_{-5.1} \pm 2.7$ | 10.3 ± 2.5 |

5.2 Fleischer–Mannel bound

Based on a few plausible assumptions, Fleischer and Mannel have proposed a very simple method for obtaining a bound on the weak phase γ from the measurement of a single ratio

$$R = \frac{\tau(B^+) \text{Br}(B^0 \rightarrow \pi^- K^+) + \text{Br}(\bar{B}^0 \rightarrow \pi^+ K^-)}{\tau(B^0) \text{Br}(B^+ \rightarrow \pi^+ K^0) + \text{Br}(B^- \rightarrow \pi^- \bar{K}^0)} \quad (75)$$

of CP-averaged branching ratios [6] (see [5] for more sophisticated generalizations of this method). The current value of this ratio obtained from Table 7 is $R = 1.06 \pm 0.18$. Neglecting the small rescattering effects parameterized by ε_a and the colour-suppressed electroweak penguin contribution q_C (observations 1 and 3), it follows from (18) that

$$R \simeq 1 - 2\varepsilon_T \cos \phi_T \cos \gamma + \varepsilon_T^2 \geq \sin^2 \gamma. \quad (76)$$

The bound excludes a region near $|\gamma| = 90^\circ$ provided that $R < 1$. It is valid for any values of ε_T and the strong-interaction phase ϕ_T and is thus independent of theoretical assumptions about the tree-to-penguin ratio in these decays.

Our calculations confirm the dynamical assumptions that go into the derivation of this bound. The neglected terms in the exact formula for R are of order $\varepsilon_a \varepsilon_T$ or $q_C \varepsilon_T$. Both are at the few percent level and can be safely neglected until the experimental error on R is much below 10%. (More accurately, we find that the bound (76) is violated by at most 1.5% and only in the region $72^\circ < \gamma < 86^\circ$.)

5.3 Strategies based on charged modes

The theoretical analysis of the charged decays $B^\pm \rightarrow \pi K$ profits from the fact that, with the exception of the strong-interaction phases ϕ and ϕ_a , the hadronic parameters entering the parameterization of the corresponding decay amplitudes in (18) can be constrained

in the limit of SU(3) symmetry [3, 4, 5]. Therefore, the QCD factorization formula is needed only to reduce the uncertainties in the estimate of SU(3)-breaking corrections. We have already seen above how SU(3) symmetry and Fierz identities help to calculate the quantity $q e^{i\omega}$ with small theoretical uncertainties. In addition, the decay amplitudes for the charged modes $B^\pm \rightarrow \pi K$ in (18) depend on the tree-to-penguin ratio $\varepsilon_{3/2}$ and the very small rescattering parameter ε_a (and the corresponding phases ϕ and ϕ_a). It is apparent from Figure 7 that our prediction for $\varepsilon_{3/2}$ has a large uncertainty due to weak annihilation contributions as well as parameter variations. The advantage of the charged $B^\pm \rightarrow \pi K$ modes is that the tree-to-penguin ratio can be determined, up to small SU(3) violations, using experimental data. Specifically, a certain combination of the parameters $\varepsilon_{3/2}$ and ε_a can be measured by comparing the CP-averaged branching fractions for the decays $B^\pm \rightarrow \pi^\pm \pi^0$ and $B^\pm \rightarrow \pi^\pm K^0$. The relation is

$$\bar{\varepsilon}_{3/2} = \frac{\varepsilon_{3/2}}{\sqrt{1 + 2\varepsilon_a \cos \phi_a \cos \gamma + \varepsilon_a^2}} \equiv R_{\text{th}} \varepsilon_{\text{exp}}, \quad (77)$$

where

$$\varepsilon_{\text{exp}} = \tan \theta_C \frac{f_K}{f_\pi} \left[\frac{2[\text{Br}(B^+ \rightarrow \pi^+ \pi^0) + \text{Br}(B^- \rightarrow \pi^- \pi^0)]}{\text{Br}(B^+ \rightarrow \pi^+ K^0) + \text{Br}(B^- \rightarrow \pi^- \bar{K}^0)} \right]^{1/2} \quad (78)$$

is an observable, and $R_{\text{th}} = 1$ in the limit of U-spin ($d \leftrightarrow s$) symmetry [3]. In the theoretical analysis of $B^\pm \rightarrow \pi K$ decays it is convenient to replace the parameter $\varepsilon_{3/2}$ by $\bar{\varepsilon}_{3/2}$. Since $\varepsilon_a = O(\epsilon_{\text{KM}})$ is very small (observation 1), both quantities take very similar values. The experimental uncertainty in the current value $\varepsilon_{\text{exp}} = 0.223 \pm 0.034$ is still large. Ultimately, however, the accuracy in the determination of $\bar{\varepsilon}_{3/2}$ is only limited by the theoretical uncertainty in the calculation of the SU(3)-breaking corrections to R_{th} . The QCD factorization approach helps reducing the model dependence in this calculation. Neglecting the tiny contributions from electroweak penguins,

$$R_{\text{th}} = \left| \frac{a_1(\pi K) + R_{\pi K} a_2(\pi K)}{a_1(\pi\pi) + a_2(\pi\pi)} \right| \frac{F_0^{B \rightarrow \pi}(m_K^2)}{F_0^{B \rightarrow \pi}(m_\pi^2)}. \quad (79)$$

The form-factor ratio can be safely set equal to 1. (Deviations are of order $(m_K^2 - m_\pi^2)/m_B^2 \approx 1\%$.) Note that there are no annihilation contributions to R_{th} . If we keep the parameter X_H governing the twist-3 contributions to the hard spectator interactions fixed vary all other input parameters over their respective ranges of uncertainty, we find that $R_{\text{th}} = 0.98 \pm 0.02$. Next, if we keep the input parameters fixed but vary X_H as shown in (71), we find a variation of about ± 0.01 . However, since our focus here is on SU(3) violations we should be more conservative and let the quantities X_H^K and X_H^π vary independently. This gives a larger variation of about ± 0.03 . Taken altogether, we obtain

$$R_{\text{th}} = 0.98 \pm 0.05. \quad (80)$$

Combining this with the experimental value of ε_{exp} gives $\bar{\varepsilon}_{3/2} = 0.218 \pm 0.034_{\text{exp}} \pm 0.011_{\text{th}}$.

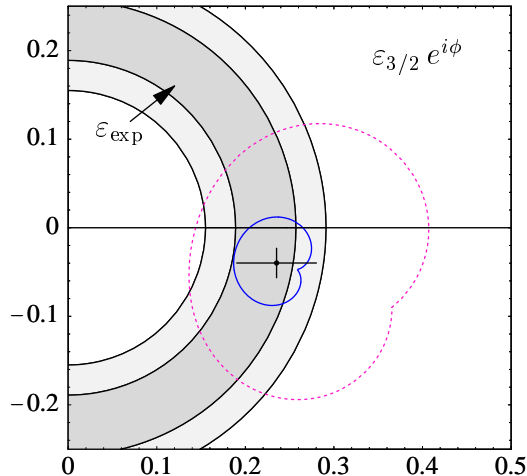


Figure 8: Comparison of the prediction for the tree-to-penguin ratio $\varepsilon_{3/2}$ in $B^\pm \rightarrow \pi K$ decays with the experimental value (at 1σ and 2σ) of the quantity ε_{exp} defined in (78). The region bounded by the solid line refers to our default annihilation model with $\varrho_A = 1$. The dashed line corresponds to $\varrho_A = 2$.

Our results for the SU(3)-breaking corrections parameterized by R_{th} and R_q (the quantity that corrects (74)) are valid up to nonfactorizable corrections that simultaneously violate SU(3) symmetry and are power-suppressed in Λ_{QCD}/m_b . The potentially most important power corrections are included in the error estimate. The remaining uncertainties are of order

$$O\left(\frac{1}{N_c} \cdot \frac{m_s - m_d}{m_b}\right), \quad (81)$$

and, by naive power counting, should not amount to more than a few percent.

Whereas our theoretical predictions for the parameter $\varepsilon_{3/2}$ were affected by large uncertainties (see Figure 7), relations (77) and (80) can be combined to obtain a much more accurate value for the related parameter $\bar{\varepsilon}_{3/2}$ provided, of course, that the experimental value of ε_{exp} has a small error. This parameter can then be used in the phenomenological analysis of $B^\pm \rightarrow \pi K$ decays. Moreover, the comparison of the so-determined value of this parameter with our prediction for the tree-to-penguin ratio $\varepsilon_{3/2}$ provides a nontrivial test of the QCD factorization approach, and ultimately could help to reduce the uncertainties in our modelling of weak annihilation contributions.

To illustrate this last point, we show in Figure 8 our prediction for $\varepsilon_{3/2} e^{i\phi}$ (corresponding to the first plot in Figure 7) and underlay as a gray band the experimental value for ε_{exp} with its 1σ and 2σ errors. (The two quantities should agree if we neglect the small deviation of R_{th} from 1, and the tiny contribution of ε_a in (77).) It is pleasing that the central experimental value is in excellent agreement with our theoretical prediction. The “smallness” of the tree-to-penguin ratio in $B \rightarrow \pi K$ decays has often been interpreted as evidence for large, nonfactorizable contributions to the decay amplitudes. Here we find that this effect is reproduced in the QCD factorization approach without

any tuning of parameters. This is an important result. A deviation of our prediction from the experimental result could have been considered as an indication of large corrections to QCD factorization, such as enhanced weak annihilation effects not covered by our simple model estimates. As an example, the dashed curve in the figure shows the allowed region obtained by increasing the value of the parameter ϱ_A in (72) from 1 to 2. Fortunately, the data provide no evidence for the existence of such large deviations from our central prediction. (However, the evidence from ε_{exp} alone does also not exclude a potentially large annihilation contribution, if it has a large phase.)

Model-independent bound on γ

A key observable in the study of the weak phase γ is the ratio of the CP-averaged branching ratios in the two $B^\pm \rightarrow \pi K$ decay modes, defined as

$$R_* = \frac{\text{Br}(B^+ \rightarrow \pi^+ K^0) + \text{Br}(B^- \rightarrow \pi^- \bar{K}^0)}{2[\text{Br}(B^+ \rightarrow \pi^0 K^+) + \text{Br}(B^- \rightarrow \pi^0 K^+)]}. \quad (82)$$

Its current value is $R_* = 0.71 \pm 0.14$. The theoretical expression for this ratio obtained using the parameterization in (18) is

$$\begin{aligned} R_*^{-1} = & 1 + 2\bar{\varepsilon}_{3/2} \cos \phi (q - \cos \gamma) + \bar{\varepsilon}_{3/2}^2 (1 - 2q \cos \gamma + q^2) \\ & - 2\bar{\varepsilon}_{3/2} \varepsilon_a \left[\sin^2 \gamma \cos \phi \cos \phi_a + (1 - q \cos \gamma) \sin \phi \sin \phi_a \right] \\ & - 2\bar{\varepsilon}_{3/2} q \sin \phi \sin \omega + O(\varepsilon_a^2, \omega^2, \varepsilon_a \omega). \end{aligned} \quad (83)$$

(The parameter q is also called δ_{EW} in the literature on this ratio.) Note that the rescattering effects described by ε_a , as well as the terms linear in the small phase ω , are suppressed by a factor of $\bar{\varepsilon}_{3/2}$ and thus reduced to the percent level. Higher-order terms in these small parameters can be safely neglected (observations 1 and 2).

From a measurement of the ratio R_* alone a bound on $\cos \gamma$ can be derived, which for $R_* < 1$ implies a nontrivial constraint on the Wolfenstein parameters $\bar{\rho}$ and $\bar{\eta}$ [3]. Only CP-averaged branching ratios are needed for this purpose. The idea is to allow the strong-interaction phases ϕ and ϕ_a in (83) to take any value between 0 and 2π . (Of course, the QCD factorization approach predicts rather restricted ranges for these strong-interaction phases. For the moment, however, we will not make use of these predictions.) This gives [3, 4]

$$R_*^{-1} < \left(1 + \bar{\varepsilon}_{3/2} |q - \cos \gamma|\right)^2 + \bar{\varepsilon}_{3/2} (\bar{\varepsilon}_{3/2} + 2\varepsilon_a) \sin^2 \gamma + O(\varepsilon_a^2, \varepsilon_a \omega, \omega^2). \quad (84)$$

Note that there is no term linear in ω on the right-hand side. Provided R_* is significantly smaller than 1, the bound implies an exclusion region for $\cos \gamma$, which becomes larger the smaller the values of R_* and $\bar{\varepsilon}_{3/2}$ turn out to be. The effect of the rescattering contribution proportional to ε_a on the right-hand side of the bound is numerically very small.

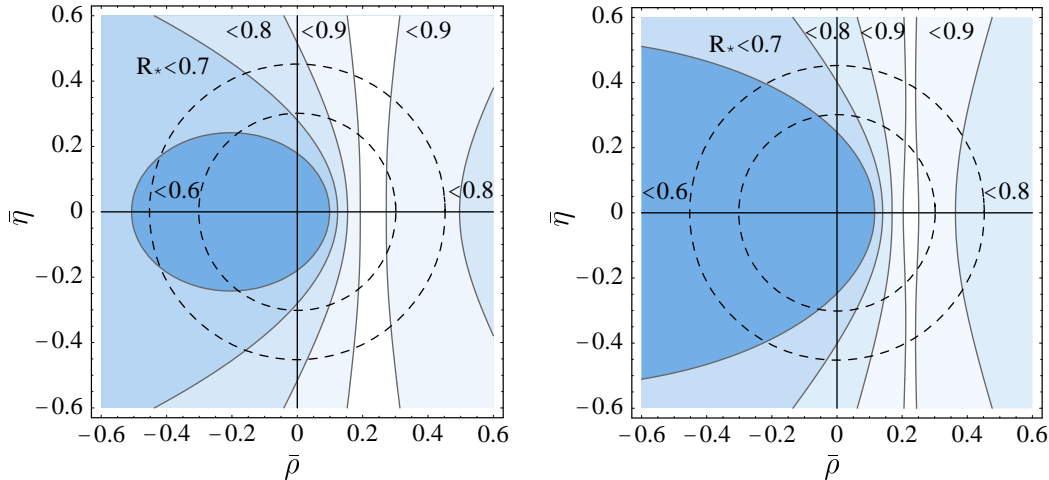


Figure 9: Theoretical constraints on the Wolfenstein parameters $(\bar{\rho}, \bar{\eta})$ implied by (still hypothetical) experimental upper bounds on the ratios R_* and ε_{exp} . The left-hand plot refers to $\varepsilon_{\text{exp}} < 0.19$, the right-hand one to $\varepsilon_{\text{exp}} < 0.25$. For a given upper bound on R_* , $\bar{\rho}$ and $\bar{\eta}$ are restricted to lie inside the corresponding shaded region. The dashed circles show the allowed region implied by the measurement of $|V_{ub}/V_{cb}|$ in semileptonic B decays.

For fixed value of q , eq. (84) excludes a region in $\cos \gamma$ provided that $R_* < 1$. However, we should take into account that the value of q itself depends on the Wolfenstein parameters $\bar{\rho}$ and $\bar{\eta}$. Hence, it is more appropriate to display the relation (84) as a constraint in the $(\bar{\rho}, \bar{\eta})$ plane. We use

$$\cos \gamma = \frac{\bar{\rho}}{\sqrt{\bar{\rho}^2 + \bar{\eta}^2}}, \quad q = \frac{\hat{q}}{R_b} = \frac{0.222 \pm 0.025}{\sqrt{\bar{\rho}^2 + \bar{\eta}^2}}, \quad (85)$$

where the numerical value $\hat{q} = q R_b = 0.222 \pm 0.025$ corresponds to $|V_{ub}/V_{cb}| = 0.085 \pm 0.017$. The experimental inputs to the bound are the measured ratios R_* and ε_{exp} of CP-averaged branching ratios. The theoretical inputs are the value of \hat{q} , the parameter R_{th} in the relation $\bar{\varepsilon}_{3/2} = R_{\text{th}} \varepsilon_{\text{exp}}$, and a value for the rescattering parameter ε_a . The accuracy of our predictions for \hat{q} and R_{th} is intrinsically limited only by effects that have a strong parametric suppression, as shown in (81). As far as ε_a is concerned, the bound becomes weaker the larger the value of ε_a . In our analysis we take $\varepsilon_a < 0.04$, corresponding to an upper bound that is twice as large as predicted by the QCD factorization approach.

Figure 9 illustrates the resulting constraint in the $(\bar{\rho}, \bar{\eta})$ plane obtained for some representative upper bounds on R_* and ε_{exp} . For comparison, the dashed circles show the constraint arising from the measurement of the ratio $|V_{ub}/V_{cb}|$ in semileptonic B decays. (Note that the information from kaon CP violation excludes $\bar{\eta} < 0$ in the Standard Model.) It is evident that, depending on the values of R_* and ε_{exp} , the constraint may be very nontrivial. If $R_* < 0.7$, then only values $|\gamma| > 90^\circ$ are allowed, which are significantly larger than those favoured by the global analysis of the unitarity triangle (see [50, 51,

52, 53] for some recent discussions of the standard analysis). For yet smaller values $R_* < 0.6$, the arising constraint would become inconsistent with the global analysis. This would be an indication of some new flavour physics beyond the Standard Model. On the other hand, if $R_* > 0.9$ then the excluded region is too small (or absent) to be of phenomenological significance. The present uncertainty in the value of R_* is too large to tell which of these possibilities is realized.

Determination of γ and constraint in the $(\bar{\rho}, \bar{\eta})$ plane

Ultimately, the goal is of course not only to derive a bound in the $(\bar{\rho}, \bar{\eta})$ plane, but to determine the Wolfenstein parameters (and thus the unitarity triangle). This requires obtaining information about the strong-interaction phase ϕ in (83), which can be achieved either through the measurement of a CP asymmetry or with the help of theory. A strategy for a model-independent determination of γ from $B^\pm \rightarrow \pi K, \pi\pi$ decays has been suggested in [1]. It generalizes a method proposed by Gronau, Rosner and London [54] to include the effects of electroweak penguins. The approach has later been refined to account for rescattering contributions to the $B^\pm \rightarrow \pi^\pm K^0$ decay amplitudes [4]. However, this method relies on the measurement of a direct CP asymmetry in addition to R_* and hence requires very high statistics. Here, we suggest an easier strategy for a theory-guided determination of $\bar{\rho}$ and $\bar{\eta}$, which does not require the measurement of a CP asymmetry. Instead, we will exploit the prediction of the QCD factorization approach that the strong-interaction phase ϕ is small, i.e.,

$$\sin \phi = O[\alpha_s(m_b), \Lambda_{\text{QCD}}/m_b]. \quad (86)$$

This implies that the deviation of $\cos \phi$ from 1 is a second-order effect in $\alpha_s(m_b)$ and/or Λ_{QCD}/m_b . More specifically, we found that $\phi \approx -(10 \pm 15)^\circ$, where the uncertainty is dominated by the weak annihilation contribution. Taking this value literally we would conclude that $\cos \phi > 0.9$; however, to be conservative we allow for a larger phase such that $\cos \phi > 0.8$. (This prediction can be tested experimentally once the direct CP asymmetry in the decays $B^\pm \rightarrow \pi^0 K^\pm$ has been measured [1, 4].) With the help of this result, a measurement of the ratio R_* can be used to obtain a narrow allowed region in the $(\bar{\rho}, \bar{\eta})$ plane, which for fixed value of $|V_{ub}/V_{cb}|$ corresponds to a determination of γ that is unique up to a sign. To this end, we rewrite (83) as

$$\cos \gamma = q + \frac{1 - R_*^{-1} + \bar{\varepsilon}_{3/2}^2(1 - q^2) - 2\bar{\varepsilon}_{3/2} \delta}{2\bar{\varepsilon}_{3/2}(\cos \phi + \bar{\varepsilon}_{3/2} q)} + O(\varepsilon_a^2, \varepsilon_a \omega, \omega^2), \quad (87)$$

where

$$\delta = \varepsilon_a \left[\sin^2 \gamma \cos \phi \cos \phi_a + (1 - q \cos \gamma) \sin \phi \sin \phi_a \right] + q \sin \phi \sin \omega. \quad (88)$$

It is safe to take $0 < \delta < 0.05$ and treat this as an independent parameter. Then, in addition to \hat{q} and R_{th} , we must specify a range for $\cos \phi$.

In evaluating the result (87), we scan the theory input parameters in the ranges $0.197 < \hat{q} < 0.247$, $0.93 < R_{\text{th}} < 1.03$, $0 < \delta < 0.05$, and $0.8 < \cos \phi < 1$ (corresponding

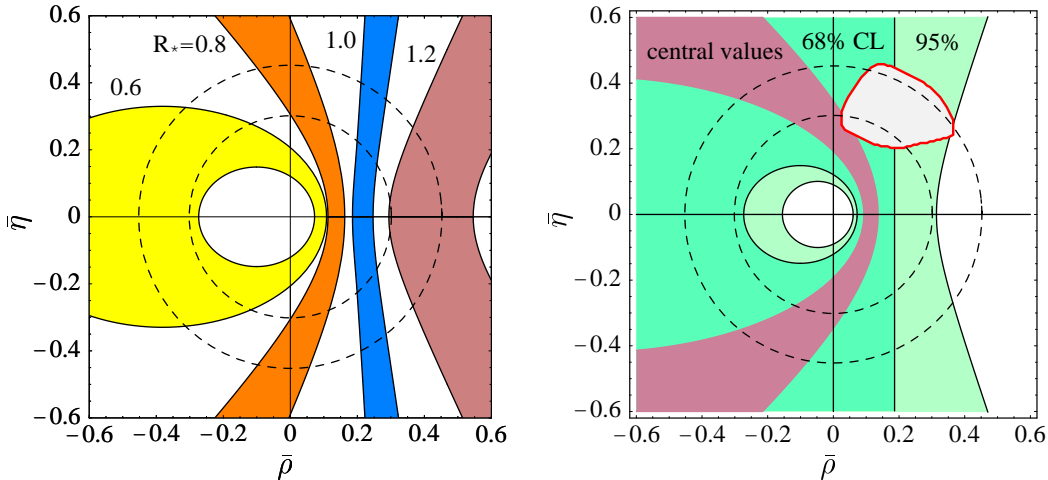


Figure 10: Left: Allowed regions in the $(\bar{\rho}, \bar{\eta})$ plane corresponding to $\varepsilon_{\text{exp}} = 0.22$ and different values of R_* as indicated. The widths of the bands reflect the total theoretical uncertainty, obtained by scanning the input parameters inside the ranges specified in the text. Right: Allowed regions at 68% and 95% confidence level obtained from the current experimental results on the branching ratios. The dark band shows the theoretical uncertainty for the central experimental values. The light gray area is the allowed region obtained from the standard global fit of the unitarity triangle [53].

to $|\phi| < 37^\circ$). The left-hand plot in Figure 10 shows the allowed regions in the $(\bar{\rho}, \bar{\eta})$ plane obtained for some representative values R_* and the current central value $\varepsilon_{\text{exp}} = 0.22$. We stress that with this method a useful constraint on the Wolfenstein parameters is obtained for any value of these parameters. When combined with a measurement of $|V_{ub}/V_{cb}|$, this determines the weak phase γ up to a sign ambiguity. Note that the theoretical accuracy of the method is high, especially if the ratio R_* turns out to be close to 1, corresponding to a value of γ as suggested by the global analysis of the unitarity triangle. In that case the theoretical uncertainty in the determination of γ is about 10° (for fixed value of $|V_{ub}/V_{cb}|$). Also, the resulting constraint is then very weakly dependent on the value of the parameter ε_{exp} . We stress that the width of the band in the $(\bar{\rho}, \bar{\eta})$ plane corresponding to $R_* = 1$ is narrower than the widths of the theoretical error bands corresponding to the “standard” constraints on the unitarity triangle derived from charmless semileptonic B decays, $B-\bar{B}$ mixing, and CP violation in $K-\bar{K}$ mixing. Only the measurement of $\sin 2\beta$ is theoretically cleaner. The uncertainty in the extraction of γ increases as one considers values of R_* significantly less than 0.8 or larger than 1.2. However, such values would be inconsistent with the global analysis of the unitarity triangle [50, 51, 52, 53] and thus provide evidence for physics beyond the Standard Model.

With the current values of the branching ratios collected in Table 7, the method proposed here is at the verge of providing a useful constraint in the $(\bar{\rho}, \bar{\eta})$ plane. This is shown in the right-hand plot in Figure 10, where we indicate the resulting allowed regions

at 68% and 95% confidence level and compare them with the allowed region (light gray area) obtained from the standard global fit of the unitarity triangle. Here and below we use the most recent result for the standard fit obtained in [53], which includes the measurements of $\sin 2\beta$ at the B -factories and adopts a conservative treatment of theoretical uncertainties that is similar in spirit to the one adopted here. In evaluating the 1σ and 2σ domains of the quantities R_* and ε_{exp} , we take into account the correlation implied by the fact that the $B^\pm \rightarrow \pi^\pm K^0$ branching ratio enters both quantities. Specifically, we vary the branching fractions for $B^\pm \rightarrow \pi^\pm \pi^0$, $\pi^\pm K^0$ and $\pi^0 K^\pm$ independently such that $\chi^2 \leq 1$ (for 1σ) or 4 (for 2σ). In this way we find that the minimum and maximum values of R_* at 95% confidence level are 0.47 and 1.07, respectively. If in the future the upper value can be reduced, the resulting allowed region in the $(\bar{\rho}, \bar{\eta})$ plane will no longer fully overlap with the standard domain.

5.4 Determination of $\sin 2\alpha$ from $B \rightarrow \pi^+ \pi^-$ decays

The methods described so far in this section provide constraints in the $(\bar{\rho}, \bar{\eta})$ plane that, in essence, correspond to a determination of the magnitude of $\gamma = \arg(V_{ub}^*)$. Independent information about the unitarity triangle can be obtained from a measurement of the time-dependent CP asymmetry in the decays $B^0, \bar{B}^0 \rightarrow \pi^+ \pi^-$, which is sensitive to the $B_d - \bar{B}_d$ mixing phase $e^{-2i\beta}$. We define

$$\begin{aligned} A_{\text{CP}}^{\pi\pi}(t) &= \frac{\text{Br}(B^0(t) \rightarrow \pi^+ \pi^-) - \text{Br}(\bar{B}^0(t) \rightarrow \pi^+ \pi^-)}{\text{Br}(B^0(t) \rightarrow \pi^+ \pi^-) + \text{Br}(\bar{B}^0(t) \rightarrow \pi^+ \pi^-)} \\ &= -S_{\pi\pi} \sin(\Delta m_B t) + C_{\pi\pi} \cos(\Delta m_B t), \end{aligned} \quad (89)$$

where

$$S_{\pi\pi} = \frac{2 \text{Im} \lambda_{\pi\pi}}{1 + |\lambda_{\pi\pi}|^2}, \quad C_{\pi\pi} = \frac{1 - |\lambda_{\pi\pi}|^2}{1 + |\lambda_{\pi\pi}|^2}, \quad \lambda_{\pi\pi} = e^{-2i\beta} \frac{e^{-i\gamma} + P_{\pi\pi}/T_{\pi\pi}}{e^{i\gamma} + P_{\pi\pi}/T_{\pi\pi}}. \quad (90)$$

The coefficient $C_{\pi\pi}$, which is a function of the weak phase γ , coincides with the direct CP asymmetry to be discussed later. The mixing-induced asymmetry $S_{\pi\pi}$ depends on γ and β . In fact, in the limit where $P_{\pi\pi}/T_{\pi\pi}$ is set to zero it follows that $\lambda_{\pi\pi} = e^{-2i(\beta+\gamma)} = e^{2i\alpha}$, and hence $S_{\pi\pi} = \sin 2\alpha$.

When the penguin contributions to the $B \rightarrow \pi\pi$ decay amplitudes are included, the relation between the coefficient $S_{\pi\pi}$ and $\sin 2\alpha$ receives hadronic corrections [8, 9, 10, 11], which can be calculated using the QCD factorization approach [14]. To illustrate the effect, we first assume that $|V_{ub}/V_{cb}|$ and the weak phase β have been determined accurately. Then using $\gamma = 180^\circ - \alpha - \beta$ the expression for $\lambda_{\pi\pi}$ in (90) becomes a function of α and our prediction for the penguin-to-tree ratio $P_{\pi\pi}/T_{\pi\pi}$. If we further assume that the unitarity triangle lies in the upper half of the $(\bar{\rho}, \bar{\eta})$ plane, then a measurement of $S_{\pi\pi}$ determines $\sin 2\alpha$ with at most a two-fold discrete ambiguity. Figure 11 shows the relation between the two quantities for the particular case where $|V_{ub}/V_{cb}| = 0.085$ and $\beta = 14.3^\circ$, corresponding to $\sin 2\beta = 0.48$ (the current world average is $\sin 2\beta = 0.48 \pm 0.16$ [55]).

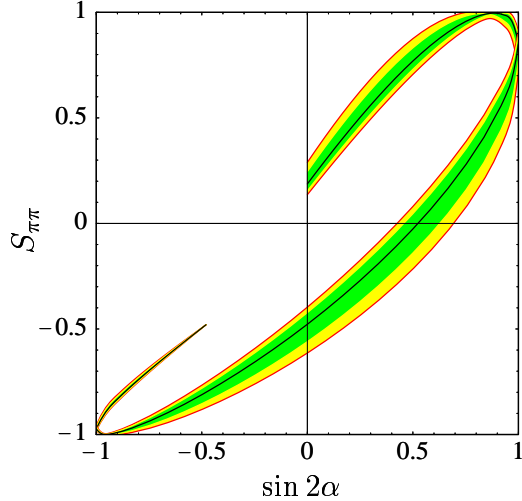


Figure 11: Relation between $\sin 2\alpha$ and the mixing-induced CP asymmetry $S_{\pi\pi}$, assuming $\sin 2\beta = 0.48$. The dark band reflects parameter variations of the first kind, the light band shows the total theoretical uncertainty. The lower portion of the band refers to values $45^\circ < \alpha < 135^\circ$, the upper one to $0 < \alpha < 45^\circ$ (right branch) or $135^\circ < \alpha < 180^\circ - \beta$ (left branch).

The dark band shows the theoretical uncertainty due to input parameter variations as specified in Table 2, whereas the light band indicates the total theoretical uncertainty including the effects of weak annihilation and twist-3 hard spectator interactions. We observe that for negative values $\sin 2\alpha$ as preferred by the global analysis of the unitarity triangle [51, 52, 53], a measurement of the coefficient $S_{\pi\pi}$ could be used to determine $\sin 2\alpha$ with a theoretical uncertainty of about ± 0.1 . Interestingly, for such values of $\sin 2\alpha$ the “penguin pollution” effect enhances the value of the mixing-induced CP asymmetry, yielding values of $S_{\pi\pi}$ between -0.5 and -1 . Such a large asymmetry should be relatively easy to observe experimentally.

Although it illustrates nicely the effect of “penguin pollution” on the determination of $\sin 2\alpha$, Figure 11 is not the most appropriate way to display the constraint on the unitarity triangle implied by a measurement of $S_{\pi\pi}$. In general, there is a four-fold discrete ambiguity in the determination of $\sin 2\alpha$, which we have reduced to a two-fold ambiguity by assuming that the triangle lies in the upper half-plane. Next, and more importantly, we have assumed that $|V_{ub}/V_{cb}|$ and β are known with precision, whereas α is undetermined. However, in the Standard Model $|V_{ub}/V_{cb}|$ and the angles α, β, γ are all functions of the Wolfenstein parameters $\bar{\rho}$ and $\bar{\eta}$. It is thus more appropriate to represent the constraint implied by a measurement of $S_{\pi\pi}$ as a band in the $(\bar{\rho}, \bar{\eta})$ plane. To this end, we write

$$e^{\mp i\gamma} = \frac{\bar{\rho} \mp i\bar{\eta}}{\sqrt{\bar{\rho}^2 + \bar{\eta}^2}}, \quad e^{-2i\beta} = \frac{(1 - \bar{\rho})^2 - \bar{\eta}^2 - 2i\bar{\eta}(1 - \bar{\rho})}{(1 - \bar{\rho})^2 + \bar{\eta}^2}, \quad \frac{P_{\pi\pi}}{T_{\pi\pi}} = \frac{r_{\pi\pi} e^{i\phi_{\pi\pi}}}{\sqrt{\bar{\rho}^2 + \bar{\eta}^2}}, \quad (91)$$

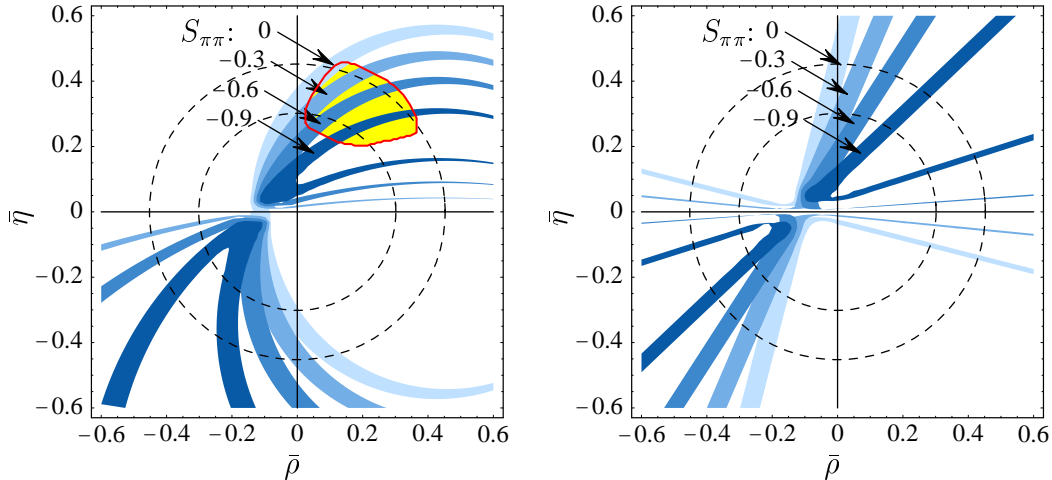


Figure 12: Allowed regions in the $(\bar{\rho}, \bar{\eta})$ plane corresponding to constant values of the mixing-induced asymmetry $S_{\pi\pi}$, assuming the Standard Model (left), and using a fixed value $\sin 2\phi_d = 0.48$ (and $\cos 2\phi_d > 0$) for the $B_d-\bar{B}_d$ mixing phase (right). The widths of the bands reflect the total theoretical uncertainty. The corresponding bands for positive values of $S_{\pi\pi}$ are obtained by a reflection about the $\bar{\rho}$ axis. The light circled area in the left-hand plot shows the allowed region obtained from the standard global fit of the unitarity triangle [53].

where $r_{\pi\pi} e^{i\phi_{\pi\pi}}$ parameterizes the large fraction in (24) without the prefactor $1/R_b$ and is thus independent of $\bar{\rho}$ and $\bar{\eta}$. We now insert these relations into (90) and draw contours of constant $S_{\pi\pi}$ in the $(\bar{\rho}, \bar{\eta})$ plane. The result is shown by the bands in the left-hand plot in Figure 12. The widths of the bands reflect the total theoretical uncertainty (including power corrections). For clarity we show only bands for negative values of $S_{\pi\pi}$; those corresponding to positive $S_{\pi\pi}$ values can be obtained by a reflection about the $\bar{\rho}$ axis (i.e., $\bar{\eta} \rightarrow -\bar{\eta}$). Note that even a rough measurement of $S_{\pi\pi}$ would translate into a rather narrow band in the $(\bar{\rho}, \bar{\eta})$ plane (this was also noted in [56]), which intersects the ring representing the $|V_{ub}/V_{cb}|$ constraint at almost right angle. This would therefore provide a very powerful constraint on the Wolfenstein parameters. We also stress that the sign of $S_{\pi\pi}$, when combined with a measurement of $|\gamma|$ (using, e.g., the method described in Section 5.3), can potentially determine whether the unitarity triangle lies in the upper or lower half-plane, and thus provide a nontrivial test of the CKM model of CP violation.

The strategy outlined above remains useful even in the hypothetical case where $B_d-\bar{B}_d$ mixing is affected by new physics beyond the Standard Model (this scenario has recently been discussed in [57, 58, 59, 60, 61]). Then the factor $e^{-2i\beta}$ in the expression for $\lambda_{\pi\pi}$ in (90) must be replaced with the mixing phase $e^{-2i\phi_d}$, where $\phi_d \neq \beta$ due to the presence of new physics. It is the value of $\sin 2\phi_d$ that is measured in the time-dependent

CP asymmetry in the decays $B^0, \bar{B}^0 \rightarrow J/\psi K_S$. From (90), we then obtain

$$\lambda_{\pi\pi}^{\text{NP}} = \left[\pm \sqrt{1 - \sin^2 2\phi_d} - i \sin 2\phi_d \right] \frac{\bar{\rho} - i\bar{\eta} + r_{\pi\pi} e^{i\phi_{\pi\pi}}}{\bar{\rho} + i\bar{\eta} + r_{\pi\pi} e^{i\phi_{\pi\pi}}}, \quad (92)$$

which still implies a constraint in the $(\bar{\rho}, \bar{\eta})$ plane for each pair of experimental values $S_{\pi\pi}$ and $\sin 2\phi_d$. The \pm sign refers to the sign of $\cos 2\phi_d$. The result obtained for $\sin 2\phi_d = 0.48$ is shown in the right-hand plot in Figure 12. In the figure we assume that $\cos 2\phi_d > 0$; the resulting bands for $\cos 2\phi_d < 0$ are, once again, obtained by a reflection about the $\bar{\rho}$ axis. We observe that the bands in the first quadrant of the $(\bar{\rho}, \bar{\eta})$ plane intersect the rings from the $|V_{ub}/V_{cb}|$ constraint at almost the same places as in the Standard Model case, implying that for $S_{\pi\pi} < 1$ (and $\cos 2\phi_d > 0$) potential new physics effects in $B_d\text{-}\bar{B}_d$ mixing have a minor impact on the results. On the other hand, the impact would be significant if $S_{\pi\pi}$ turned out to be positive.

5.5 Predictions for CP-averaged branching ratios

Whereas so far in this section we have focused on methods that require minimal input from the QCD factorization approach, we now discuss in detail our theoretical predictions for the $B \rightarrow \pi K, \pi\pi$ branching ratios. These predictions follow from the theory described in this work without relying on further phenomenological input. All branching fractions discussed in this section are averaged over CP-conjugate modes (even though for neutral K and B mesons this is not indicated by the notation). We use $\tau_{B^+} = 1.65$ ps and $\tau_{B^0} = 1.56$ ps for the B -meson lifetimes.

Absolute predictions for branching fractions

Two out of the seven decay modes, $B^\pm \rightarrow \pi^\pm \pi^0$ and $B^\pm \rightarrow \pi^\pm K^0$, are (almost) independent of the CKM phase γ , since the corresponding decay amplitudes have to a very good approximation only a single weak phase. The predicted branching fractions for these modes are (setting $\gamma = 55^\circ$ for concreteness)

$$10^6 \text{Br}(B^\mp \rightarrow \pi^\mp \pi^0) = \left[5.3_{-0.4}^{+0.8} (\lambda_B, \alpha_2^\pi) \pm 0.3 (X_H) \right] \times \left[\frac{|V_{ub}|}{0.0035} \frac{F_0^{B \rightarrow \pi}(0)}{0.28} \right]^2, \\ 10^6 \text{Br}(B^\mp \rightarrow \pi^\mp \bar{K}^0) = \left[14.1_{-4.0}^{+6.4} (m_s) \pm 8.1_{-3.6} (X_A) \right] \times \left[\frac{F_0^{B \rightarrow \pi}(0)}{0.28} \right]^2, \quad (93)$$

where the first error is due to parameter variations as shown in Table 2, whereas the second one accounts for the uncertainty due to power corrections from weak annihilation and twist-3 hard spectator contributions. The dominant contributions to the uncertainty are shown in parentheses. Note that the decays $B^\pm \rightarrow \pi^\pm \pi^0$ do not receive weak annihilation contributions. The $B^\pm \rightarrow \pi^\pm K^0$ branching ratio is to a good approximation proportional to $(m_s/110 \text{ MeV})^{-1.35}$. The largest uncertainty for the $\pi^\pm \pi^0$ final state is a 50% normalization uncertainty from the current errors on $|V_{ub}|$ and the $B \rightarrow \pi$ form

factor. The systematics of theoretical errors is different for the πK final states. Their absolute branching fractions are (approximately) proportional to the square of the penguin amplitude $a_4 + r_\chi^K a_6 + r_A b_3$, which is sensitive to the penguin annihilation coefficient b_3 (see the left-hand plot in Figure 6). The dominant theoretical errors therefore come from the annihilation parameter X_A and from the strange-quark mass (through r_χ^K). The theoretical errors detailed here are characteristic for the absolute branching fractions of all $\pi\pi$ and πK final states, respectively.

The central values in (93) agree well with the current data summarized in Table 7. In particular, we find that the QCD factorization approach prefers large branching fractions for the πK final states. This arises due to an enhancement of the QCD penguin amplitude relative to naive factorization. Weak annihilation contributions play only a minor role in this enhancement. Without annihilation the $B^\pm \rightarrow \pi^\pm K^0$ branching fraction would be reduced to 12.1×10^{-6} . Hence the effect is not negligible, but there is no need for a largely enhanced annihilation contribution (this is in contrast to the findings of [17]). In fact, the good agreement of our prediction with the data provides circumstantial evidence against the idea that annihilation effects could be much enhanced with respect to our estimates. For instance, increasing the parameter ϱ_A in (72) from 1 to 2 would increase the corresponding error on the branching ratio from ${}_{-3.6}^{+8.1}$ to ${}_{-9.2}^{+26.4}$, in which case it would require considerable fine-tuning of the strong-interaction phase of X_A to reproduce the experimental value of the branching ratio.

It has also been suggested in the literature that one needs a large enhancement from penguin diagrams with a charm loop (so-called “charming penguins”) to understand the overall πK branching fractions [62]. The leading perturbative contribution from the penguin diagrams in Figure 3, however, turns out to be very small. There exists also a power-suppressed contribution from these diagrams, when one of the quarks the gluon decays into becomes soft. In this case, the gluon is “semi-hard” and probes the charm-quark loop at a scale of order $\mu_h \sim (\Lambda_{\text{QCD}} m_b)^{1/2}$. The penguin function $G(s, x)$ in (56) tends to a constant for small x , which implies that the contribution from the semi-hard region to the function $G_K(s)$ in (55) is suppressed by two (not one!) powers of the heavy-quark mass relative to the leading perturbative contribution. Hence, although the strong coupling constant in the semi-hard region is larger than $\alpha_s(m_b)$, a large nonperturbative enhancement of the charm-penguin contribution appears implausible. (It is possible to obtain a first-order power correction by invoking a higher Fock component in the wave function of the emission meson, as discussed in [15]. However, in this case the penguin loop continues to be a hard subprocess, and so contributes a factor of $\alpha_s(m_b)$.) In a recent article [63] a non-perturbative charming penguin contribution has been fitted to experimental data under the assumption that this effect is responsible for any deviation of the measured branching fractions from those expected within the Standard Model with $\bar{\rho}$ and $\bar{\eta}$ determined by the standard unitarity-triangle fit. It is worth noting that such a fit is technically equivalent to fitting the annihilation contribution to the QCD penguin amplitude, indirectly related to X_A [eq. (72)] in our notation. If a modification of this amplitude were required (for which the present data does not provide strong motivation, as will become more evident below), we would attribute its physical origin

to weak annihilation rather than charm penguins, given the power-counting detailed above.

In Figure 13, we show the dependence of the absolute branching fractions of the various $B \rightarrow \pi K, \pi\pi$ decay modes (except for $B^\pm \rightarrow \pi^\pm\pi^0$) on the weak phase γ . In each plot, the solid line gives the central prediction of the QCD factorization approach at next-to-leading order in α_s . For comparison, the short-dashed line shows the result at leading order, corresponding to naive factorization. The dark-shaded band is obtained by varying all input parameters as specified in Table 2, and by varying the renormalization scale between $m_b/2$ and $2m_b$. It also includes the uncertainties due to the errors on the CKM parameters $|V_{ub}/V_{cb}| = 0.085 \pm 0.017$ and $|V_{cb}| = 0.041 \pm 0.003$. The variation due to $|V_{ub}/V_{cb}|$ alone is indicated by the long-dashed lines. The light-shaded band adds to this the uncertainties inherent to our modelling of power corrections due to twist-3 hard spectator and weak annihilation corrections, as discussed in Sections 4.2 and 4.3. The annihilation contributions dominate the uncertainty in all cases (see Figure 7). They imply a considerable uncertainty in the overall normalization of the πK modes. For the purposes of our discussion here the different sources of theoretical uncertainty are added in quadrature. Later, when our focus is on constraining CKM parameters, we will be more conservative and scan over the entire theory parameter space (corresponding to linear addition of errors).

The next-to-leading order effects included in the QCD factorization approach significantly enhance the branching fractions for the $B \rightarrow \pi K$ modes with respect to their values obtained in the naive factorization model. No such enhancement occurs for the decays $B^0 \rightarrow \pi^+\pi^-$ and $B^\pm \rightarrow \pi^\pm\pi^0$. As a result, the empirical finding that $B \rightarrow \pi K$ branching ratios are larger than the $B \rightarrow \pi\pi$ branching ratios is reproduced in our approach without any tuning of parameters.

Predictions for ratios of branching fractions

The uncertainty in the overall magnitude of the penguin amplitude due to weak annihilation effects, and the overall scale uncertainty in the predictions for the branching fractions due to hadronic form factors and CKM elements, are largely eliminated by taking ratios of branching fractions. The dependence of the six relevant ratios on the weak phase γ is displayed in Figure 14, in which the curves and bands have the same interpretation as in the previous figure. (The results presented here are consistent with the preliminary results published in [16], which did not include annihilation contributions. However, the treatment of theoretical uncertainties in [16] differs from the present work.) Table 8 gives numerical predictions and theoretical uncertainties for some selected values of the angle γ . It is evident that annihilation effects are less important for the ratios. The small error on the ratios involving πK final states shows the potential of these ratios to constrain γ . Comparing our results with the preliminary experimental data collected in Tables 7 and 8 (and shown by the horizontal bands), we note a preference for large values of γ ; however, the experimental errors are still too large to assign much significance to this observation.

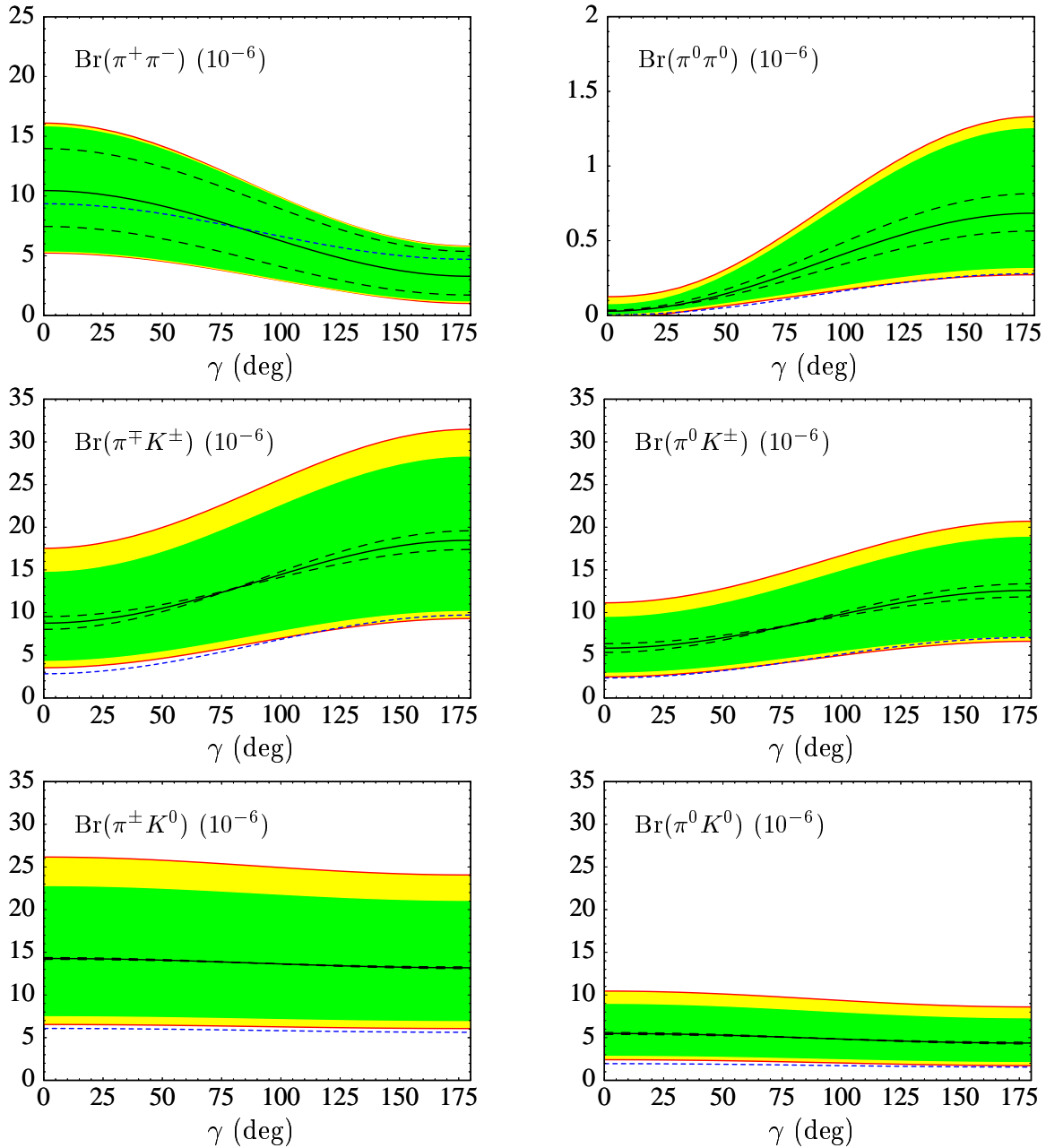


Figure 13: Absolute CP-averaged branching fractions as functions of γ . Central values are shown by the solid line. The inner (dark) band corresponds to the variation of the theory input parameters (including $|V_{ub}/V_{cb}|$), whereas the outer (light) band also includes the uncertainty from weak annihilation and twist-3 hard spectator contributions (see text for details). The long-dashed lines indicate the sensitivity to $|V_{ub}/V_{cb}|$. The short-dashed curve shows the result obtained using naive factorization.

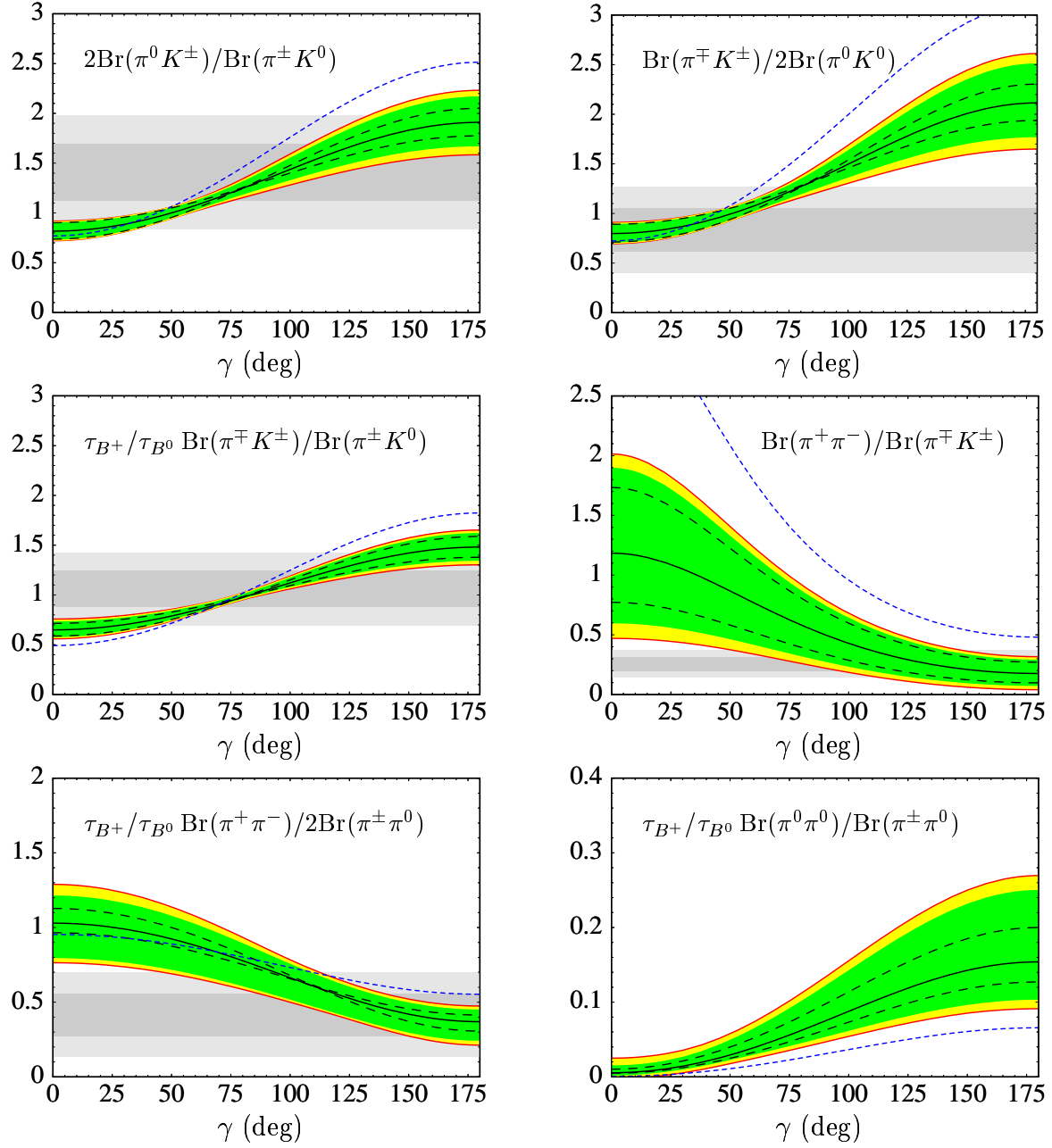


Figure 14: Ratios of CP-averaged branching fractions as functions of γ . The meaning of the curves and bands is the same as in Figure 13. The horizontal bands show the 1σ and 2σ error bands for the current experimental results.

Table 8: Predicted ratios of CP-averaged branching fractions for selected values of γ . The last column shows the experimental values deduced from Table 7. Our averages ignore correlations between the individual measurements.

| Ratio | 40° | 70° | 100° | 130° | Experiment |
|---|-----------------|-----------------|-----------------|-----------------|-----------------|
| $\frac{2\text{Br}(\pi^0 K^\pm)}{\text{Br}(\pi^\mp K^0)}$ | 0.94 ± 0.07 | 1.16 ± 0.07 | 1.44 ± 0.16 | 1.70 ± 0.25 | 1.41 ± 0.29 |
| $\frac{\text{Br}(\pi^\mp K^\pm)}{2\text{Br}(\pi^0 K^0)}$ | 0.92 ± 0.08 | 1.17 ± 0.08 | 1.50 ± 0.19 | 1.83 ± 0.34 | 0.83 ± 0.22 |
| $\frac{\tau_{B^+}}{\tau_{B^0}} \frac{\text{Br}(\pi^\mp K^\pm)}{\text{Br}(\pi^\pm K^0)}$ | 0.74 ± 0.07 | 0.91 ± 0.04 | 1.12 ± 0.07 | 1.32 ± 0.12 | 1.06 ± 0.18 |
| $\frac{\text{Br}(\pi^+\pi^-)}{\text{Br}(\pi^\mp K^\pm)}$ | 0.96 ± 0.60 | 0.67 ± 0.38 | 0.43 ± 0.25 | 0.27 ± 0.18 | 0.26 ± 0.06 |
| $\frac{\tau_{B^+}}{\tau_{B^0}} \frac{\text{Br}(\pi^+\pi^-)}{2\text{Br}(\pi^\pm\pi^0)}$ | 0.96 ± 0.25 | 0.83 ± 0.20 | 0.66 ± 0.15 | 0.50 ± 0.13 | 0.42 ± 0.14 |

An important remark in this context concerns the ratio involving the neutral mode $B^0 \rightarrow \pi^0 K^0$, which seems to prefer a small value of γ . Our theoretical results indicate that to a good approximation (compare the two plots in the first row in Figure 14)

$$\frac{2\text{Br}(B^\pm \rightarrow \pi^0 K^\pm)}{\text{Br}(B^\pm \rightarrow \pi^\pm K^0)} \approx \frac{\text{Br}(B^0 \rightarrow \pi^\mp K^\pm)}{2\text{Br}(B^0 \rightarrow \pi^0 K^0)}. \quad (94)$$

This relation is in slight disagreement (albeit by no more than 2σ) with present data. Some authors have interpreted this fact as an indication of large rescattering phases (see, e.g., [64]). However, the validity of (94) is a model-independent consequence of isospin symmetry, which is valid to linear order in the small tree-to-penguin ratios [4]. Therefore, we expect that with more precise data the values of the two ratios in (94) will come closer to each other.

Finally, we wish to stress that the difference between the QCD factorization results and naive factorization are largest for the ratio of the $\pi^+\pi^-$ and $\pi^\mp K^\pm$ final states. Whereas we can accommodate the low experimental value of this ratio for $\gamma > 50^\circ$ (at the 2σ level), this would not be possible for any value of γ if one were to use the naive factorization model.

It is evident from Figure 14 that in many cases the error on $|V_{ub}/V_{cb}|$ constitutes one of the largest uncertainties in the predictions for the ratios of branching fractions. This is true, in particular, for the interesting ratio of the $\pi^+\pi^-$ and $\pi^\pm K^\mp$ final states. For instance, if $|V_{ub}/V_{cb}|$ is 20% lower than its current central value, then our prediction for the $B^0 \rightarrow \pi^+\pi^-$ branching ratio is reduced by 40%, whereas the result for the $B^0 \rightarrow \pi^\mp K^\pm$ branching fraction remains almost unaffected. This shows that for future analyses of rare B decays it will be important to reduce the theoretical uncertainty in the value of $|V_{ub}|$.

We can unfold the strong dependence of the ratios on $|V_{ub}/V_{cb}|$ by presenting the predictions for the branching fractions as functions of the Wolfenstein parameters $\bar{\rho}$ and

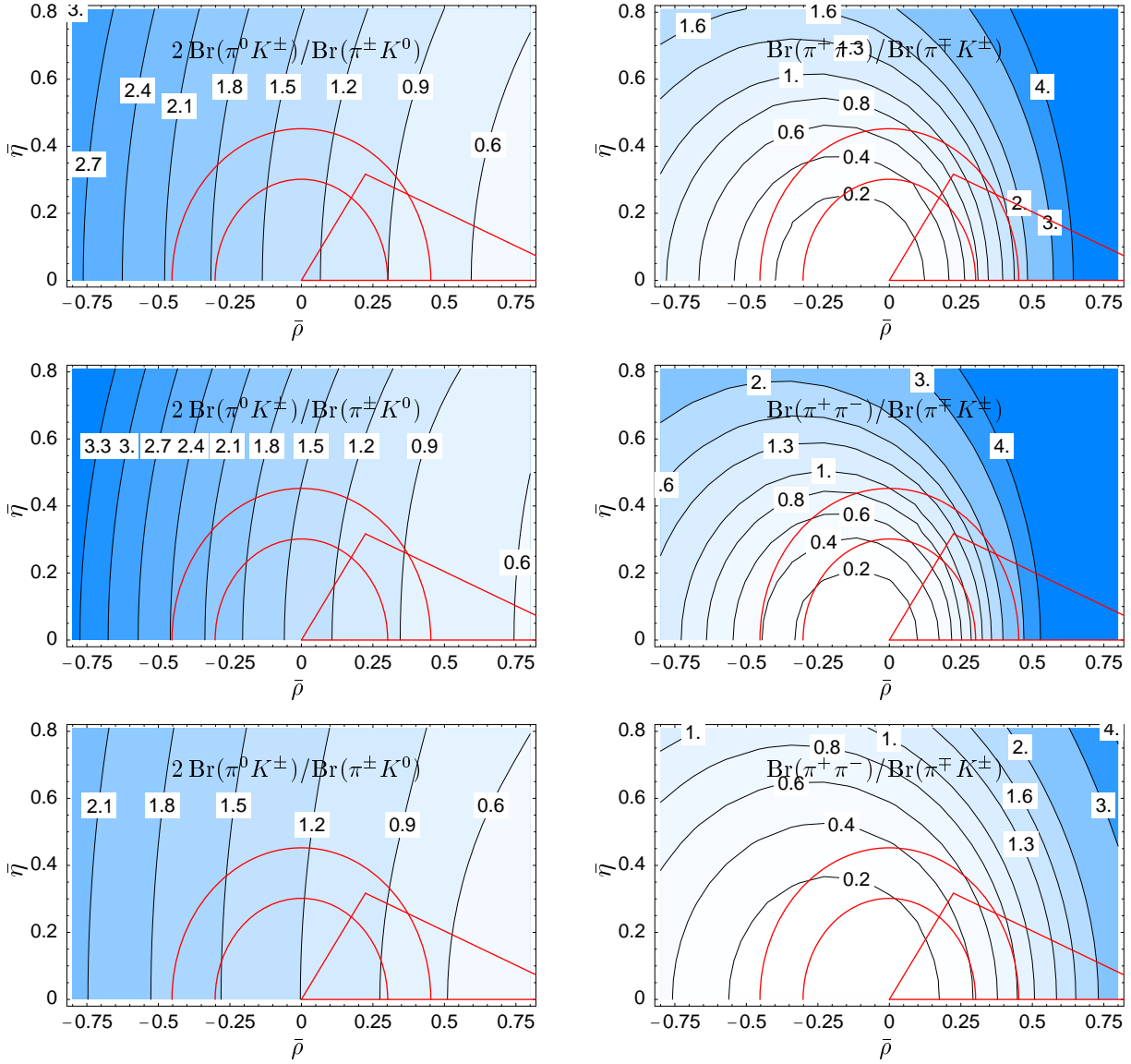


Figure 15: Two ratios of CP-averaged branching fractions as functions of the Wolfenstein parameters $\bar{\rho}$ and $\bar{\eta}$. The upper row corresponds to our central values; the middle (lower) row corresponds to the upper (lower) theoretical value including all uncertainties. We only show the upper half-plane ($\bar{\eta} > 0$). The current standard best-fit unitarity triangle and the annulus given by $|V_{ub}/V_{cb}|$ are overlaid to guide the eye.

$\bar{\eta}$. This is illustrated in Figure 15 for the two cases of the ratios $2\text{Br}(\pi^0 K^\mp)/\text{Br}(\pi^\mp \bar{K}^0)$ and $\text{Br}(\pi^+\pi^-)/\text{Br}(\pi^\pm K^\mp)$. The other two ratios involving πK final states exhibit a dependence similar to the first of these two examples. For not too large values of $\bar{\eta}$, any of the three ratios involving only πK final states is a direct measure of $\bar{\rho}$, since the dominant dependence on the CKM parameters arises from $\epsilon_{\text{KM}} \cos \gamma = \tan^2 \theta_C \bar{\rho}$. For positive $\bar{\rho}$ the theoretical uncertainty is relatively small, as can be deduced by comparing the three panels of Figure 15 that refer to $2\text{Br}(\pi^0 K^\mp)/\text{Br}(\pi^\mp \bar{K}^0)$. (Note that the contour lines in this plot do not coincide with those of constant R_*^{-1} inferred from Figure 10, since there the parameter $\epsilon_{3/2}$ is assumed to be fixed and extracted from data, whereas here it is determined from theory and hence proportional to $|V_{ub}/V_{cb}|$.) The ratio $\text{Br}(\pi^+\pi^-)/\text{Br}(\pi^\mp K^\pm)$ exhibits a rather different behaviour. The circular contours reflect the increase of the $\pi^+\pi^-$ branching fraction with $|V_{ub}|$. The offset of the center to negative values of $\bar{\rho}$ results from the interference of the two contributions with different weak phases to the decay amplitudes, which for $\bar{\rho} > 0$ is constructive (destructive) for the $\pi\pi$ (πK) final states (and vice versa for $\bar{\rho} < 0$).

The current experimental values for the CP-averaged branching fractions are still afflicted by large errors, so a fit of $(\bar{\rho}, \bar{\eta})$ to these ratios may appear premature. Nonetheless, it is useful to carry out such an analysis at the present stage, not only to exhibit its potential once the errors decrease, but also to gauge the limitations eventually set by the theoretical uncertainties. Figure 16 shows the results separately for each of the five ratios of CP-averaged branching fractions that have been measured so far. Consider first the dark-shaded band in each plot, which covers the region allowed by theory given the current central experimental value. The light-shaded bands in Figure 16 represent the theoretically allowed regions obtained by using experimental values for the ratios shifted up or downwards by two standard deviations. Hence, the width of each band thus reflects the (largely irreducible) theory uncertainty given a certain value of the observable, while the current constraint on $\bar{\rho}$ and $\bar{\eta}$ provided by each observable separately can roughly be taken to be the entire region bounded by the two light-shaded bands.

Global fit in the $(\bar{\rho}, \bar{\eta})$ plane

The information from all CP-averaged $B \rightarrow \pi K, \pi\pi$ branching fractions (and, in the future, from the corresponding CP asymmetries) can be combined into a single global fit, giving regions for the Wolfenstein parameters $\bar{\rho}$ and $\bar{\eta}$ that are allowed by theory. We will now determine these regions, using two slightly different treatments of theoretical uncertainties. Because our focus is to determine fundamental parameters of the Standard Model, we adopt a more conservative error analysis than in the previous paragraphs of this section and scan all theory input parameters over their respective ranges of uncertainty (rather than adding theoretical uncertainties in quadrature). The same conservative treatment was used in the analysis of the weak phase γ in Section 5.3.

It is evident from our previous discussion that ratios of CP-averaged branching fractions provide the most powerful constraints on the Wolfenstein parameters, since they are afflicted with relatively small theoretical uncertainties. However, there are two reasons

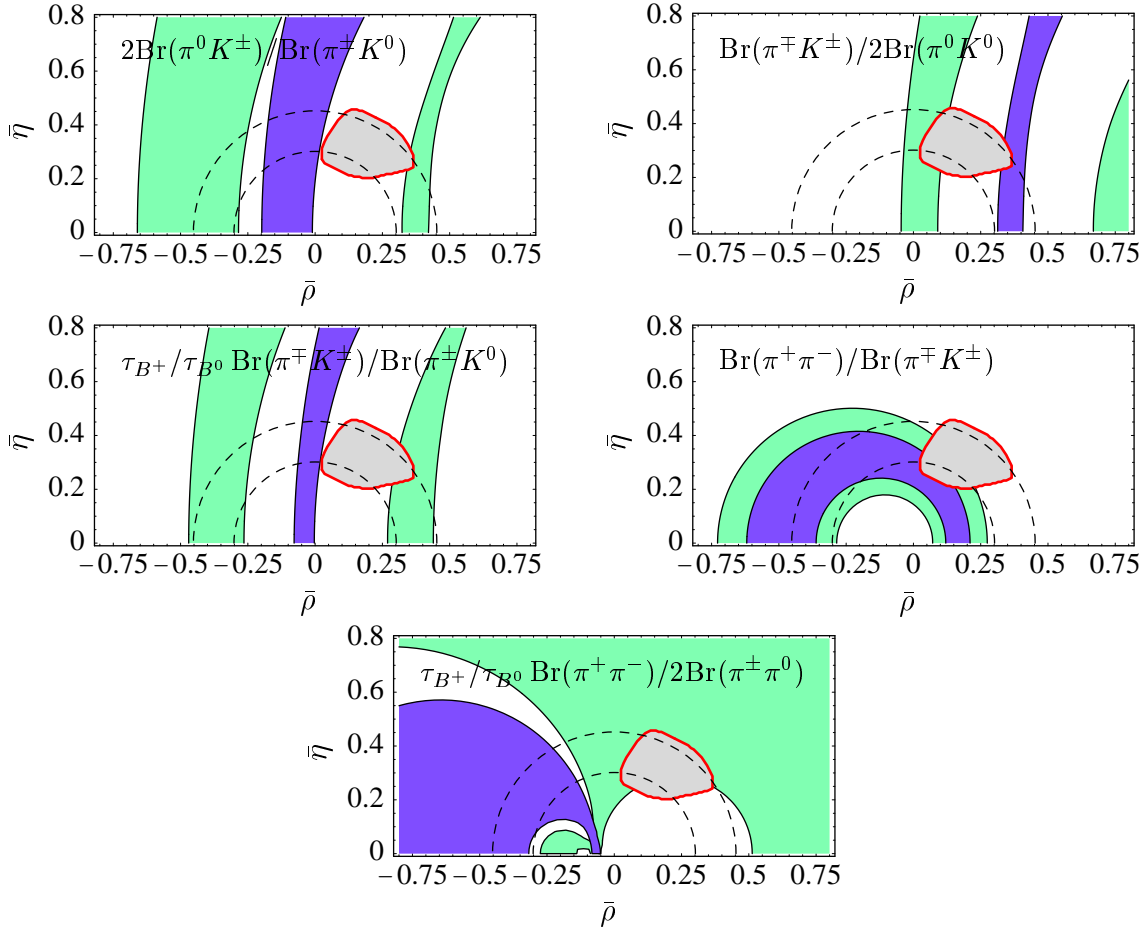


Figure 16: Regions in the $(\bar{\rho}, \bar{\eta})$ plane allowed by theory given the current central experimental values of the ratios of branching fractions (dark bands), and the experimental values $\pm 2\sigma$ standard deviations (light bands). Only the upper half-plane ($\bar{\eta} > 0$) is shown. The dashed circles indicate the allowed region implied by the measurement of $|V_{ub}/V_{cb}|$ in semileptonic B decays. The light circled area shows the allowed region obtained from the standard global fit of the unitarity triangle [53].

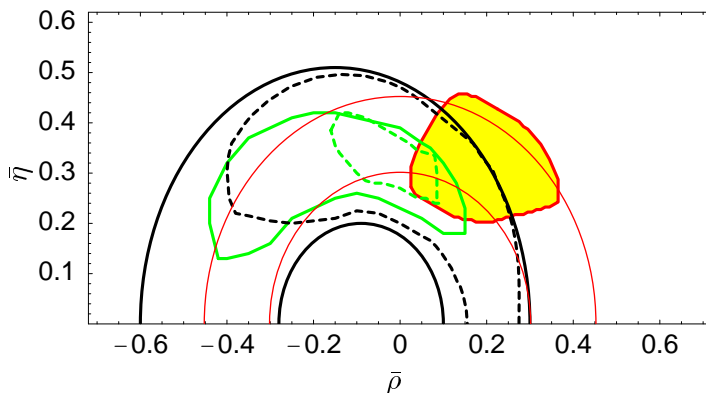


Figure 17: 95% confidence region in the $(\bar{\rho}, \bar{\eta})$ plane obtained from a fit to the CP-averaged $B \rightarrow \pi K, \pi\pi$ branching fractions. The dark curve gives the envelope of the 95% confidence level contours, the lighter curve the envelope of the set of χ^2_{\min} points. Here the solid lines refer to a cut on the χ^2_{\min} value, which corresponds to a 5% confidence level of the fit for a given model. The dashed lines refer to all models which have a χ^2_{\min} per degree of freedom of less than 1. See text for further explanations.

for not performing a global fit to the ratios directly (see also the discussion in Appendix C of [53]): first, with the present large experimental errors there are significant differences in the results of the fit depending on whether the ratios or inverse ratios are used, leading to an element of arbitrariness; secondly, even if two quantities have gaussian errors, their ratio does not. It is therefore preferable to perform the global fit for the individual branching ratios, despite the fact that the predictions for the branching fractions have larger (and correlated) theoretical uncertainties.

We now present two versions of such a fit. In the first method, we find the allowed region from $\bar{\rho}$ and $\bar{\eta}$ by determining first the 95% confidence level contour for a given theoretical input, and then scanning over all models in the theory parameter space that survive a 5% confidence cut. The theory parameter space is given by the set of all input parameters confined to the ranges specified in Table 2, variation of the renormalization scale μ between $m_b/2$ and $2m_b$, and scanning of the parameters X_H and X_A in the ranges described in (71) and (72). The resulting 95% confidence region is bounded by the dark solid lines in Figure 17. The grey solid line inside this region envelopes the set of χ^2_{\min} points of all models that pass the 5% confidence cut. The dashed dark and grey lines have the same interpretation except that only theory models with a χ^2_{\min} per degree of freedom of less than 1 are selected. The $(\bar{\rho}, \bar{\eta})$ range so determined is compared with the standard CKM fit (also at 95% confidence level) [53], which uses information from semileptonic B decays ($|V_{ub}|$ and $|V_{cb}|$), $K-\bar{K}$ mixing (ϵ_K), and $B-\bar{B}$ mixing (Δm_{B_d} , Δm_{B_s} , and $\sin 2\beta$). The constraint corresponding to $|V_{ub}/V_{cb}| = 0.085 \pm 0.017$ is indicated by the solid annulus.

A fit to CP-averaged branching fractions cannot distinguish between $\bar{\eta}$ and $-\bar{\eta}$, and so

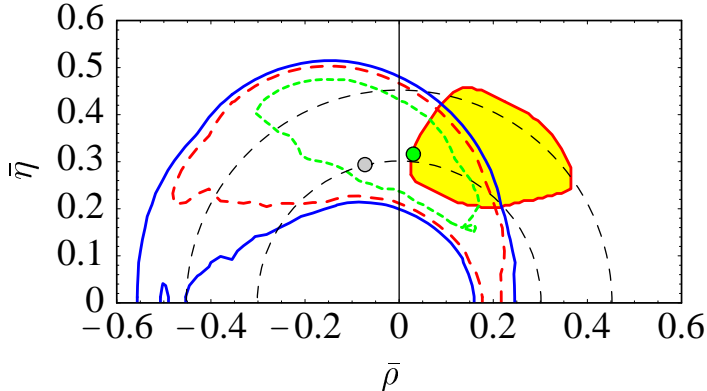


Figure 18: 95% (solid), 90% (dashed) and 68% (short-dashed) confidence level contours in the $(\bar{\rho}, \bar{\eta})$ plane obtained from a global fit to the CP-averaged $B \rightarrow \pi K, \pi\pi$ branching fractions, using the scanning method of [53]. The dark dot shows the overall best fit, whereas the light dot indicates the best fit for the default parameter set. See text for further explanations.

for simplicity only the upper half of the $(\bar{\rho}, \bar{\eta})$ plane is shown in the figure. At present our contours are symmetric about the $\bar{\rho}$ axis. In the future, data on direct CP asymmetries in the various $B \rightarrow \pi K, \pi\pi$ modes should be included in the fit, in which case it will become possible to obtain information about the sign of $\bar{\eta}$.

Before interpreting the results of this analysis, we discuss a second method for performing the global fit, which follows the strategy outlined in [53]. It differs from the method explained above in two ways. First, the large overall scale uncertainty (of almost 40%) due to the error on the value of the form factor $F_0^{B \rightarrow \pi}(0)$, which is common to the theoretical predictions for all branching fractions (see, e.g., (93)), is eliminated by fitting the form factor to the data. In that way, the sensitivity to the Wolfenstein parameters is increased in the same way as it would be by using ratios; however, the statistical problems of using ratios (see above) are avoided. Specifically, we start from the χ^2 function

$$\chi^2(S) = \sum_i \left(\frac{E_i - S T_i}{\sigma_i} \right)^2, \quad (95)$$

where E_i are the experimental values for the branching ratios, σ_i are their errors, and T_i are the corresponding theoretical predictions obtained with the fixed form factor $F_0^{B \rightarrow \pi}(0) = 0.28$. The scale factor S parameterizes the deviations of the product $(F_0^{B \rightarrow \pi}(0) |V_{cb}|)^2$ from its central value. For a given set of theory parameters, we determine

$$S = \frac{\sum_i E_i T_i / \sigma_i^2}{\sum_i (T_i / \sigma_i)^2} \quad (96)$$

such that $\chi^2(S)$ is minimized, provided that the value of S is allowed by the theory ranges for the form factor (see Table 2) and $|V_{cb}|$. For most choices of theory parameters this condition is satisfied. If it is not, we choose the value of S inside the allowed range

that is closest to the optimal value in (96). Next, we scan over all theory parameters and determine the global minimum of χ^2 in the $(\bar{\rho}, \bar{\eta})$ plane. We then plot contours of constant $\Delta\chi^2 = \chi^2 - \chi_{\min}^2$ corresponding to the 68%, 90% and 95% confidence levels. The second difference with respect to our first scanning method is that these contours refer to a constant χ^2 , whereas in the first method the χ^2 is different for each of the theory models considered. The results of this analysis are shown in Figure 18. The best fit has an excellent $\chi^2 = 2.1$ (for 3 degrees of freedom), corresponding to a confidence level of 54%. The parameters of the particular theory model corresponding to this fit are all very reasonable. In particular, the quantity X_A parameterizing the weak annihilation terms is even smaller in magnitude than our default value. Hence, a good global fit to the data can be obtained without using extreme choices of input parameters, or invoking phenomenological recipes such as largely enhanced annihilation or charm-penguin contributions. The default parameter set in Table 2 also yields a good fit, which has $\chi^2 = 4.57$ and 21% confidence level. Note that at 90% confidence level the allowed range obtained by combining our results with the measurement of $|V_{ub}/V_{cb}|$ in semileptonic B decays excludes $\bar{\eta} = 0$, thus establishing the existence of a CP-violating phase in $b \rightarrow u$ transitions.

The results of the two scanning methods shown in Figures 17 and 18 are similar (though the range obtained in the first method is somewhat more conservative). The allowed region for $\bar{\rho}$ and $\bar{\eta}$ obtained from our analysis of rare hadronic B decays is compatible with the standard global fit using information from semileptonic B decays, $K-\bar{K}$ mixing and $B-\bar{B}$ mixing. However, the best fits to the rare-decay branching fractions prefer a larger value of γ (of about 90°). This has been noted by many other authors in the past, usually based on the naive factorization approximation and without a theoretical error estimate. Here we have put this analysis on a firmer theoretical footing. On the other hand, we see that small values of γ are also allowed, provided the value of $|V_{ub}|$ is lower than its standard central value. Combining our results with the standard fit would reduce the allowed region in the $(\bar{\rho}, \bar{\eta})$ plane by about a factor 2, indicating that even with present experimental (and theoretical) errors the information obtained from rare hadronic decays provides important constraints on the Wolfenstein parameters.

It will be interesting to follow how the comparison of the standard fit and the fit to rare hadronic B decays will develop as the data become more precise. If the two fits remain consistent with each other even as the allowed regions shrink in size, this would constitute a highly nontrivial test of the CKM model, in which for the first time the phase of the V_{ub} matrix element (which enters through tree-penguin interference) is restricted by both direct and indirect measurements. If, on the other hand, the two regions would not overlap at a reasonable confidence level, this may suggest that the standard theory of weak interactions does not account completely for either the $B-\bar{B}$ mixing amplitude (since this is what determines the left-most side of the allowed region in the standard fit) or the loop-induced flavour-changing amplitudes in $B \rightarrow \pi K, \pi\pi$ decays. (Another option would be to abandon the theoretical framework advocated here, but we understandably leave it to others to pursue this avenue.)

5.6 Predictions for CP asymmetries

The QCD factorization approach predicts the strong-interaction phases and hence the direct CP asymmetries in the heavy-quark limit. In the following, we define the asymmetries as

$$A_{\text{CP}}(f) = \frac{\text{Br}(B \rightarrow f) - \text{Br}(\bar{B} \rightarrow \bar{f})}{\text{Br}(B \rightarrow f) + \text{Br}(\bar{B} \rightarrow \bar{f})}, \quad (97)$$

where $\bar{B} = \bar{B}^0, B^-$ contains a b quark (rather than antiquark). The dependence of the CP asymmetries on the weak phase γ is displayed in Figure 19. The asymmetries are typically predicted to be small, concurrent with the fact that strong-interaction phases are suppressed in the heavy-quark limit [14]. Even the largest asymmetries for the πK final states are predicted to be of order 10% or less. An exception to this rule is the final state $f = \pi^0\pi^0$, for which the asymmetry is sensitive to QCD penguins and to the coefficient a_2 , both of which have large uncertainties and a potentially large relative phase.

While our approach predicts the generic magnitude of the CP asymmetries, their precise values remain uncertain. This is not surprising, since in contrast to the branching ratios the asymmetries are more sensitive to – and in fact generated by – corrections to naive factorization. Hence, they are subject to larger relative uncertainties. In particular, the CP asymmetries are proportional to the sines of strong-interaction phases, which are of order $\alpha_s(m_b)$ or Λ_{QCD}/m_b . Only the leading perturbative contributions to these phases are calculable. On the contrary, the CP-averaged branching fractions depend on the cosines of strong-interaction phases, which are equal to 1 in the heavy-quark limit.

First measurements of CP asymmetries have been published by the CLEO [65] and Belle [49] Collaborations. All results are compatible with no asymmetry, with typical 1σ errors of about 20%. These errors are not yet small enough to draw meaningful conclusions, except that very large asymmetries appear already improbable. In the future, accurate measurements of CP asymmetries will test the generic prediction of the QCD factorization approach that strong-interaction phases are small. If this prediction is confirmed, further analysis of the CP asymmetries should help to determine the sign of γ , which cannot be probed using CP-averaged branching fractions. In addition, data on CP asymmetries may help to further constrain annihilation contributions and other theoretical input parameters in the QCD factorization approach.

6 Comparison with other work

A general overview of the various approaches to the evaluation of the matrix elements in exclusive hadronic B decays has been given in [15]. In that reference we have commented on the strategies and methods that had been employed previously and explained how they are related to QCD factorization. In this section we discuss recent papers on the subject and clarify the differences with our work. We divide these papers into four categories: those using our QCD factorization formalism, those using a perturbative PQCD approach, those in which nonperturbative effects are estimated using light-cone

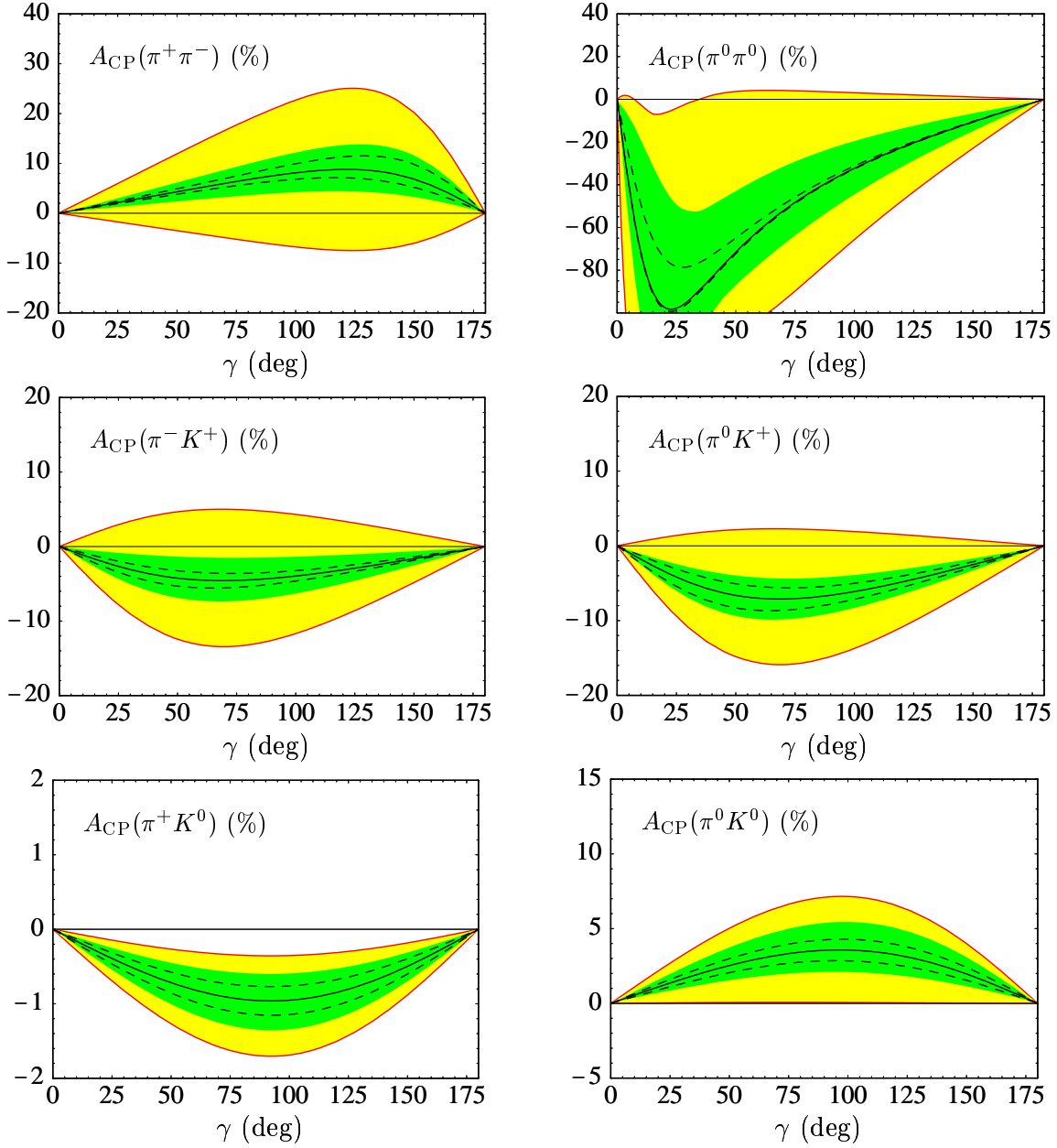


Figure 19: Direct CP asymmetries as functions of γ , assuming $\gamma > 0$. For negative γ , the signs of the asymmetries are reversed. The meaning of the curves and bands is the same as in Figure 13. The asymmetries vanish in naive factorization, so no corresponding line is drawn.

sum rules or model calculations, and finally those containing phenomenological analyses. We consider each of these in turn.

Before discussing other approaches to nonleptonic B -decays it may be helpful to summarize again the conceptual basis of the QCD factorization approach. The key ingredient is the systematic analysis of Feynman graphs in the heavy-quark limit, from which we deduce the factorization of infrared singularities into hadronic light-cone distribution amplitudes and form factors. This enables us to establish the factorization formula (25). The separation of long- and short-distance contributions to the decay amplitudes, necessary to establish factorization, holds only to leading power in Λ_{QCD}/m_b and is based on considerations analogous to those used to demonstrate factorization in other applications of QCD to hard processes (such as deep inelastic scattering, Drell–Yan production, and electromagnetic form factors of hadrons at large momentum transfer). The factorization formula leads to a model-independent treatment of exclusive hadronic B decays in the heavy-quark limit. A consistent counting scheme for powers of Λ_{QCD}/m_b and a systematic identification of all the leading contributions are crucial for establishing this result. The framework proposed in [14, 15] is general and provides a starting point for further theoretical developments, such as the improved understanding of the nonperturbative input (e.g., the $B \rightarrow \pi$ form factor and the light-cone distribution amplitudes) and estimates of power corrections.

6.1 Analyses within QCD factorization

Several authors have used the framework of QCD factorization for applications to two-body hadronic B decays [18, 19, 20, 21, 22, 23]. We now compare the results reported in these papers with ours and comment on apparent differences and discrepancies.

Muta et al. have generalized the results of our previous work [14] by including electroweak penguin contributions, and have applied the QCD factorization approach to the decays $B \rightarrow \pi K$, $\pi\pi$. We would like to point out the following differences with respect to the present work:

- The hard-scattering kernels are derived only for symmetric light-cone distribution amplitudes.
- In evaluating the α_s corrections to the penguin coefficients a_4 and a_6 , the existence of the two distinct types of penguin contractions shown in Figure 3 is not taken into account. As discussed in Section 3.3, this leads to incorrect terms proportional to $\alpha_s(C_4 + C_6)$ in these coefficients.
- An incomplete projector for the twist-3, two-particle distribution amplitude of the pion is employed. This gives an incorrect contribution proportional to C_{8g}^{eff} in a_6 .
- We also observe a disagreement with the remaining terms in the correction of order α_s to a_6 , which concerns the function $G'_{M_2}(s_q)$ in [18]. All three components, the s_q -dependent part, the constant, and the coefficient of the logarithm, differ from our

findings. We note that the μ -dependence of G'_{M_2} is in conflict with the requirement of renormalization-group invariance of the product $r_\chi^M(\mu) a_6(\mu)$. In addition, the contributions from the radiative vertex corrections to a_6 and a_8 are missing.

- A minor difference comes from the fact that we neglect electroweak penguin contributions to a_4 and a_6 , while these are included in [18]. On the other hand, Muta et al. omit the contributions proportional to C_1 , C_2 and $C_{7\gamma}^{\text{eff}}$ to the electromagnetic penguin coefficients a_8 and a_{10} .
- The twist-3 contributions to the spectator hard-scattering amplitudes and annihilation effects are not discussed. As we have seen, these corrections are the potentially most important source of theoretical uncertainty.

The formulae given in [18] have also been applied to discuss B decays into vector–pseudoscalar final states [19] and final states containing η and η' [20]. The previous comments apply also to these papers, as they do to [21], which relies on the same expressions except for dropping the formally power-suppressed terms proportional to a_6 and a_8 .

In a series of papers, Du et al. have discussed B decays into two light pseudoscalar mesons [22]. We focus on the two last papers in [22], which contain the most complete and updated results. Similarly to the present work, electroweak penguin contributions and chirally-enhanced twist-3 components of the pion distribution amplitude are included in these papers, but no weak annihilation effects are considered. The hard-scattering kernels are given only for symmetric distribution amplitudes, and explicit results are presented for the case of $B \rightarrow \pi\pi$ decays. We will therefore not distinguish between $\pi\pi$ and πK final states in the present discussion. The formulae for the coefficients a_i can be directly compared with our results. A minor difference concerns the tiny electroweak penguin contributions to the coefficients a_1, \dots, a_6 , which we decided to neglect in our approximation scheme, but which are retained in [22]. Next we recall from Section 3.3 that in the approximation of including twist-3 contributions only when they are chirally enhanced, the equations of motion require the use of asymptotic distribution amplitudes Φ_p , Φ_σ . Du et al. have considered a more general situation, which would affect the cancellation of endpoint singularities and the renormalization-scale dependence of some results. Use of the appropriate asymptotic distribution amplitudes eliminates these spurious ambiguities. Finally, we note two minor discrepancies:

- Our expression for the twist-3, hard spectator interaction in (57) contains a factor

$$\frac{2\mu_P}{m_b} \frac{\Phi_M(x)}{x} \frac{\Phi_p(y)}{\bar{y}} \quad (98)$$

in the integrand, whereas the corresponding result given in eq. (37) of the third paper in [22] has

$$\frac{2\mu_P}{M_B} \frac{\Phi_M(x)}{x} \frac{\Phi_\sigma(y)}{6\bar{y}^2}. \quad (99)$$

Using the asymptotic forms of the twist-3 distribution amplitudes Φ_p and Φ_σ , we find that the two results differ by a factor of y .

- In our result for the twist-3 penguin contribution P_3^p in (54), the coefficient of C_1 , for example, is

$$\frac{4}{3} \ln\left(\frac{m_b}{\mu}\right) + \frac{2}{3} - \hat{G}(s_p). \quad (100)$$

The equivalent expression given in eq. (23) of the third paper in [22] reads

$$\left(1 + \frac{2}{3} A_\sigma\right) \ln\left(\frac{m_b}{\mu}\right) + \frac{7}{12} + \frac{1}{2} A_\sigma - G'(s_p) - G^\sigma(s_p). \quad (101)$$

Using asymptotic twist-3 distribution amplitudes, one may check that $G'(s_p) + G^\sigma(s_p) = \hat{G}(s_p)$ and $A_\sigma = 1/2$. The two results then agree up to a constant $1/6$. This difference can be traced back to an inconsistent use of twist-3 projectors in four space-time dimensions within a d -dimensional loop calculation, before the subtraction of ultraviolet poles is performed (see the last reference in [22]). Analogous differences occur in the other terms in a_6 and a_8 .

Apart from these discrepancies, the expressions agree with our results for symmetric distribution amplitudes.

Cheng and Yang have applied the QCD factorization approach to a study of the decays $B \rightarrow \phi K$ [23]. Annihilation topologies are discussed and argued to be important numerically. A few minor discrepancies with our results occur in the expressions for the coefficients $a_{3,\dots,10}$. The penguin contraction of the operators $Q_{4,6}$ is treated incorrectly, as discussed in Section 3.3. Photonic penguin contractions of the operators $Q_{1,2}$ contributing to $a_{8,10}$ are omitted. Also, QCD corrections to $a_{6,8}$ are not considered, presumably because the corresponding amplitudes are formally power suppressed. Similarly to the results of [22], the twist-3 kernel for the hard spectator interaction contains an additional factor of y . Finally, we briefly comment on the analysis of weak annihilation contributions. In [23] the final state consists of a vector meson and a kaon rather than two pseudoscalar mesons. The decay amplitudes are estimated in the approximation of using leading-twist distribution amplitudes for the ϕ meson, but including chirally-enhanced twist-3 contributions for the kaon. Taking this systematic difference into account, we can still compare the results of [23] with our expressions. The two agree in the case of $(V-A) \otimes (V-A)$ operators, but the results for $(S-P) \otimes (S+P)$ operators are different. The latter are the ones that depend on the twist-3 contributions, but we do not have sufficient information to trace back the origin of the discrepancy.

6.2 The PQCD approach

Recently, Keum, Li and Sanda have presented an extensive study of $B \rightarrow \pi K$ decays within a perturbative hard-scattering (or ‘‘PQCD’’) approach [17]. While the underlying goal of a separation of soft and hard physics in the B -decay matrix elements is similar

in spirit to QCD factorization, there are fundamental differences in the implementation of this idea.

In the PQCD approach, the $B \rightarrow \pi$ and $B \rightarrow K$ form factors are assumed to be perturbatively calculable. This assumption is justified by invoking Sudakov effects to regulate the infrared-sensitive contribution from the endpoint region in the integral over the light-cone momentum of the outgoing spectator quark. In other words, the contribution from the region where the spectator quark is soft is supposed to be strongly suppressed, and therefore the exchange of a hard gluon is always required. Instead of being of leading order (in the QCD coupling constant), as in the generic case of a $B \rightarrow \pi$ form factor dominated by soft physics, the form factor is now counted as being of order α_s in perturbation theory. Thus, the hierarchy of the various contributions to the decay amplitudes in PQCD is very different from that in our approach:

- In the PQCD approach, the $B \rightarrow \pi K$ matrix element is a quantity of order α_s . To this order, therefore, all the Wilson coefficients can then be taken in the leading logarithmic approximation.
- The “nonfactorizable” hard gluon-exchange contributions to the kernels T_i^I in (25) enter at order α_s^2 and are therefore omitted. Note, however, that it is essential to consider such effects in order to establish factorization. This has never been done explicitly in the PQCD framework.
- The form-factor terms containing the kernels T_i^I and the hard-scattering terms containing the kernels T_i^{II} in the factorization formula are treated as being of the same order in the PQCD approach. The former are called “factorizable” and the latter “nonfactorizable”. Because both terms vanish simultaneously in the limit $\alpha_s \rightarrow 0$, naive factorization is not recovered in any limit of QCD. This is in contrast to our interpretation of the QCD factorization formula, for which naive factorization is recovered in the heavy-quark limit.

After this brief synopsis of the key features of the PQCD scheme, we now examine critically the main assumptions of this approach in the context of $B \rightarrow \pi K$ decays.

Importance of Sudakov effects and calculability of the $B \rightarrow \pi$ form factor

In the PQCD approach the transverse momenta of the quarks are kept explicitly when evaluating contributions that are potentially infrared sensitive. For instance, the gluon-exchange kernel for the $B \rightarrow \pi$ form factor is written as

$$H \sim \frac{1}{(x_3 m_b^2 + \vec{k}_{3\perp}^2)[x_1 x_3 m_b^2 + (\vec{k}_{1\perp} - \vec{k}_{3\perp})^2]} + \dots, \quad (102)$$

where the ellipses represent less singular terms. Here x_1 (x_3) is the light-cone momentum fraction of the spectator quark in the B meson (pion). In the conventional collinear expansion adopted in our work, the transverse momenta $\vec{k}_{i\perp}^2 \sim \Lambda_{\text{QCD}}^2$ would be treated

as higher-twist effects and dropped (more precisely, the amplitude would be expanded in powers of transverse momenta). It then follows that $H \sim 1/x_3^2$, and so the convolution with the leading-twist pion distribution amplitude $\Phi_\pi(x_3) \sim x_3(1-x_3)$ would lead to an integral $\int dx_3/x_3$, which is infrared divergent. This well-known result can be interpreted as a sign of the dominance of soft endpoint contributions in the $B \rightarrow \pi$ form factor [66, 67].

In [17] (see also [68]) this divergence is regulated by keeping the transverse momenta. Then a Fourier transform from transverse momentum space into impact parameter space (b space) is performed, and a Sudakov factor is included for each of the meson distribution amplitudes. This factor strongly suppresses the region of large b , and the $B \rightarrow \pi$ form factor is therefore assumed to be perturbatively calculable.

It should be noted that retaining the transverse momentum dependence in H , which is only part of the complete higher-twist contribution, is a model-dependent procedure. It is precisely in the critical endpoint region $x_3 \rightarrow 0$ that the leading two-particle Fock-state description that underlies this analysis breaks down. A further puzzle to us is the assumption made in [68] that the spectator quark in the B meson has a large momentum component in the “-” direction, $k_1^- = x_1 m_b / \sqrt{2}$, when the pion momentum is in the “+” direction. This is used to derive the Sudakov factor for the B meson in analogy to the case of a fast light meson. Since the spectator quark in the B meson is intrinsically soft, we see no justification for such an assumption.

In conclusion, we believe that the perturbative evaluation of the $B \rightarrow \pi$ form factor, which is one of the central ingredients of the PQCD analysis in [17], is not justified. The relevance of Sudakov form factors in hadronic B decays should be investigated in a more systematic way. However, it seems unlikely to us that Sudakov logarithms are sufficiently important at the scale m_b to eliminate the soft contributions to heavy-to-light form factors and thus render them calculable in a model-independent way. A complete description of the $B \rightarrow \pi$ transitions at large recoil in the heavy-quark limit and the derivation of a (hypothetical) factorization theorem for these processes has, to our knowledge, never been presented. For recent progress in this direction and further critical discussions of the problem see [33, 69].

Dynamical enhancement of penguin contributions (“fat penguins”)

Keum et al. claim a dynamical enhancement of (factorizable) contributions to the matrix elements of penguin operators (such as Q_4 and Q_6) in the effective weak Hamiltonian. The first reason given in support of this assertion is a dynamical enhancement of the $B \rightarrow \pi$ form factor of the scalar density $\bar{u}b$ contained in (the Fierz-transformed form of) Q_6 , relative to the form factor of the vector current $\bar{u}\gamma^\mu b$ relevant for other operators. A dynamically different structure for the form factor of the scalar density in PQCD is claimed, and a strong sensitivity of the effect to the model employed for the B -meson light-cone distribution amplitude is noted. However, an enhancement of this nature is not possible, because the form factor of the scalar density is related to that of the vector

current by the equations of motion, leading to

$$\langle \pi^+ | \bar{u}b | \bar{B}^0 \rangle = F_0^{B \rightarrow \pi}(q^2) \frac{m_B^2}{m_b}. \quad (103)$$

The erroneous conclusion in [17] is the consequence of an incorrect treatment of the twist-3 contribution to the pion distribution amplitude (see below).

The second reason given in favor of a penguin enhancement is the choice of a low scale μ in the (leading-order) penguin coefficients $a_4(\mu)$ and $a_6(\mu)$. This is motivated by arguing that μ should be a typical scale intrinsic to the dynamics of the $B \rightarrow \pi$ form factor in the PQCD evaluation. However, the scale μ is unphysical and must be canceled by vertex corrections to the operator matrix elements, and in the case of $a_6(\mu)$ also by the running quark masses. Such corrections have been properly included in the present work, but they were neglected in [17]. The scale μ in $a_{4,6}$ may depend on the scale of non-factorizable hard spectator interactions, but it is clearly independent of the internal dynamics of the form factor. The arguments made in favour of a low scale μ and correspondingly increased penguin coefficients are therefore not well justified.

Relevance of annihilation topologies

In their analysis, Keum et al. find that penguin annihilation contributions are numerically very important and give a dominant contribution to some of the $B \rightarrow \pi K$ decay amplitudes. We have investigated these effects in the present work and found them to give a significant correction (compatible with being a power correction of canonical size), but not a dominant contribution. Nevertheless, it must be emphasized that weak-annihilation diagrams contribute at subleading power in the heavy-quark expansion and, in general, are not calculable in a QCD-based factorization approach. Therefore, the question about the relevance of these effects warrants further investigation.

Generation of large, calculable strong-interaction phases

It is claimed that large strong-interaction phases are generated by hard gluon exchange with the spectator quark in the B meson, as well as by weak annihilation diagrams. Let us consider the hard spectator interactions in detail. In that case the effect is calculable within the QCD factorization approach and found to be real to leading order. The source of the imaginary part found in [17] is as follows. The quark propagator entering the hard-scattering diagram is written as

$$H_q \sim \frac{1}{x_2 x_3 m_b^2 - (\vec{k}_{2\perp} + \vec{k}_{3\perp})^2 + i\epsilon}. \quad (104)$$

Working to leading power we would drop the transverse components and find a real contribution to the kernel. Keum et al., on the other hand, keep the transverse momenta and hence generate an imaginary part proportional to $\delta(\vec{k}_{2\perp}^2 - x_2 x_3 m_b^2)$, where $k_{\perp} = k_{2\perp} + k_{3\perp}$. Again, this treatment is model dependent. The Fourier transform of the

kernel into impact parameter space results in a Bessel function with the imaginary part proportional to $m_b b J_0(\sqrt{x_2 x_3} m_b b)$. In the evaluation of the matrix element this function is convoluted with the Sudakov factor. Since the Bessel function is oscillating rapidly, with the amplitude of $m_b b J_0$ growing like $\sqrt{m_b b}$, the result of this convolution is very sensitive to the details of the b -space cut-off. This implies that the estimate of the strong-interaction phase is both model dependent and numerically sensitive to effects that are poorly under control. Similar comments hold for the estimate of the strong-interaction phases from the annihilation contributions, which are generated in an analogous way.

Finally, we remark that the simple γ_5 structure of the twist-3 projection for the pion employed by Keum et al. is incomplete. The proper treatment is discussed in Section 3.3. The wrong twist-3 projection is, in particular, inconsistent with gauge invariance. Moreover, the correct asymptotic behaviour of the twist-3 pion distribution amplitude $\Phi_p(x)$ is proportional to a constant, whereas the functional form $\sim x(1-x)$ is assumed in [17]. This problem affects all decay amplitudes, including the $B \rightarrow \pi$ form factor, the corresponding spurious penguin enhancement, and the nonfactorizable spectator interactions and annihilation contributions.

Other works using the PQCD approach

Other analyses in the spirit of the PQCD approach were presented in [70, 71, 72, 73], to which similar comments apply. In [72], the presence of a “recoil-phase” effect was advocated, which was claimed to originate within the PQCD framework. This phase should affect, e.g., the $B \rightarrow \pi$ form factor, which was assumed to be dominated by hard gluon exchange. It was argued that, when the gluon is exchanged between the spectator quark and the b quark, the b -quark propagator could go on the mass shell because $m_B > m_b + m_{\text{spect}}$. This in turn would lead to a complex phase in the form factor. In our opinion this conclusion is unwarranted, since bound-state effects have to be factorized before a perturbative treatment can be justified and thus cannot influence the hard-scattering process. Another fundamental objection to the “recoil phase” is that it would contradict the fact that the $B \rightarrow \pi$ form factor is a real quantity.

6.3 Estimates of nonperturbative effects

Recently, Khodjamirian has suggested to study hadronic matrix elements for two-body B decays in the framework of light-cone QCD sum rules [43]. As an example, he discusses the matrix elements of the current–current operators Q_1^u and Q_2^u for $B \rightarrow \pi^+ \pi^-$ decays. The idea is to generalize the light-cone QCD sum-rule analysis of the $B \rightarrow \pi$ form factor directly to the case of hadronic two-body modes. The starting point is the correlation function

$$F_\alpha(p, q, k) = - \int d^4x e^{i(p-q)x} \int d^4y e^{i(p-k)y} \langle 0 | T [j_\alpha^{(\pi)}(y) Q_i^u(0) j^{(B)}(x)] | \pi^-(q) \rangle, \quad (105)$$

where $j_\alpha^{(\pi)} = \bar{u} \gamma_\alpha \gamma_5 d$ and $j^{(B)} = m_b \bar{b} i \gamma_5 d$ are interpolating currents for the emission pion and the B meson, respectively. The explicit pion state $\pi^-(q)$ represents the recoil

pion that absorbs the spectator quark. According to the QCD sum rule philosophy, the correlator is evaluated in two ways: by a direct calculation in QCD, and by inserting complete sets of hadronic states between the operator Q_i^u and the interpolating currents, extracting the desired ground-state contribution with the help of quark–hadron duality. The two sides of the equation are expressed in the form of dispersion relations, and the usual Borel transformation is applied. To leading order in α_s , the factorized result for the matrix element is recovered. A particular type of power correction is then estimated as a further illustration. This contribution comes from higher twist, three-particle (quark–antiquark–gluon) Fock components of the recoil pion, where the (nonfactorizable) gluon couples to the quark lines of the emission current. In the heavy-quark limit the resulting expression is demonstrated to scale as Λ_{QCD}/m_b relative to the leading contribution. It is estimated to be of relative size λ_E/m_B with $\lambda_E \approx 0.05\text{--}0.15\text{ GeV}$. Note that this correction has no rescattering phase. Its numerical effect is small, but comparable to the perturbative corrections at leading power. Additional nonfactorizable contributions exist but have not yet been investigated. Examples are the gluon-exchange effects that correspond to the vertex corrections and the spectator scattering diagrams in the QCD factorization formula. In the sum-rule approach these effects are in principle contained in similar diagrams, together with certain hadronic corrections of subleading power. A potential difficulty will be to disentangle power corrections to the asymptotic result given by the QCD factorization formula from uncertainties intrinsic to the sum rule method, such as the assumption of quark–hadron duality and the approximation of the emission pion by an interpolating current. It is not fully clear how this can be achieved in a controlled and systematic fashion.

Some recent papers [74, 75, 76] have tried to model soft final-state interactions via the rescattering of certain hadronic channels such as $B \rightarrow D\bar{D} \rightarrow \pi\pi$. We consider such an approach to be problematical for a variety of reasons. There are many more intermediate channels beyond those taken into account. Systematic cancellations among these channels, which are predicted to occur in the heavy-quark limit, are missed when only a few intermediate states are retained (see the discussion in Sections 3.4 and 7.2 of [15]). Moreover, the hadronic dynamics of multi-body decays is very complicated and in general not under theoretical control. The main problem of such models is the lack of a systematic approximation scheme based on parametric expansions. In our opinion, the use of a purely hadronic language, suitable for kaon decays, is not very helpful in the case of B decays, where the number of channels and the energy release are large.

In [74], the coefficients a_i obtained from the QCD factorization approach have been used in conjunction with a hadronic description of final-state interactions. The general caveats concerning hadronic rescattering models apply also here. Moreover, such an approach faces a manifest double-counting problem, since rescattering effects in the heavy-quark limit are already contained in the QCD coefficients a_i .

A nonperturbative treatment of “charming penguins”, matrix elements with charm loops of the type shown in Figure 3, was proposed in [77]. In this calculation operators with flavour structure $(\bar{c}b)(\bar{s}c)$ were split into nonlocal products of currents $(\bar{c}b)$ and $(\bar{s}c)$. These were connected by intermediate virtual D -meson states to yield transitions such

as $B \rightarrow D \rightarrow K\pi$ under the separate action of the currents. However, the operators $(\bar{c}b)(\bar{s}c)$ are local operators in the effective theory at the b -mass scale. They would become nonlocal only if probed at the far higher scale of M_W , but certainly not at a scale of order m_D , as implied in [77]. We therefore see no basis for the method adopted in this paper.

6.4 Phenomenological analyses

There are several recent analyses in the literature that approach hadronic B decays in a more phenomenological way. Some of the most extensive studies of this type have been presented by Ali et al. [78], who elaborate on the concept of “generalized factorization” [79]. In these analyses, part of the order- α_s vertex and penguin contributions calculated in the present work are included. As a consequence, the decay amplitudes receive strong-interaction phases due to the Bander–Silverman–Soni mechanism [37], and nonzero CP asymmetries are obtained. However, no systematic attempt to include all such effects (or to prove factorization) is made. Also, these authors rely on ad hoc model assumptions such as an “effective number of colours” $N_c \neq 3$, which is introduced to parameterize nonfactorizable corrections.

A recent study of $B \rightarrow \pi K$ decays presented in [80] emphasizes general, model-independent parameterizations of the decay amplitudes such as our parameterization in (18), avoiding as much as possible the use of dynamical input. For instance, strong-interaction phases are a priori allowed to take any value in the construction of bounds on CKM parameters. Information on these phases may then be inferred indirectly. Such an approach is complementary to the more ambitious goal of exploiting theoretical insight into the hadronic matrix elements. In fact, the smallness of the rescattering effects parameterized by $\varepsilon_\alpha e^{i\phi_\alpha}$ in (18), which is a prediction of the QCD factorization approach, represents a useful input to such a phenomenological analysis.

Many other phenomenological studies of two-body hadronic B decays have been performed in the literature. Recent examples are [81, 82, 83, 84, 85, 86], where simplifying assumptions are made and no systematic estimates of theoretical uncertainties are undertaken.

7 Conclusions

In this paper we have presented a detailed study of $B \rightarrow \pi K$ and $B \rightarrow \pi\pi$ decays based on the QCD factorization formula. This approach allows us to perform a systematic and model-independent calculation of two-body hadronic B decays in the heavy-quark limit. We have evaluated the hard-scattering kernels entering the matrix elements for $B \rightarrow \pi K$, $\pi\pi$ decays at next-to-leading order in α_s , thus obtaining predictions for the decay amplitudes including the leading, “nonfactorizable” corrections. We have included the contributions from electroweak penguins, taking into account the corresponding order- α_s corrections to the dominant terms (enhanced by m_t^2/M_W^2 or $1/\sin^2\theta_W$) in a consistent

approximation scheme. All hard-scattering kernels have been derived for general, asymmetric distribution amplitudes, as appropriate for K mesons.

In addition to computing the model-independent leading-twist results, we have identified and estimated those power corrections which are expected to be the largest. We have analyzed the complete set of contributions from light-cone wave functions of twist 3 with a chiral enhancement factor $m_\pi^2/(m_u+m_d)$ or $m_K^2/(m_q+m_s)$, as well as the contributions from weak annihilation topologies, including both twist-2 and twist-3 components in the light-meson wave functions. We distinguish three classes of power corrections: the contributions from operators with (pseudo-) scalar currents ($\sim a_{6,8}$), twist-3 effects in the hard spectator interactions, and weak annihilation corrections. While the first two effects are proportional to the chiral enhancement factor, the annihilation terms are quadratic polynomials in this factor. Since these are power-suppressed effects, we do not expect the factorization formula to work in these cases. In fact, naively evaluating these terms in a “hard-scattering” framework one encounters logarithmic endpoint singularities. (Incidentally, the terms of order α_s related to $a_{6,8}$ are free of such infrared singularities, but divergent terms are present for the other two contributions.) Therefore, while our results at leading twist are model-independent predictions of QCD in the heavy-quark limit, some model dependence is currently unavoidable in the description of power corrections. We choose to regulate these divergences by introducing a simple cut-off, leading to the complex phenomenological parameters X_H and X_A . The motivation for this model-dependent approach to power corrections is twofold: we obtain systematic order-of-magnitude estimates, while automatically keeping track of relative suppressions or enhancements from Wilson coefficients and CKM factors. In addition, we can investigate the sensitivity of the observables on the model parameters. It turns out that annihilation graphs may in principle give sizable corrections. On the other hand, twist-3 effects in the hard spectator contributions appear generally to be less prominent.

Using this framework, we have performed a detailed comparison with the available experimental data on $B \rightarrow \pi K$ and $B \rightarrow \pi\pi$ branching ratios. The data are beginning to be sufficiently precise to allow for detailed phenomenological analyses. An important result is that in the QCD factorization approach the $B \rightarrow \pi K$ branching fractions can be larger than the $B \rightarrow \pi\pi$ ones without any tuning of the theoretical input parameters, and without invoking large phenomenological power corrections. An acceptable fit to the branching fractions is obtained even if we impose that $\gamma < 90^\circ$ as implied by the standard constraints on the unitarity triangle. This is in contrast to the naive factorization model, in which the observed branching fractions can either not be reproduced at all or require a large CKM angle γ , in conflict with other indirect determinations. Encouraged by this success, we have derived constraints in the $(\bar{\rho}, \bar{\eta})$ plane from a global fit to the $B \rightarrow \pi K$, $\pi\pi$ branching ratios, which already provide useful additional information on the unitarity triangle. Clearly, the experimental situation will continue to improve and allow us to further test our framework and exploit it in phenomenological studies of hadronic B decays. An important role in these analyses will be played by the tree-to-penguin ratio $\varepsilon_{3/2}$, which can be reliably determined from $B^\pm \rightarrow \pi^\pm \pi^0$ and $B^\pm \rightarrow \pi^\pm K^0$ decays and can be unambiguously confronted with the theoretical predictions. This will

be a valuable check that the power corrections are not surprisingly large. The absence of penguin and annihilation contributions in the $B^\pm \rightarrow \pi^\pm \pi^0$ mode is a crucial feature in this analysis. A more precise measurement of this decay will thus be particularly useful.

We would like to conclude by emphasizing again the strategy underlying our treatment of weak annihilation contributions and non-leading, but chirally-enhanced spectator interactions. While the present data do not require these effects to be larger than expected, the data also do not definitively exclude this possibility. Our error analysis is based on allowing the parameters ϱ_A and ϱ_H to be smaller than 1 (reflecting the range of our expectations), but the error estimates sometimes depend sensitively on the precise choice of this upper limit, in particular in the case of ϱ_A . With more precise data one may contemplate fitting ϱ_A to data (in practice this implies fitting the QCD penguin amplitude) in order to decide upon the plausibility of the adopted range of values. The discovery of large annihilation contributions would by itself constitute valuable insight into the strong-interaction dynamics of nonleptonic decays, but would evidently limit the utility of the QCD factorization approach. The present data make this scenario appear unlikely, but we look forward to further information to validate our error estimation. In this case, important and reliable information on flavour physics will become available from $B \rightarrow \pi K$ and $B \rightarrow \pi\pi$ decays, as well as from a large class of other two-body hadronic decays into light pseudoscalar and vector mesons.

Acknowledgments: We are grateful to A. Höcker and H. Lacker for helpful discussions and for providing us with a data file of their CKM fit results. We also thank G. Martinelli and L. Silvestrini for useful discussions. The research of M.N. is supported in part by the National Science Foundation. C.T.S. acknowledges partial support from PPARC through Grant No. GR/K55738.

References

- [1] M. Neubert and J.R. Rosner, Phys. Rev. Lett. **81** (1998) 5076 [[hep-ph/9809311](#)].
- [2] R. Fleischer, Phys. Lett. B **365** (1996) 399 [[hep-ph/9509204](#)].
- [3] M. Neubert and J.R. Rosner, Phys. Lett. B **441** (1998) 403 [[hep-ph/9808493](#)].
- [4] M. Neubert, J. High Ener. Phys. **02** (1999) 014 [[hep-ph/9812396](#)]; Nucl. Phys. B (Proc. Suppl.) **86** (2000) 477 [[hep-ph/9909564](#)].
- [5] R. Fleischer, Eur. Phys. J. C **6**, 451 (1999) [[hep-ph/9802433](#)];
A.J. Buras and R. Fleischer, Eur. Phys. J. C **11**, 93 (1999) [[hep-ph/9810260](#)].
- [6] R. Fleischer and T. Mannel, Phys. Rev. D **57** (1998) 2752 [[hep-ph/9704423](#)].
- [7] R. Fleischer, Phys. Lett. B **459** (1999) 306 [[hep-ph/9903456](#)].
- [8] M. Gronau and D. London, Phys. Rev. Lett. **65** (1990) 3381.

- [9] J.P. Silva and L. Wolfenstein, Phys. Rev. D **49** (1994) 1151 [[hep-ph/9309283](#)].
- [10] Y. Grossman and H.R. Quinn, Phys. Rev. D **58** (1998) 017504 [[hep-ph/9712306](#)].
- [11] J. Charles, Phys. Rev. D **59** (1999) 054007 [[hep-ph/9806468](#)].
- [12] A.E. Snyder and H.R. Quinn, Phys. Rev. D **48** (1993) 2139.
- [13] Z. Ligeti, M. Luke and M.B. Wise, Preprint LBNL-47551 [[hep-ph/0103020](#)].
- [14] M. Beneke, G. Buchalla, M. Neubert and C.T. Sachrajda, Phys. Rev. Lett. **83** (1999) 1914 [[hep-ph/9905312](#)].
- [15] M. Beneke, G. Buchalla, M. Neubert and C.T. Sachrajda, Nucl. Phys. B **591** (2000) 313 [[hep-ph/0006124](#)].
- [16] M. Beneke, G. Buchalla, M. Neubert and C.T. Sachrajda, Preprint PITHA-00-13 [[hep-ph/0007256](#)], to appear in the Proceedings of the 30th International Conference on High-Energy Physics (ICHEP 2000), Osaka, Japan, 27 July–2 August 2000.
- [17] Y.Y. Keum, H.-n. Li and A.I. Sanda, Preprint KEK-TH-642 [[hep-ph/0004004](#)]; Phys. Rev. D **63** (2001) 054008 [[hep-ph/0004173](#)]; Y.Y. Keum and H.-n. Li, Phys. Rev. D **63** (2001) 074006 [[hep-ph/0006001](#)].
- [18] T. Muta, A. Sugamoto, M.Z. Yang and Y.D. Yang, Phys. Rev. D **62** (2000) 094020 [[hep-ph/0006022](#)].
- [19] M.Z. Yang and Y.D. Yang, Phys. Rev. D **62** (2000) 114019 [[hep-ph/0007038](#)].
- [20] M.Z. Yang and Y.D. Yang, Preprint OCHA-PP-166 [[hep-ph/0012208](#)].
- [21] X.G. He, J.P. Ma and C.Y. Wu, Phys. Rev. D **63** (2001) 094004 [[hep-ph/0008159](#)].
- [22] D.-s. Du, D.-s. Yang and G.-h. Zhu, Phys. Lett. B **488** (2000) 46 [[hep-ph/0005006](#)]; Preprints [hep-ph/0008216](#), [hep-ph/0102077](#), [hep-ph/0103211](#).
- [23] H.-Y. Cheng and K.-C. Yang, Preprint [hep-ph/0012152](#).
- [24] J.D. Bjorken, Nucl. Phys. B (Proc. Suppl.) **11** (1989) 325.
- [25] M.J. Dugan and B. Grinstein, Phys. Lett. B **255** (1991) 583.
- [26] H.D. Politzer and M.B. Wise, Phys. Lett. B **257** (1991) 399.
- [27] A.J. Buras, M. Jamin and M.E. Lautenbacher, Nucl. Phys. B **400** (1993) 75 [[hep-ph/9211321](#)].
- [28] M. Ciuchini, E. Franco, G. Martinelli and L. Reina, Phys. Lett. B **301** (1993) 263 [[hep-ph/9212203](#)]; Nucl. Phys. B **415** (1994) 403 [[hep-ph/9304257](#)].

- [29] N.G. Deshpande and X.-G. He, Phys. Rev. Lett. **74** (1995) 26 [E: **74** (1995) 4099] [hep-ph/9408404].
- [30] G. Buchalla, A.J. Buras and M.E. Lautenbacher, Rev. Mod. Phys. **68** (1996) 1125 [hep-ph/9512380].
- [31] A.J. Buras, P. Gambino and U.A. Haisch, Nucl. Phys. B **570** (2000) 117 [hep-ph/9911250].
- [32] A.G. Grozin and M. Neubert, Phys. Rev. D **55** (1997) 272 [hep-ph/9607366].
- [33] M. Beneke and T. Feldmann, Nucl. Phys. B **592** (2001) 3 [hep-ph/0008255].
- [34] V.M. Braun and I.E. Filyanov, Z. Phys. C **44** (1989) 157; Z. Phys. C **48** (1990) 239.
- [35] B.V. Geshkenbein and M.V. Terentev, Phys. Lett. B **117** (1982) 243; Sov. J. Nucl. Phys. **40** (1984) 487 [Yad. Fiz. **40** (1984) 758]; Yad. Fiz. **39** (1984) 873.
- [36] T. Becher, B.D. Pecjak and M. Neubert, Preprint CLNS 01-1723 [hep-ph/0102219].
- [37] M. Bander, D. Silverman and A. Soni, Phys. Rev. Lett. **43** (1979) 242.
- [38] G.P. Korchemsky, D. Pirjol and T.-M. Yan, Phys. Rev. D **61** (2000) 114510 [hep-ph/9911427].
- [39] A. Khodjamirian et al., Phys. Rev. D **62** (2000) 114002 [hep-ph/0001297]; A. Khodjamirian and R. Rückl, in: *Heavy Flavours II*, A.J. Buras and M. Lindner eds. (World Scientific, Singapore, 1998) pp. 345 [hep-ph/9801443].
- [40] P. Ball, J. High Ener. Phys. **09** (1998) 005 [hep-ph/9802394].
- [41] D. Melikhov and B. Stech, Phys. Rev. D **62** (2000) 014006 [hep-ph/0001113].
- [42] A. Abada et al., Nucl. Phys. B (Proc. Suppl.) **83** (2000) 268 [hep-lat/9910021].
- [43] A. Khodjamirian, Preprint CERN-TH-2000-325 [hep-ph/0012271].
- [44] C.N. Burrell and A.R. Williamson, Preprint UTPT-01-02 [hep-ph/0101190].
- [45] A.F. Falk, A.L. Kagan, Y. Nir and A.A. Petrov, Phys. Rev. D **57** (1998) 4290 [hep-ph/9712225].
- [46] M. Gronau and J.L. Rosner, Phys. Rev. D **59** (1999) 113002 [hep-ph/9809384].
- [47] D. Cronin-Hennessy et al. (CLEO Collaboration), Phys. Rev. Lett. **85** (2000) 515.
- [48] L. Cavoto (BaBar Collaboration), talk at the 36th Rencontres de Moriond on QCD and Hadronic Interactions, Les Arcs, France, 17–24 March 2001, to appear in the Proceedings.

- [49] T. Iijima (Belle Collaboration), talk at the 4th International Conference On *B* Physics And CP Violation (BCP4), Ise-Shima, Japan, 19–23 February 2001, to appear in the Proceedings.
- [50] A. Ali and D. London, *Eur. Phys. J. C* **9**, 687 (1999) [[hep-ph/9903535](#)].
- [51] S. Plaszczynski and M.-H. Schune, talk given at 8th International Symposium on Heavy Flavour Physics, Southampton, UK, 25–29 July 1999, Preprint LAL-99-67 [[hep-ph/9911280](#)].
- [52] M. Ciuchini et al., Preprint LAL-00-77 [[hep-ph/0012308](#)].
- [53] A. Höcker, H. Lacker, S. Laplace and F. Le Diberder, Preprint LAL-01-06 [[hep-ph/0104062](#)].
- [54] M. Gronau, J.L. Rosner and D. London, *Phys. Rev. Lett.* **73** (1994) 21 [[hep-ph/9404282](#)].
- [55] J. Beringer (BaBar Collaboration), talk at the 36th Rencontres de Moriond on QCD and Hadronic Interactions, Les Arcs, France, 17–24 March 2001, to appear in the Proceedings.
- [56] G. Buchalla and A.J. Buras, *Phys. Rev. D* **54** (1996) 6782 [[hep-ph/9607447](#)].
- [57] A.L. Kagan and M. Neubert, *Phys. Lett. B* **492** (2000) 115 [[hep-ph/0007360](#)].
- [58] J.P. Silva and L. Wolfenstein, *Phys. Rev. D* **63** (2001) 056001 [[hep-ph/0008004](#)].
- [59] G. Eyal, Y. Nir and G. Perez, *J. High Ener. Phys.* **0008** (2000) 028 [[hep-ph/0008009](#)].
- [60] Z.-z. Xing, Preprint [hep-ph/0008018](#).
- [61] A.J. Buras and R. Buras, *Phys. Lett. B* **501** (2001) 223 [[hep-ph/0008273](#)].
- [62] M. Ciuchini, E. Franco, G. Martinelli and L. Silvestrini, *Nucl. Phys. B* **501** (1997) 271 [[hep-ph/9703353](#)].
- [63] M. Ciuchini et al., Preprint [hep-ph/0104018](#).
- [64] W.-S. Hou and K.-C. Yang, *Phys. Rev. Lett.* **84** (2000) 4806 [[hep-ph/9911528](#)].
- [65] S. Chen et al. (CLEO Collaboration), *Phys. Rev. Lett.* **85** (2000) 525 [[hep-ex/0001009](#)].
- [66] A. Szczepaniak, E.M. Henley and S.J. Brodsky, *Phys. Lett. B* **243** (1990) 287.
- [67] G. Burdman and J.F. Donoghue, *Phys. Lett. B* **270** (1991) 55.

- [68] H.-n. Li and H.-L. Yu, Phys. Rev. D **53** (1996) 2480 [hep-ph/9411308].
- [69] A.P. Szczepaniak and A. Radyushkin, Phys. Rev. D **59** (1999) 034017 [hep-ph/9810438].
- [70] C.-D. Lu, K. Ukai and M.-Z. Yang, Phys. Rev. D **63** (2001) 074009 [hep-ph/0004213].
- [71] C.-H. Chen and H.-n. Li, Phys. Rev. D **63** (2001) 014003 [hep-ph/0006351].
- [72] B.F.L. Ward, Preprint hep-ph/0006357.
- [73] C.-D. Lu and M.-Z. Yang, Preprint HUPD-0012 [hep-ph/0011238].
- [74] Z.-z. Xing, Phys. Lett. B **493** (2000) 301 [hep-ph/0007136].
- [75] P. Zenczykowski, Phys. Rev. D **63** (2001) 014016 [hep-ph/0009054].
- [76] K. Terasaki, Preprint YITP-00-65 [hep-ph/0011358].
- [77] C. Isola et al., Preprint BA-TH-404-00 [hep-ph/0101118].
- [78] A. Ali and C. Greub, Phys. Rev. D **57** (1998) 2996 [hep-ph/9707251];
A. Ali, G. Kramer and C.-D. Lu, Phys. Rev. D **58** (1998) 094009 [hep-ph/9804363];
Phys. Rev. D **59** (1999) 014005 [hep-ph/9805403].
- [79] M. Bauer, B. Stech and M. Wirbel, Z. Phys. C **34** (1987) 103;
M. Neubert and B. Stech, in: *Heavy Flavours II*, ed. A.J. Buras and M. Lindner
(World Scientific, Singapore, 1998) pp. 294 [hep-ph/9705292].
- [80] A.J. Buras and R. Fleischer, Eur. Phys. J. C **16**, 97 (2000) [hep-ph/0003323].
- [81] H.-Y. Cheng and K.-C. Yang, Phys. Rev. D **62** (2000) 054029 [hep-ph/9910291].
- [82] Y.-L. Wu and Y.-F. Zhou, Phys. Rev. D **62** (2000) 036007 [hep-ph/0002227].
- [83] Y.F. Zhou, Y.L. Wu, J.N. Ng and C.Q. Geng, Phys. Rev. D **63** (2001) 054011 [hep-ph/0006225].
- [84] X.H. Guo, O. Leitner and A.W. Thomas, Phys. Rev. D **63** (2001) 056012 [hep-ph/0009042].
- [85] C. Isola and T.N. Pham, Preprint CPHT-S-085-0900 [hep-ph/0009210].
- [86] W.N. Cottingham, H. Mehrban and I.B. Whittingham, Preprint hep-ph/0102012.